2006

MIMO communication systems: receiver design and diversity-multiplexing tradeoff analysis

Wei Mo
Iowa State University

MIMO communication systems: receiver design and diversity-multiplexing tradeoff analysis

by

Wei Mo

A dissertation submitted to the graduate faculty

in partial fulfillment of the requirements for the degree of

DOCTOR OF PHILOSOPHY

Major: Electrical Engineering

Program of Study Committee:
Zhengdao Wang, Major Professor
Julie Dickerson
Aleksandar Dogandžić
Sang W. Kim
Yao Ma
Huaiqing Wu

Iowa State University

Ames, Iowa

2006

TABLE OF CONTENTS

LIST OF FIGURES

LIST OF ACRONYMS

APP	a posteriori probability
AWGN	additive white Gaussian noise
BER	bit error rate
BLAST	Bell labs layered space-time
BPSK	binary phase shift keying
CDMA	code division multiple access
CIS	coordinated independent sleeping
CSI	channel sate information
DMT	diversity-multiplexing tradeoff
DW-ILSP	decoupled weighted iterative least squares with projection
EM	expectation-maximization
IID	independent and identically distributed
ILSP	iterative least squares with projection
LDPC	low-density parity-check
LLR	log likeilhood ratio
LPR	log-probability ratio
LSD	list sphere decoder
MAP	maximum a posteriori
MCRB	modified Cramér-Rao bound
MIMO	multi-input multi-output

ML	maximum-likelihood
MMSE	minimum mean square error
MRC	maximum ratio combining
MSE	mean-square error
OFDM	orthogonal frequency-division multiplexing
OSSIC	ordered successive softer interference cancellation
PDF	probability density function
QAM	quadrature amplitude modulation
QPSK	quadrature phase shift keying
RIS	randomized independent sleeping
RS	Reed-Solomon
SEP	symbol error probability
SER	symbol error rate
SIMO	single-input multiple-output
SNR	diversity-multiplexing tradeoff

ACKNOWLEDGEMENTS

Looking back at the years I spent at Iowa State University, I truly feel being blessed with many wonderful friendships and collaborations. I would like to express my thanks to those who helped me with various aspects of my study, research and life at Ames.

My deepest gratitude and respect first go to my advisor, Dr. Zhengdao Wang, for his expert guidance and for his kindness, encouragement and support over the years. It was his wonderful lectures on digital communications (EE 521 Digital Communications) that first attracted me into this field of telecommunications and later into this specific area of MIMO communications. His creative thinking and insightful ideas have often inspired me. I appreciate the confidence that he has shown in my abilities and the patience he has exhibited in teaching me a lot of valuable things.

I am very grateful to Dr. Julie A. Dickerson, Dr. Aleksandar Dogandžić, Dr. Sang W. Kim, Dr. Yao Ma, and Dr. Huaiqing Wu for serving on my committee.

I also wish to acknowledge Dr. Daji Qiao for his useful discussions, important suggestions and numerous proofreads during the collaboration on the research project of wireless sensor network.

My interaction with the members and visitors in Communication and Signal Processing Group, Systems and Control Group, has been of exceptional value of me. My respect and recognition go to these students: Jialing Liu, Lei Zhao, Jinghua Jin, Dongbo Zhang, Benhong Zhang, Xiaofan Yang and Peng Yu.

This thesis is dedicated to my wife, daughter and parents.

ABSTRACT

After a few decades' evolution of wireless communication systems, to ensure reliable high-speed communication over unreliable wireless channels is still one of the major challenges facing researchers and engineers. The use of multiple antennas at transmitter and receiver, known as multiple-input multiple-output (MIMO) communications, is one promising technology delivering desired wireless services. The main goal of this thesis is to study two important issues in wireless MIMO communication systems: receiver design for coded MIMO systems, and diversity-multiplexing tradeoff analysis in general fading channels.

In the first part of this thesis, we decompose the receiver design problem into two sub-problems: MIMO channel estimation and MIMO detection. For the MIMO channel estimation, we develop an expectation-maximization (EM) based semi-blind channel and noise covariance matrix estimation algorithm for space-time coding systems under spatially correlated noise. By incorporating the proposed channel estimator into the iterative receiver structure, both the channel estimation and the error-control decoding are improved significantly. We also derive the modified Cramér-Rao bounds (MCRB) for the unknown parameters as the channel estimation performance metric, and demonstrate that the proposed channel estimation algorithm can achieve the MCRB after several iterations. For the MIMO detection, we propose a novel low-complexity MIMO detection algorithm, which has only cubic order computational complexity, but with near-optimal performance. For a 4×4 turbo-coded system, we show that the proposed detector had the same performance as the *maximum a posteriori* (MAP) detector for BPSK modulation, and 0.1 dB advantage over the approximated MAP detector (list sphere decoding algorithm) for 16-QAM modulation at BER $= 10^{-4}$.

In the second part of this thesis, we derive the optimal diversity-multiplexing tradeoff for

general MIMO fading channels, which include different fading types as special cases. We show that for a MIMO system with long coherence time, the optimal diversity-multiplexing tradeoff is also a piecewise linear function, and only the first segment is affected by different fading types. We proved that under certain full-rank assumptions spatial correlation has no effect on the optimal tradeoff. We also argued that non-zero channel means in general are not beneficial for multiplexing-diversity tradeoff.

CHAPTER 1. INTRODUCTION

1.1 Overview of wireless MIMO communication systems

High data rate wireless communications is of interests in emerging wireless local area network and next generation wireless systems. Designing high speed communication systems that can support reliable transmissions over wireless channels constitutes a significant research and engineering challenge. The use of multiple antennas at transmitter and receiver, commonly referred to as multiple-input multiple-output (MIMO) communications, is one promising technology delivering desired wireless services. The seminal work by Foschini and Gans [31] and, independently, Telatar [102] suggested that MIMO systems have the potential of achieving remarkable spectral efficiency under "rich" multipath environments. The Bell Labs Layered Space-Time (BLAST) scheme has demonstrated spectral efficiencies ranging from 20 to 40 bits per second per Hertz, which is almost impossible with conventional methods [116].

It is well known that, compared with wireline communication systems, one major impairment for wireless communication systems is the complicated time-varying channels with possibly multi-path fading, shadowing, pass loss, interference, and so on. This may leads to severe data rate loss or performance degradation, or both. One effective way to combat fading channel is to use the so-called "diversity" techniques, which means that other replicas of the transmitted signal must be sent to the receiver in other formats (or through other paths). The intuition is to take advantage of the low probability of concurrent deep fades in all independent paths to lower the probability of error. The commonly used diversity techniques include temporal diversity, frequency diversity and spatial (antenna) diversity. In many cases, wireless channel is slow time-varying (no temporary diversity), non-frequency selective (no frequency diversity), thus spatial diversity is needed to improve the performance. Such spatial diversity

can be achieved by the use of MIMO systems. For example, the same signal can be transmitted over N_T different transmit antennas, and received by N_R receive antennas. Since the signal goes through $N_T \times N_R$ independent paths, it is possible to achieve the diversity of $N_T \times N_R$ by appropriately combining these signals. On the other hand, fading channels may also be beneficial for a wireless communication system. By increasing the independent fading paths between the transmitter and receiver, the degrees of freedom of the whole system are increased as well. If the different degrees of freedom are used to transmit different signals, the total data rate can be increased significantly. This is why MIMO systems can provide much higher spectral efficiency than single-antenna systems.

To date, many transmission schemes for MIMO systems have been proposed in the literature. These schemes may be roughly divided into two categories: *space-time coding* techniques and *spatial multiplexing* schemes. Space-time coding techniques (such as Alamouti's scheme [3]) exploit spatial diversity to yield good performance and easy decodability at the expense of less spectral efficiency. On the other hand, spatial multiplexing schemes like BLAST can provide spatial-multiplexing gain to enhance the overall data throughput and achieve significant fractions of the data rate promised in theory. However, the corresponding data detection at the receiver is much more complicated due to the interferences introduced by MIMO channels. Combined with strong error-control codes, both of these two schemes can deliver high-rate data with good performance, provided that the frame length is long enough and good channel estimation is available at the receiver.

In order to use MIMO communication systems to ensure reliable high-speed information transmission over unreliable wireless fading channels, there are still many technical issues in both theoretical analysis and practical design. These issues include, but not limited to, i) practical issues: transmitter design (such as space-time coding, power and/or rate adaptation), receiver design (such as channel state/statistics estimation and symbol detection), error-control coding (such as low-density parity-check (LDPC) coding and turbo coding), equalization, feedback from the receiver to transmitter, etc. ii) theoretical issues: MIMO capacity analysis, error performance analysis, optimal (capacity-achieving) signaling design, diversity-

multiplexing tradeoff, etc. In what follows, we briefly introduce two issues (one practical and one theoretical) addressed in this thesis: iterative receiver design for coded MIMO systems and diversity-multiplexing tradeoff in MIMO fading channels.

1.2 Iterative receiver design for coded MIMO systems

In almost all of modern communication systems, error-control codes are used to improve the system performance in terms of error probability. Here, we also consider a coded MIMO system as shown in Fig. 1.1. At the transmitter, the information bit stream $\boldsymbol{u}$ is encoded to coded bit stream $\boldsymbol{c}$ through error-control encoder, then modulated to vector signal $\boldsymbol{s}$ by MIMO modulator, and transmitted using multiple transmit antennas. At the receiver, the received vector signal $\boldsymbol{y}$ from multiple receive antennas is a mixed-version of $\boldsymbol{s}$ due to MIMO channel matrix $\boldsymbol{H}$, plus some noise. The optimal way to recover the information bits is to find the maximum-likelihood estimate of each information bit based on the received data $\boldsymbol{y}$'s, and the constraints imposed by the MIMO channel $\boldsymbol{H}$ and the error-control code. However, the prohibitive computational complexity makes it impossible to implement. The most commonly used alternative is to separate the detection and the decoding of the coded bits $\boldsymbol{c}$. Such receiver structure has two modules: MIMO demodulator and error-control decoder as shown in Fig. 1.1. Since the MIMO channel matrix $\boldsymbol{H}$ is usually unknown at the receiver, the MIMO demodulator block includes both channel estimator and MIMO detector.

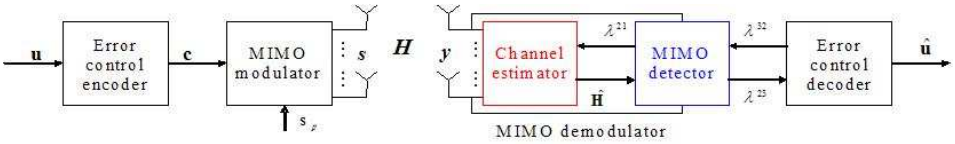

Figure 1.1 Discrete-time transmitter and receiver structure for coded MIMO communication systems

Recently there have been increasing interests in iterative receiver design [17, 51, 58, 100]. In an iterative receiver, there are iterations between MIMO demodulator and error-control decoder, where soft information of coded bits is exchanged between them such that the symbol

detection and the channel estimation can be refined and ultimately improve decoding performance. It has been shown that such "turbo principle" is very effective and computationally efficient in other joint detection and decoding problems [51, 104]. Since the error-control encoder and decoder are relatively standard, we here focus in detail on the MIMO demodulator design.

In this thesis, we will study the MIMO demodulator design for two different transmission schemes: space-time coding and spatial multiplexing. For space-time coding scheme, e.g., orthogonal space-time codes [101], the MIMO detection is much easier due to the special structure of space-time codewords at the expense of less spectral efficiency. Thus, we can assume the optimal MIMO detection, i.e., *maximum a posterior* (MAP) detector, and design efficient MIMO channel estimator for space-time coding scheme. For spatial multiplexing scheme, with much higher spectral efficiency, we can use more redundancy to estimate the MIMO channel, and still achieve the same data rate as the space-time coding scheme. For example, more pilot symbols can be inserted into the data transmission without violating the overall data rate requirement, and improve the MIMO channel estimation significantly. Therefore, we can assume perfect channel state information, and design low-complexity near-optimal MIMO detector.

In summary, the iterative receiver design for coded MIMO systems is decoupled into two sub-problems: MIMO channel estimation and MIMO detection.

1.2.1 MIMO channel estimation

Both space-time coding and spatial multiplexing schemes require channel state information (CSI) at the receiver for coherent detection, and the performance depends on the quality of channel estimation. Differential schemes do not require CSI at the receiver, but they usually suffer a 3 dB loss in SNR when the detection is based on two consecutive received blocks [53]. Therefore, estimation of the MIMO channel is a major challenge for multi-antenna systems. At the same time, it is also a non-trivial problem because of the large number of parameters involved and that the parameters have to be estimated within the channel coherence time.

Existing channel estimation algorithms can be classified as training based algorithms [14, 88, 9], and blind or semi-blind algorithms [107, 39, 20, 63, 77]. For training based channel estimation, MIMO channels are estimated using only pilot symbols and the corresponding received signals, and then the estimates are used to detect data symbols. In order to achieve better channel estimation, more pilot symbols are usually needed which results in rate loss. On the other hand, blind or semi-blind algorithms utilize the received signals of both pilot symbols and data symbols to estimate the channel. Inspired by iterative detection and decoding schemes, most of the state-of-the-art semi-blind channel estimation algorithms are carried out under the joint channel estimation, detection and decoding framework, since the soft information of data symbols fed back from the error-control decoder can greatly improve the channel estimation.

1.2.2 MIMO detection

For spatial multiplexing schemes, we assume that the channel matrix $\boldsymbol{H}$ is perfectly known at the receiver, then the task of MIMO detectors is to provide the decision (hard or soft) on transmitted symbols $\boldsymbol{s}$ given the received signal $\boldsymbol{y}$. Such MIMO detection problem also shows up in other setups, including the multi-user detection [108], filter banks [106], modulated coding [117], and multi-carrier CDMA schemes [113]. The solution to the MIMO detection problem can also offer benefits to designing these systems.

There are two classes of MIMO detectors: hard-decision detectors and soft-decision detectors. The first one is useful for detecting uncoded transmissions, where the decision of MIMO detectors will be used as final decision. The second one is usually used in coded MIMO systems, where an iterative detection and decoding scheme needs soft information being exchanged between detection and decoding modules following the "turbo principle", see e.g., [49]. Since soft information can be fed back from the error-control decoder to the MIMO detector, soft-decision detectors often incorporates *a priori* information on symbols in $\boldsymbol{s}$ into detector design.

Among hard-decision detectors, the maximum-likelihood (ML) detector is optimum, which

is equivalent to finding the closest lattice point to the given received vector $\boldsymbol{y}$ in the space of all possible symbol vectors. Denoting the alphabet size of the scalar constellation transmitted from each antenna by M, the ML detector needs to search over a total of M^{N_T} vectors rendering the complexity exponential in the number of transmit antennas. It is prohibitive even for moderate systems, e.g., $N_T = 6$ with QPSK modulation. Existing sub-optimal hard-decision detectors include zero-forcing or decorrelating detectors, linear minimum mean square-error (MMSE) detectors [79], successive interference cancellation with iterative least squares [64], multistage cancellation [108], and BLAST nulling/cancelling [116, 47]. They have total complexity in the order of $\mathcal{O}(N_T^2)$ to $\mathcal{O}(N_T^3)$, but there is usually a significant performance gap from the ML detector. Sphere decoding [29, 80, 110, 48] has near-optimal performance but with complexities higher than the cubic order, especially for moderate systems (e.g., $N_T \leq 10$).

For soft-decision detection, the optimal detector is MAP detector, which can output the soft information on transmitted symbols or the underlying coded bits. However, the computational complexity of MAP detector is the same as that of the ML detector, which limits its practical application. Some sub-optimal soft-decision detectors have been proposed in the literature, e.g., parallel soft interference cancellation [17], soft interference cancellation with linear MMSE filtering [111], and BLAST nulling/cancelling with prior information [119]. Although they have low complexity at cubic to biquadratic order, none of them can achieve near-optimal performance at the medium frame length. List sphere decoding [51] and iterative tree search detection [21] have near-optimal performance at the expense of much higher complexities than those sub-optimal algorithms.

1.3 Diversity-multiplexing tradeoff in MIMO fading channels

As explained in Section 1.1, MIMO systems can be configured to provide spatial diversity by transmitting the same symbol through different antennas, or increase the total transmission rate by transmitting independent information streams through different antennas. *Can we achieve both of these two advantages simultaneously?*

While traditional design focused on maximizing either the spatial diversity or the transmis-

sion rate, Zheng and Tse gave a novel asymptotic view of MIMO systems in their seminal work [124] by considering them jointly, and answered the previous question. Their result shows that both of the two advantages mentioned above can be achieved simultaneously, but there is a tradeoff between them. In other words, having more spatial diversity results in less transmission rate, and vice versa. From a diversity-multiplexing tradeoff (DMT)'s point of view, we say a coding (transmission) scheme has a spatial multiplexing gain r and a diversity gain d, if the transmission rate scales like $r \log \mathrm{SNR}$ and the average error probability decays like SNR^{-d}. The essential result of the paper is the characterization of the optimal diversity-multiplexing tradeoff for a MIMO system under independent and identically distributed (i.i.d) Rayleigh fading channel. It was proved that the optimal diversity gain $d(r)$ is a simple piecewise linear function of multiplexing gain r.

Following similar ideas, optimal tradeoff curves have been calculated in different scenarios. For example, the DMT for the non-coherent MIMO channel is considered in [122]. The tradeoff result in multiple-access channels is obtained in [103]. In [120], the authors derived the DMT for cooperative wireless systems. The DMT result for multi-access relay channels is provided in [15]. To determine which point of the optimal DMT curve a MIMO system should operate on, the authors of [52] considered an additional end-to-end distortion constraint. Inner and outer bounds are derived for the DMT of a 2×2 broadcast/multiple access channel [115].

Popular schemes such as Alamouti, V-BLAST and D-BLAST are evaluated using diversity and multiplexing tradeoff as a metric in [124]. This kind of tradeoff has been serving as a new performance benchmark to compare different schemes and evaluate new ones [94, 5]. Meanwhile, the lack of optimality of existing schemes shown by [124] inspires the design of new MIMO schemes that achieve the optimal tradeoff curve [32].

1.4 Problem formulations and main results

In this section, we motivate the specific problems we wish to address, briefly describe the approaches, informally present our main results, and summarize the contributions.

In the first part of this thesis, we focus on the iterative receiver design for coded MIMO

systems. Two different transmission schemes are considered here: space-time coding and spatial multiplexing. For the space-time coding scheme, the MIMO detection is relatively easy due to the special structure of space-time codes. For example, with orthogonal space-time codes, different symbols can be detected separately with optimal detector. Thus, we assume that the MAP detector is employed, and the iterative receiver design is boiled down to MIMO channel estimator design.

Problem 1. *Find an efficient semi-blind MIMO channel estimator for space-time coding systems under unknown spatially correlated noise.*

Since the channel information is required at the MIMO detection module for coherent detection, an accurate channel estimation plays an important role in MIMO receiver design. We consider a space-time coding system with iterative receiver structure. The additive noise is assumed to be spatially correlated, which can model the co-channel interference. Within the iterative receiver structure (c.f. Fig. 1.1), the MIMO detector is MAP detector, and error-control decoder is standard soft-input soft-output decoder (e.g., LDPC decoder or turbo decoder). Our goal is to design the MIMO channel estimator to estimate both the channel matrix and the noise covariance matrix.

The main approach we apply is based on expectation-maximization (EM) algorithm, which is a general iterative method for computing ML estimates in the scenarios where ML algorithm cannot be easily performed. Our results state as follows. We develop an EM-based semi-blind channel and noise covariance matrix estimation algorithm. By incorporating the proposed channel estimator into the iterative receiver structure, the accuracy of channel estimation is improved significantly, and can achieve the theoretical bounds (modified Cramér-Rao bounds) after several iterations. In terms of error rate performance, after several iterations, we can reach the same performance as the ideal coherent scenario, where the channel is assumed to be perfectly known at the receiver. For such a spatially correlated noise scenario, simulation results show that estimation algorithms assuming white noise have much worse performance than the one of the proposed algorithm.

The contributions of this work could be summarized as: 1) proposing an efficient semi-

blind channel and noise estimation algorithm for space-time coding systems under spatially correlated noise; 2) deriving the modified Cramér-Rao bounds for the unknown parameters; and 3) demonstrating the importance of taking into account spatial correlation of the noise when the noise is spatially correlated. Part of this work can be found in [23, 72].

For the spatial-multiplexing transmission schemes, the spectral efficiency can be much higher than the space-time coding schemes. With the same total data rate as the space-time coding systems, spatial multiplexing schemes can exploit more training symbols to get more accurate channel estimation. Therefore, when we design the iterative receiver for spatial multiplexing systems, we assume that the channel state information is perfectly known at the receiver, and the remaining problem is how to design a good MIMO detector.

Problem 2. *Design a low-complexity near-optimal MIMO detection algorithm for spatial multiplexing systems.*

It has been shown in [51] that spatial multiplexing combined with strong error-control codes can achieve near-capacity on MIMO systems with perfect channel estimation at the receiver. But the success of such iterative receiver structure requires a good MIMO detection module. Provided that the perfect CSI is available at the receiver, MAP detection is optimum but with exponential complexity, which is prohibitive for large systems (many antennas or large constellation size). Existing sub-optimal detection algorithms include zero-forcing, minimum mean-square error, nulling/cancelling, successive or parallel interference cancellation, and sphere decoding algorithms. But these sub-optimal algorithms either have high complexity (biquadratic-order or higher), or do not produce soft information, or have far-from-optimum performance. Our goal is to design a low-complexity MIMO detection algorithm with near-optimal performance.

The approach used in our design is to incorporate the prior information of the transmitted symbol provided by error-control decoder into the BLAST nulling/cancelling algorithm, which leads to the following results to Problem 2. We propose a novel low-complexity MIMO detection algorithm, namely ordered successive softer interference cancellation (OSSIC), which has only cubic-order computational complexity. For a 4×4 turbo-coded system, the proposed detector

has the same performance as the MAP detector for BPSK modulation, and 0.1 dB advantage over the approximated MAP detector (list sphere decoding algorithm) for 16-QAM modulation at BER $= 10^{-4}$.

Our novelties and contributions of this work are: 1) incorporating the prior information from error-control decoder into the original nulling/cancelling algorithm, and making nulling, cancelling and ordering steps *a posteriori* probabilities (APP) based; 2) developing a "square-root" algorithm to reduce the complexity of the proposed detector to the cubic order; 3) achieving near-optimal performance with much lower complexity than the optimal detector. Part of this work is published in [71].

In the second part of this thesis, we discuss another theoretical issue in MIMO communication systems: diversity-multiplexing tradeoff in MIMO fading channels. In Zheng and Tse's work [124], the optimal diversity-multiplexing tradeoff is characterized by a simple piecewise linear function for i.i.d Rayleigh fading channels. In practical MIMO communication scenarios, there exist many channel conditions that cannot be accurately modeled as i.i.d Rayleigh fading. Our question then is, *can we extend Zheng and Tse's results to a general fading channel condition?* Such question leads us to the third problem to be addressed in this thesis.

Problem 3. *Characterize the optimal diversity-multiplexing tradeoff in general fading channels.*

Our technique for this generalization is based on the intuition that the optimal tradeoff performance is determined by the joint probability density function (pdf) of the eigenvalues of the Gram matrix of the MIMO channel, especially the eigenvalue behavior near zeros. The main results of this work are as follows. We derive the optimal diversity-multiplexing tradeoff for general MIMO fading channels, which include different fading types as special cases. We show that for a MIMO system with long coherence time, the optimal diversity-multiplexing tradeoff is also a piecewise linear function, and only the first segment is affected by different fading types. We proved that under certain full-rank assumptions spatial correlation has no effect on the the optimal tradeoff. We also argued that non-zero channel means in general are not beneficial for diversity-multiplexing tradeoff.

Our main contribution is that, the answers to Problem 3 can facilitate a more comprehensive understanding of the limiting performance of MIMO systems under generalized fading conditions. The techniques we developed can also be used to analyze the diversity-multiplexing tradeoff in multiple-access and broadcast channels. The results of this work have been reported in [123].

The rest of the thesis is organized as follows: Chapter 2 presents an EM-based channel and noise estimation algorithm for uncoded single-input multiple-output (SIMO) systems, which is extended to coded MIMO systems under spatially correlated noise in Chapter 3. In Chapter 4, we propose a low-complexity near-optimal MIMO detection algorithm for coded MIMO systems. Chapter 5 discusses the optimal diversity-multiplexing tradeoff in general MIMO fading channels. At last, Chapter 6 concludes the thesis and point out some directions for future work. For completeness, another two projects that were done during my Ph.D. study, asymptotic performance analysis for cooperative diversity system [70], and lifetime study for wireless sensor networks [68, 69], are also presented in Appendix A and Appendix B, respectively.

CHAPTER 2. MAXIMUM LIKELIHOOD CHANNEL AND NOISE ESTIMATION FOR UNCODED SIMO SYSTEMS

2.1 Introduction

Expectation-maximization (EM) and related algorithms (see [22, 73, 66]) have been applied to carrier phase recovery [76], demodulation for unknown carrier phase [83], timing estimation [34], and channel estimation [55]–[19] in single-input single-output (SISO) communication systems, and, more recently, to symbol detection [65]–[20] and channel estimation [4] in smart antenna systems. In this chapter, we present an EM algorithm for semi-blind ML estimation of both the channel and spatial noise covariance matrices in a single-input multi-output (SIMO) smart antenna scenario. The proposed algorithm can also be used to estimate multipath channels in unknown colored noise. This is unlike previous work in [55, 19, 4], where EM algorithms were applied to SISO and multi-input single-output (MISO) channel estimation in white noise.

The signal and noise models are introduced in Section 2.2. In Section 2.3, we derive the EM algorithm for estimating the unknown channel and noise parameters and in Section 2.4, we compute modified and estimated Cramér-Rao bounds (CRBs) for these parameters. The EM channel estimates are incorporated into the receiver design in Section 2.5. In Section 2.6, we give some numerical examples. We conclude the chapter in Section 2.7.

2.2 Measurement Model

Consider a single-input multi-output (SIMO) flat-fading channel with equiprobable constant-modulus symbols. Denote by $\boldsymbol{y}(t)$ an $n_R \times 1$ data vector (snapshot) received by an array of n_R

antennas at time t and assume that we have collected N snapshots. Under a single-user slow flat-fading scenario, $\boldsymbol{y}(t)$ can be modeled as

$$\boldsymbol{y}(t) = \boldsymbol{h} \cdot u(t) + \boldsymbol{e}(t), \quad t = 1, 2, \ldots, N, \tag{2.1}$$

where

- $\boldsymbol{h}$ is an unknown $n_R \times 1$ channel response vector;
- $u(t)$ is an unknown symbol received by the array at time t;
- $\boldsymbol{e}(t)$ is temporally white and circularly symmetric zero-mean complex Gaussian noise vector with unknown positive definite spatial covariance matrix Σ.

The channel $\boldsymbol{h}$ and noise covariance matrix Σ are assumed to be constant for $t \in \{1, 2, \ldots, N\}$. The spatially correlated noise model accounts for co-channel interference (CCI) and receiver noise[1]. We further assume that the symbols $u(t)$ belong to an M-ary constant-modulus constellation

$$\mathcal{U} = \{u_1, u_2, \ldots, u_M\}, \tag{2.2}$$

where

$$|u_m| = 1, \quad m = 1, 2, \ldots, M. \tag{2.3}$$

[The constant-modulus assumption can be relaxed, see Appendix 2.A.] We model $u(t)$, $t = 1, 2, \ldots, N$ as independent, identically distributed (i.i.d.) random variables with probability mass function

$$p(u(t)) = \frac{1}{M} i(u(t)), \tag{2.4}$$

where

$$i(u) = \begin{cases} 1, & u \in \{u_1, u_2, \ldots, u_M\}, \\ 0, & \text{otherwise} \end{cases}. \tag{2.5}$$

Our goal is to estimate the unknown channel and noise parameters $\boldsymbol{h}$ and Σ. To allow unique estimation of the channel $\boldsymbol{h}$ (e.g. to resolve the phase ambiguity), we further assume that N_T

[1]This noise model has been used in numerous recent publications to account for unstructured interference, see e.g. [26] and references therein.

known (training) symbols

$$u_T(t) \in \mathcal{U}, \quad t = 1, 2, \ldots, N_T, \tag{2.6}$$

are embedded in the transmission scheme and denote the corresponding snapshots received by the array as $\boldsymbol{y}_T(\tau),\ \tau = 1, 2, \ldots, N_T$. Then, the measurement model (2.1) holds for the training symbols as well, with $\boldsymbol{y}(t)$ and $u(t)$ replaced by $\boldsymbol{y}_T(\tau)$ and $u_T(\tau)$, respectively.

In the following section, we derive an EM algorithm for computing the ML estimates of $\boldsymbol{h}$ and Σ under the above measurement model.

2.3 ML Estimation

The EM algorithm is a general iterative method for computing ML estimates in the scenarios where ML estimation cannot be easily performed by directly maximizing the likelihood function of observed measurements. Each EM iteration consists of maximizing the expected complete-data log-likelihood function, where the expectation is computed with respect to the conditional distribution of the unobserved data given the observed measurements. A good choice of unobserved data allows easy maximization of the expected complete-data log-likelihood. The algorithm converges monotonically to a local or the global maximum of the observed-data likelihood function, see e.g. [66, Ch. 3]. Here, the unknown symbols $u(t)$, $t = 1, 2, \ldots, N$ are modeled as the unobserved (or missing) data. Given $u(t)$, the corresponding *observed* snapshot $\boldsymbol{y}(t)$ is distributed as a complex multivariate Gaussian vector with probability density function (pdf):

$$f(\boldsymbol{y}(t)|u(t), \boldsymbol{h}, \Sigma) = \frac{1}{|\pi\Sigma|} \cdot \exp\Big\{ -[\boldsymbol{y}(t) - \boldsymbol{h}u(t)]^H \Sigma^{-1} [\boldsymbol{y}(t) - \boldsymbol{h}u(t)] \Big\}, \tag{2.7}$$

where "$(\cdot)^H$" denotes the Hermitian (conjugate) transpose. The above expression also holds for the training data, with $\boldsymbol{y}(t)$ and $u(t)$ replaced by $\boldsymbol{y}_T(\tau)$ and $u_T(\tau)$. The joint distribution of $\boldsymbol{y}(t)$, $u(t)$ (for $t = 1, 2, \ldots, N$), and $\boldsymbol{y}_T(\tau)$ (for $\tau = 1, 2, \ldots, N_T$) can be written as

$$\prod_{t=1}^{N} p(u(t)) f(\boldsymbol{y}(t)|u(t), \boldsymbol{h}, \Sigma) \cdot \prod_{\tau=1}^{N_T} f(\boldsymbol{y}_T(\tau)|u_T(\tau), \boldsymbol{h}, \Sigma), \tag{2.8}$$

which is also known as the *complete-data likelihood function*. The *observed-data likelihood function* to be maximized is then

$$\begin{aligned}&\Big[\sum_{u(1)\in\mathcal{U}}\sum_{u(2)\in\mathcal{U}}\cdots\sum_{u(N)\in\mathcal{U}}\prod_{t=1}^{N}p(u(t))\;f(\boldsymbol{y}(t)|u(t),\boldsymbol{h},\Sigma)\Big]\cdot\prod_{\tau=1}^{N_T}f(\boldsymbol{y}_T(\tau)|u_T(\tau),\boldsymbol{h},\Sigma)\\ =&\prod_{t=1}^{N}\Big[\sum_{m=1}^{M}\frac{1}{M}\cdot f(\boldsymbol{y}(t)|u_m,\boldsymbol{h},\Sigma)\Big]\cdot\prod_{\tau=1}^{N_T}f(\boldsymbol{y}_T(\tau)|u_T(\tau),\boldsymbol{h},\Sigma).\end{aligned}\tag{2.9}$$

In Appendix 2.A, we derive the EM algorithm for maximizing (2.9): Iterate between

Step 1:

$$\boldsymbol{h}^{(k+1)}=\frac{1}{N+N_T}\Big\{\sum_{t=1}^{N}\Big[\boldsymbol{y}(t)\sum_{m=1}^{M}u_m^*\cdot\rho_m^{(k)}(t)\Big]+\sum_{\tau=1}^{N_T}\boldsymbol{y}_T(\tau)u_T(\tau)^*\Big\},\tag{2.10}$$

where

$$\rho_m^{(k)}(t)=\frac{\exp\{-[\boldsymbol{y}(t)-\boldsymbol{h}^{(k)}u_m]^H(\Sigma^{(k)})^{-1}[\boldsymbol{y}(t)-\boldsymbol{h}^{(k)}u_m]\}}{\sum_{n=1}^{M}\exp\{-[\boldsymbol{y}(t)-\boldsymbol{h}^{(k)}u_n]^H(\Sigma^{(k)})^{-1}[\boldsymbol{y}(t)-\boldsymbol{h}^{(k)}u_n]\}},\tag{2.11}$$

and

Step 2:

$$\Sigma^{(k+1)}=R_{yy}-\boldsymbol{h}^{(k+1)}(\boldsymbol{h}^{(k+1)})^H.\tag{2.12}$$

Here

$$R_{yy}=\frac{1}{N+N_T}\Big[\sum_{t=1}^{N}\boldsymbol{y}(t)\boldsymbol{y}(t)^H+\sum_{\tau=1}^{N_T}\boldsymbol{y}_T(\tau)\boldsymbol{y}_T(\tau)^H\Big]\tag{2.13}$$

is the sample correlation matrix of the observed data and "*" denotes complex conjugation. Note that the terms in the summation over t in (2.10) can be computed in parallel. To ensure that the estimates of the spatial noise covariance matrix in (2.12) are positive definite with probability one, the following condition should be satisfied:

$$N+N_T\geq n_R+1,\tag{2.14}$$

see also the discussion in Appendix 2.A. Expression (2.11) can be further simplified by canceling out terms in the numerator and denominator:

$$\rho_m^{(k)}(t)=\frac{\exp[2\,\mathrm{Re}\{\boldsymbol{y}(t)^H(\Sigma^{(k)})^{-1}\boldsymbol{h}^{(k)}u_m\}]}{\sum_{n=1}^{M}\exp[2\,\mathrm{Re}\{\boldsymbol{y}(t)^H(\Sigma^{(k)})^{-1}\boldsymbol{h}^{(k)}u_n\}]},\tag{2.15}$$

where we have used the constant-modulus property of the transmitted symbols. In the $(k+1)$st iteration, Step 1 requires computing $(\Sigma^{(k)})^{-1}$, which can be done using the matrix inversion

lemma in e.g., [42, Cor. 18.2.10]:

$$(\Sigma^{(k)})^{-1} = R_{yy}^{-1} + \frac{R_{yy}^{-1}\boldsymbol{h}^{(k)}(\boldsymbol{h}^{(k)})^H R_{yy}^{-1}}{1-(\boldsymbol{h}^{(k)})^H R_{yy}^{-1}\boldsymbol{h}^{(k)}}, \tag{2.16}$$

where R_{yy}^{-1} needs to be evaluated only once, before the iteration starts. Then, $(\Sigma^{(k)})^{-1}\boldsymbol{h}^{(k)}$ simplifies to:

$$(\Sigma^{(k)})^{-1}\boldsymbol{h}^{(k)} = \frac{R_{yy}^{-1}\boldsymbol{h}^{(k)}}{1-(\boldsymbol{h}^{(k)})^H R_{yy}^{-1}\boldsymbol{h}^{(k)}}. \tag{2.17}$$

In the following, we discuss phase correction of the EM channel estimates.

2.3.1 Phase Correction

We describe a method for correcting the phases of the channel estimates in the EM iteration. Observe that the first product term in (2.9) is due to the unknown symbols, whereas the second term

$$\prod_{\tau=1}^{N_T} f(\boldsymbol{y}_T(\tau)|u_T(\tau),\boldsymbol{h},\Sigma) \tag{2.18}$$

is due to the training symbols, and is equal to the likelihood function for the case where *only* the training data are available. For i.i.d. symbols considered here [see (2.4)], the first term in (2.9) has M equal maxima (due to the phase ambiguity), which could cause the above EM iteration to converge to a local maximum of the likelihood function. We correct the phase of the EM channel estimates $\boldsymbol{h}^{(k)}$ to ensure that (2.18) is maximized. For example, for a QPSK constellation, we find which of the following four vectors: $\boldsymbol{h}^{(k)}$, $\boldsymbol{h}^{(k)}\exp(j\pi/2)$, $\boldsymbol{h}^{(k)}\exp(-j\pi/2)$, and $\boldsymbol{h}^{(k)}\exp(j\pi)$ maximizes the training-data likelihood function in (2.18) and update $\boldsymbol{h}^{(k)}$ accordingly. This test is computationally very efficient and may not need to be performed at every step of the EM iteration.

2.4 Cramér-Rao Bounds

We derive the CRB matrix for the unknown parameters under the measurement model in Section 2.2. First, define the vector of the unknown channel and noise parameters $\boldsymbol{\zeta} = [\boldsymbol{\eta}^T, \boldsymbol{\psi}^T]^T$, where $\boldsymbol{\eta} = [\mathrm{Re}(\boldsymbol{h})^T, \mathrm{Im}(\boldsymbol{h})^T]^T$ and $\boldsymbol{\psi} = [\mathrm{Re}\{\mathrm{vech}(\Sigma)\}^T, \mathrm{Im}\{\underline{\mathrm{vech}}(\Sigma)\}^T]^T$. (The

vech and vech operators create a single column vector by stacking elements below the main diagonal columnwise; vech includes the main diagonal, whereas vech omits it.) Define also the vector of the observed data

$$\boldsymbol{\upsilon} = [\boldsymbol{y}(1)^T, \boldsymbol{y}(2)^T, \ldots, \boldsymbol{y}(N)^T, \boldsymbol{y}_T(1)^T, \boldsymbol{y}_T(2)^T, \ldots, \boldsymbol{y}_T(N_T)^T]^T \tag{2.19}$$

and the vector of the unobserved data

$$\boldsymbol{u} = [u(1), u(2), \ldots, u(N)]^T. \tag{2.20}$$

Then, the CRB matrix for the unknown parameters $\boldsymbol{\zeta}$ is computed as (see [66, Ch. 3.8.1]):

$$\mathrm{CRB}(\boldsymbol{\zeta}) = \left\{ \mathrm{E}_{\upsilon}[\boldsymbol{s}(\boldsymbol{\upsilon};\boldsymbol{\zeta})\boldsymbol{s}(\boldsymbol{\upsilon};\boldsymbol{\zeta})^T] \right\}^{-1}, \tag{2.21}$$

where the expectation is performed with respect to the distribution of $\boldsymbol{\upsilon}$ and $\boldsymbol{s}(\boldsymbol{\upsilon};\boldsymbol{\zeta})$ is the observed-data score vector. The observed-data score vector can be computed as (see [66, eq. (3.42)]):

$$\boldsymbol{s}(\boldsymbol{\upsilon};\boldsymbol{\zeta}) = \mathrm{E}_{\mathrm{u}|\boldsymbol{\upsilon}}[\boldsymbol{s}_{\mathrm{c}}(\boldsymbol{\upsilon},\boldsymbol{u};\boldsymbol{\zeta})|\boldsymbol{\upsilon}], \tag{2.22}$$

where $\boldsymbol{s}_{\mathrm{c}}(\boldsymbol{\upsilon},\boldsymbol{u};\boldsymbol{\zeta})$ is the complete-data score vector, obtained by differentiating the complete-data log-likelihood function [i.e. the logarithm of (2.8)] with respect to $\boldsymbol{\zeta}$. Computing the expectations in (2.21) and (2.22) is discussed in Appendix 2.B, where the expression for $\boldsymbol{s}_{\mathrm{c}}(\boldsymbol{\upsilon},\boldsymbol{u};\boldsymbol{\zeta})$ is also given.

2.5 Detection

We now utilize the channel and noise estimators proposed in Section 2.3 to detect the unknown transmitted symbols $u(t)$. We apply the (estimated) maximum *a posteriori* (MAP) detector:

$$\widehat{u}(t) = \arg\max_{u(t)\in\mathcal{U}} \frac{\exp\{-[\boldsymbol{y}(t) - \widehat{\boldsymbol{h}}u(t)]^H \widehat{\Sigma}^{-1}[\boldsymbol{y}(t) - \widehat{\boldsymbol{h}}u(t)]\}}{\sum_{n=1}^{M} \exp\{-[\boldsymbol{y}(t) - \widehat{\boldsymbol{h}}u_n]^H \widehat{\Sigma}^{-1}[\boldsymbol{y}(t) - \widehat{\boldsymbol{h}}u_n]\}} \tag{2.23}$$

$$= \arg\min_{u(t)\in\mathcal{U}} [\boldsymbol{y}(t) - \widehat{\boldsymbol{h}}u(t)]^H \widehat{\Sigma}^{-1}[\boldsymbol{y}(t) - \widehat{\boldsymbol{h}}u(t)] \tag{2.24}$$

$$= \arg\max_{u(t)\in\mathcal{U}} \mathrm{Re}\{\boldsymbol{y}(t)^H R_{yy}^{-1}\widehat{\boldsymbol{h}} \cdot u(t)\}, \tag{2.25}$$

where $\widehat{\boldsymbol{h}} = \boldsymbol{h}^{(\infty)}$ and $\widehat{\Sigma} = \Sigma^{(\infty)}$ are the ML estimates obtained from the EM iteration (2.10)–(2.12) upon convergence. To derive (2.25), we have used the identity (2.17) and the constant-modulus property of the transmitted symbols. Interestingly, the detector in (2.25) is a function of the channel estimate $\widehat{\boldsymbol{h}}$ *only*, through the $R_{yy}^{-1}\widehat{\boldsymbol{h}}$ term. Note that the above detection problem is equivalent to finding $m \in \{1, 2, \ldots, M\}$ that maximizes $\rho_m^{(\infty)}(t)$ in (2.15) [see also (2.11)]. The detector (2.24) and EM algorithm (2.10)–(2.12) can be easily modified to account for unequal prior probabilities of the transmitted symbols.

2.6 Simulation Results

We evaluate the performance of the proposed estimation and detection algorithms using numerical simulations. We consider an array of $n_R = 5$ receiver antennas. Our performance metrics are the mean-square error (MSE) and symbol error rate (SER), averaged over 5000 random channel realizations generated using an i.i.d. Rayleigh fading model with unit-variance channel coefficients. The transmitted symbols were generated from an uncoded QPSK modulated constellation (i.e. $M = 4$) with normalized energy. We added a three-symbol training sequence ($N_T = 3$), which was utilized to obtain the initial channel estimate $\boldsymbol{h}^{(0)}$, computed using least squares. The initial estimate of the noise covariance matrix was chosen as $\Sigma^{(0)} = R_{yy}$. The signal was corrupted by additive complex Gaussian noise with spatial noise covariance matrix Σ whose (p, q)th element is

$$\Sigma_{p,q} = \sigma^2 \cdot 0.9^{|p-q|} \cdot \exp[j(\pi/2)(p-q)], \tag{2.26}$$

which is the noise covariance model used in [109] (see also references therein). The bit signal-to-noise ratio (SNR) per receiver antenna was defined as

$$\text{SNR} = 10\log_{10}\left[\frac{1}{\sigma^2 \cdot \log_2(M)}\right] = 10\log_{10}\left(\frac{1}{2\sigma^2}\right) \quad \text{(dB)}. \tag{2.27}$$

In the cases where the EM algorithm did not converge within 40 iterations, it was restarted using a randomly selected initial value for the channel coefficients[2]. [We implemented the same

[2]Note that fast convergence of the EM algorithm or utilizing the above restart method do not guarantee convergence to the global maximum of the observed-data likelihood function. Hence, our simulation results

restart procedure in all algorithms whose performance is analyzed in this section.] We also applied the phase correction technique in Section 2.3.1 at every step of the EM iteration.

In the first set of simulations, the bit SNR was set to -1 dB. In Figs. 2.1 and 2.2, we show the average MSEs (and corresponding average CRBs) for the ML estimates of the channel coefficients[3] and selected elements of the spatial noise covariance matrix Σ (obtained using the proposed EM algorithm) as functions of the block length N. Fig. 2.1 also compares the MSE performance of the proposed EM algorithm with

- the decoupled weighted iterative least squares with projection (DW-ILSP) method in [84] and
- an EM algorithm that assumes spatially white noise.

For completeness, we summarize below our implementation of DW-ILSP method:

1. Given an initial estimate of $\boldsymbol{h} = \boldsymbol{h}^{(0)}$, $k = 0$.
2. At $k = k + 1$ iteration, for $t = 1, \ldots, N$,
   (a) Weighted least-square estimate of transmitted symbols:
   $$\hat{u}(t) = \frac{(\boldsymbol{h}^{(k)})^H R_{yy}^{-1} \boldsymbol{y}(t)}{(\boldsymbol{h}^{(k)})^H R_{yy} \boldsymbol{h}^{(k)}}. \tag{2.28}$$
   (b) Project onto nearest constellation point:
   $$\hat{u}(t) = \text{proj}[\hat{u}(t)]. \tag{2.29}$$
   (c) least-square estimate of channel:
   $$\boldsymbol{h}^{(k+1)} = \frac{1}{N} \sum_{t=1}^{N} R_{yy}^{-(1/2)} \boldsymbol{y}(t) \hat{u}(t)^*. \tag{2.30}$$
3. Repeat step 2) until converagence.

This method is initialized with the least-square estimate using the pilot codewords

$$\boldsymbol{h}^{(k+1)} = \frac{1}{N_T} \sum_{\tau=1}^{N_T} R_{yy}^{-(1/2)} \boldsymbol{y}_T(\tau) \hat{u}_T(\tau)^*. \tag{2.31}$$

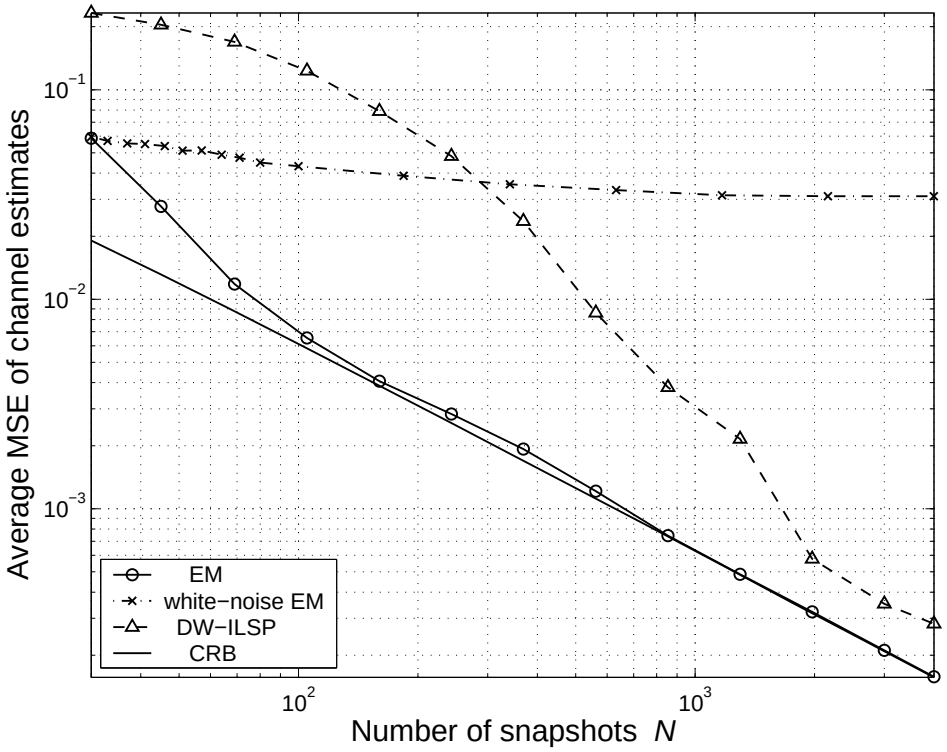

Figure 2.1 Average mean-square errors and corresponding Cramér-Rao bounds for the channel estimates obtained using the proposed EM algorithm, DW-ILSP method, and an EM algorithm for spatially white noise, as functions of N for $N_T = 3$ and SNR $= -1$ dB.

For low SNR (-1 dB), few training symbols ($N_T = 3$) and short block lengths, the proposed EM algorithm clearly outperforms the DW-ILSP method. In this scenario, the proposed method attains the CRB for $N = 100$ symbols, compared with more than 4000 symbols needed for the DW-ILSP method. [Note also that in fading channels the block length N is limited by the coherence time of the channel.] The average numbers of iterations needed for the EM, white-noise EM, and DW-ILSP algorithms to converge were $9, 9$, and 6, respectively. For $N = 100$, restart was needed in less than 0.1% of the total number of trials. A single EM iteration has higher computational complexity than a DW-ILSP iteration for the same N, and the complexity of both iterations increases linearly with N. However, the proposed EM algorithm

represent upper bounds on the performance achievable by the exact ML method.

[3]Here, averaging is performed over *both* the channel coefficients for different antennas (i.e. elements of $\widehat{\boldsymbol{h}}$) and random channel and training-data realizations.

typically needs a smaller N to attain the same MSE. To demonstrate the importance of incorporating the spatial color of the noise in channel estimation, we also show the performance of an EM algorithm that assumes spatially white noise in the scenario where the noise is *colored* [with covariance (2.26)]. The EM algorithm for spatially white noise follows from (2.10)–(2.12) by substituting $\Sigma^{(k)} = (\widehat{\sigma}^2)^{(k)} I_{n_R}$ into Step 1 in (2.10) and applying the following Step 2: $(\widehat{\sigma}^2)^{(k+1)} = \mathrm{tr}(\Sigma^{(k+1)})/n_R$, where $\Sigma^{(k+1)}$ was defined in (2.12), and I_{n_R} denotes the identity matrix of size n_R. For low SNR (-1 dB) and few training symbols ($N_T = 3$), the white-noise EM algorithm breaks down.

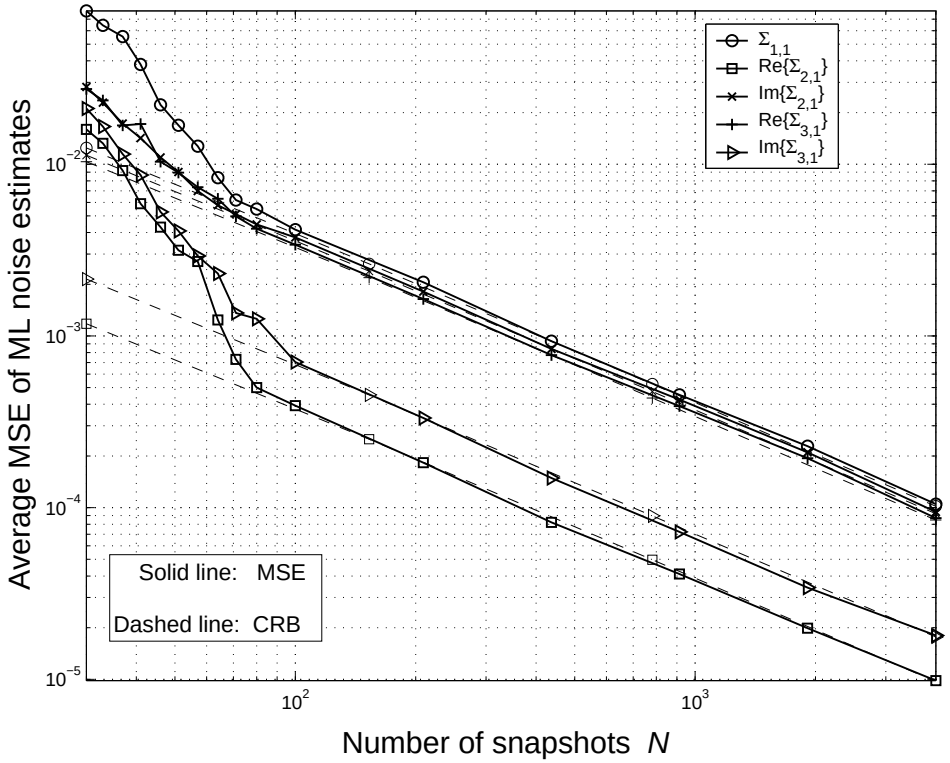

Figure 2.2 Average mean-square errors and corresponding Cramér-Rao bound for the ML estimates of $\Sigma_{1,1}$, $\mathrm{Re}\{\Sigma_{2,1}\}$, $\mathrm{Im}\{\Sigma_{2,1}\}$, $\mathrm{Re}\{\Sigma_{3,1}\}$, $\mathrm{Im}\{\Sigma_{3,1}\}$ obtained using the proposed EM algorithm, as functions of N for $N_T = 3$ and SNR $= -1$ dB.

In Fig. 2.2, we show the average MSEs for the ML estimates of $\Sigma_{1,1}$, $\mathrm{Re}\{\Sigma_{2,1}\}$, $\mathrm{Im}\{\Sigma_{2,1}\}$, $\mathrm{Re}\{\Sigma_{3,1}\}$, and $\mathrm{Im}\{\Sigma_{3,1}\}$ (obtained using the proposed EM algorithm) and the corresponding

CRBs as functions of N.

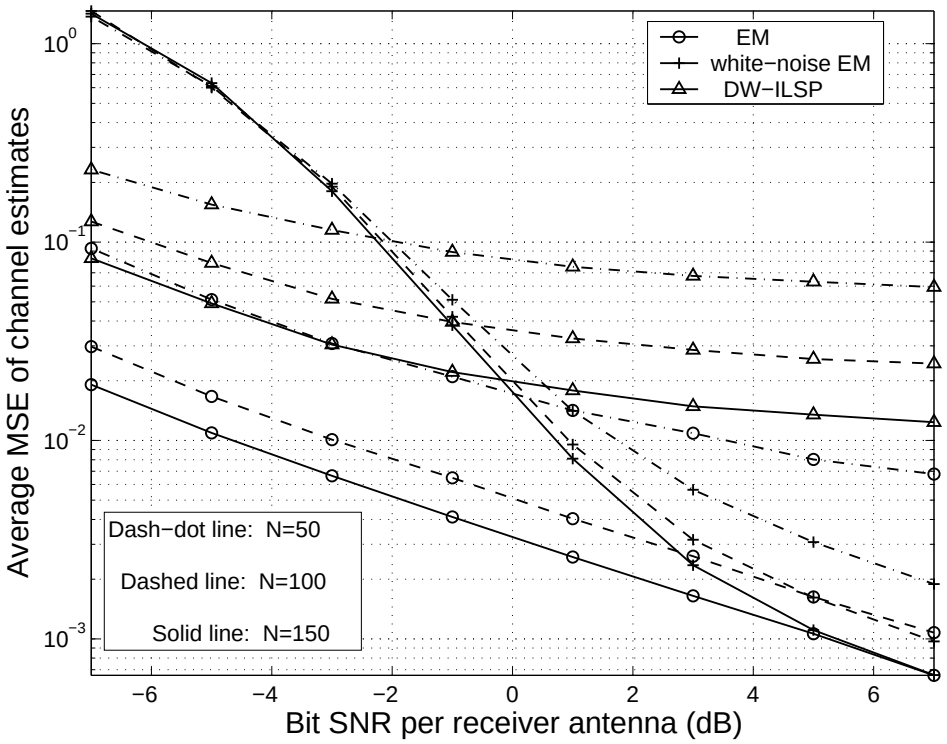

Figure 2.3 Average mean-square errors for the channel estimates obtained using the proposed EM algorithm, DW-ILSP method, and EM algorithm for spatially white noise, as functions of the bit SNR per receiver antenna for block lengths $N = 50, 100$, and 150.

In Fig. 2.3, the average MSEs for the channel estimates obtained by the proposed EM algorithm for spatially correlated noise, DW-ILSP method, and EM algorithm for spatially white noise are shown as functions of the bit SNR per receiver antenna for block lengths $N = 50, 100$, and 150. When the average MSE is 0.03 and $N = 100$, the EM algorithm has an advantage of about 9 dB over the DW-ILSP algorithm; this advantage further grows as N decreases. An intuitive explanation for this performance improvement is that the EM algorithm exploits additional information provided by the prior distribution of the unknown symbols in (2.4). Note also that the number of parameters in the random-symbol measurement model in Section 2.2 equals $n_R^2 + 2n_R$, and, therefore, is independent of N. This is in contrast with the DW-ILSP and other deterministic ML methods (e.g. [93], see also [24]) where the number of parameters grows with N. For low SNRs, the white-noise EM algorithm performs poorly,

see also Fig. 2.1. However, for high SNRs and small block lengths, it outperforms the EM algorithm for spatially correlated noise. Hence, in this scenario, the fact that the white-noise EM algorithm estimates a small number of parameters $(2n_R + 1)$ becomes more important than accounting for spatial noise covariance (which, in addition, is poorly estimated due to the small block length).

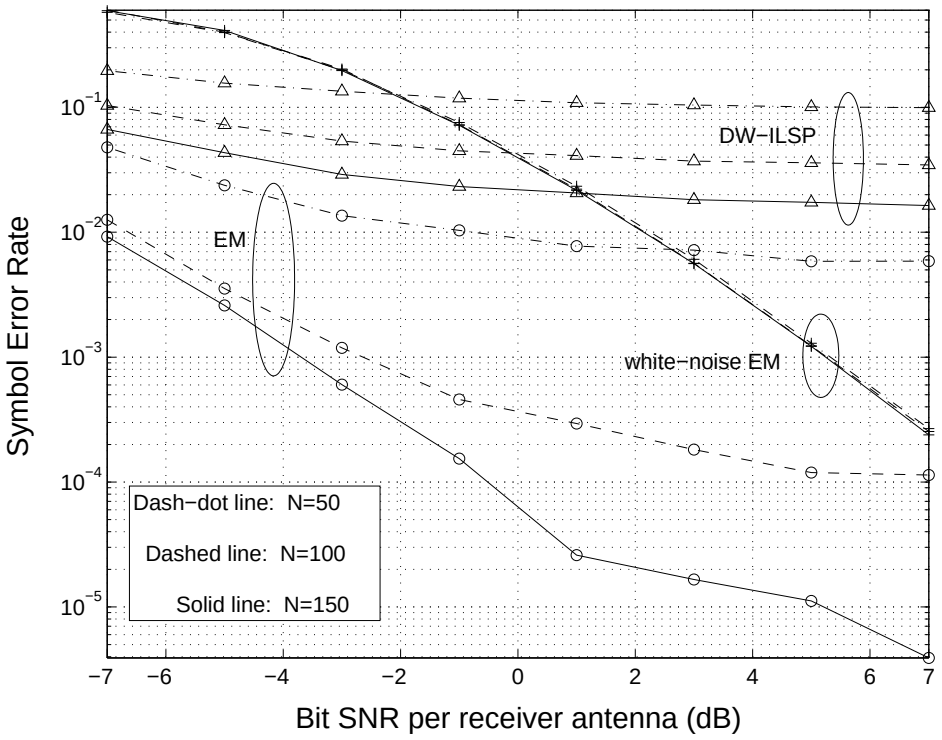

Figure 2.4 Symbol error rates of the EM-based and DW-ILSP detectors, as functions of the bit SNR per receiver antenna for block lengths $N = 50, 100$, and 150.

In Fig. 2.4, we compare symbol error rates of the detector (2.25) which uses the ML estimates of $\boldsymbol{h}$ and Σ [obtained from the EM iteration (2.10)–(2.12)] with

- the DW-ILSP detector in [84] and
- a white-noise detector

$$\arg \max_{u(t)\in\mathcal{U}} \mathrm{Re}\{\boldsymbol{y}(t)^H \widehat{\boldsymbol{h}}_{\text{white EM}} \cdot u(t)\}, \tag{2.32}$$

where $\widehat{\boldsymbol{h}}_{\text{white EM}}$ is computed using the EM algorithm for spatially white noise.

The symbol error rates are shown as functions of the bit SNR per receiver antenna for block lengths $N = 50, 100$, and 150. For the given range of SNRs and block lengths, the proposed detector significantly outperforms the DW-ILSP detector. As expected, the white-noise detector performs poorly for low SNRs due to poor channel estimates provided by the white-noise EM algorithm. Similarly, for high SNRs and small block lengths it outperforms the detector in (2.25) due to the fact that the white-noise EM algorithm outperforms the EM algorithm for spatially correlated noise in this scenario. The performance of the detector (2.25) improves significantly as the block length increases due to the improved channel estimation. In contrast, the performance of the white-noise detector is insensitive to the choice of the block length (for the block lengths considered in Fig. 2.4), which can be explained by the fact that the white-noise EM algorithm estimates a small number of parameters (and thus requires a relatively small data size).

2.7 Summary

We developed an expectation-maximization algorithm for semi-blind estimation of single-input multi-output fading channels in spatially correlated noise having unknown covariance. We also derived a method for phase correction of the EM channel estimates and computed the Cramér-Rao bounds for the unknown parameters. The proposed channel and noise estimators were incorporated into the receiver design. We presented numerical simulations that demonstrated the performance of the proposed methods, and compared them with the existing techniques.

In next chapter, we will extend the proposed methods to the multi-input multi-output (MIMO) systems with coded transmission. For coded transmission, an iterative receiver structure will be employed as explained in Chapter 1, where iterations between channel estimator and error control decoder will further improve the channel estimation accuracy.

2.8 Appendix 2.A EM Algorithm Derivation

We relax the constant-modulus assumption (2.3) and first derive the EM algorithm for the general case where the symbols $u(t)$, $t = 1, 2, \ldots, N$, $u_T(\tau)$, $\tau = 1, 2, \ldots, N_T$ belong to an arbitrary constellation. This algorithm is then simplified to the constant-modulus scenario in Sections 2.2 and 2.3.

By taking the logarithm of (2.8) and neglecting terms that do not depend on the parameters $\boldsymbol{h}$ and Σ, we obtain the complete-data log-likelihood function

$$\begin{aligned}\mathcal{L}(\boldsymbol{h}, \Sigma) \;=\; &-(N+N_T)\cdot\big\{\ln|\Sigma| \\ &+\mathrm{tr}[\Sigma^{-1}\cdot(R_{yy}-\boldsymbol{r}_{y\mathrm{u}}\boldsymbol{h}^H-\boldsymbol{h}\boldsymbol{r}_{y\mathrm{u}}^H+r_{\mathrm{uu}}\boldsymbol{h}\boldsymbol{h}^H)]\big\},\end{aligned} \tag{2.33}$$

where $|\cdot|$ denotes the determinant and

$$R_{yy} \;=\; \frac{1}{N+N_T}\Big[\sum_{t=1}^{N}\boldsymbol{y}(t)\boldsymbol{y}(t)^H+\sum_{\tau=1}^{N_T}\boldsymbol{y}_T(\tau)\boldsymbol{y}_T(\tau)^H\Big], \tag{2.34}$$

$$\boldsymbol{r}_{y\mathrm{u}} \;=\; \frac{1}{N+N_T}\Big[\sum_{t=1}^{N}\boldsymbol{y}(t)u(t)^*+\sum_{\tau=1}^{N_T}\boldsymbol{y}_T(\tau)u_T(\tau)^*\Big], \tag{2.35}$$

$$r_{\mathrm{uu}} \;=\; \frac{1}{N+N_T}\big[\sum_{t=1}^{N}|u(t)|^2+\sum_{\tau=1}^{N_T}|u_T(\tau)|^2\big] \tag{2.36}$$

are the *natural complete-data sufficient statistics* for estimating $\boldsymbol{h}$ and Σ, see e.g. [8]. At the kth iteration, the E step computes the conditional expectation of the complete-data log-likelihood given the observed data $\boldsymbol{\upsilon}$ [see (2.19)] at the current parameter estimates $\boldsymbol{h}^{(k)}$ and $\Sigma^{(k)}$:

$$\begin{aligned}Q(\boldsymbol{h}, \Sigma; \boldsymbol{h}^{(k)}, \Sigma^{(k)}) = &-(N+N_T)\cdot\big\{\ln|\Sigma| \\ &+\mathrm{tr}[\Sigma^{-1}\cdot(R_{yy}-\boldsymbol{r}_{y\mathrm{u}}^{(k)}\boldsymbol{h}^H-\boldsymbol{h}(\boldsymbol{r}_{y\mathrm{u}}^{(k)})^H+r_{\mathrm{uu}}^{(k)}\boldsymbol{h}\boldsymbol{h}^H)]\big\},\end{aligned} \tag{2.37}$$

where $\boldsymbol{r}_{y\mathrm{u}}^{(k)} = \mathrm{E}_{\mathrm{u}|\boldsymbol{\upsilon}}[\boldsymbol{r}_{y\mathrm{u}}|\boldsymbol{\upsilon}; \boldsymbol{h}^{(k)}, \Sigma^{(k)}]$ and $r_{\mathrm{uu}}^{(k)} = \mathrm{E}_{\mathrm{u}|\boldsymbol{\upsilon}}[r_{\mathrm{uu}}|\boldsymbol{\upsilon}; \boldsymbol{h}^{(k)}, \Sigma^{(k)}]$. The above expression is obtained from (2.33) by replacing $\boldsymbol{r}_{y\mathrm{u}}$ and r_{uu} with their conditional expectations $\boldsymbol{r}_{y\mathrm{u}}^{(k)}$ and $r_{\mathrm{uu}}^{(k)}$. The M step maximizes the above Q function with respect to $\boldsymbol{h}$ and Σ to produce

$$\boldsymbol{h}^{(k+1)}, \Sigma^{(k+1)} = \arg\max_{\boldsymbol{h},\Sigma} Q(\boldsymbol{h}, \Sigma; \boldsymbol{h}^{(k)}, \Sigma^{(k)}). \tag{2.38}$$

The maximization of $\mathcal{L}(\boldsymbol{h}, \Sigma)$ in (2.33) with respect to $\boldsymbol{h}$ and Σ has well-known solutions given by $\boldsymbol{r}_{yu}/r_{uu}$ and $R_{yy} - \boldsymbol{r}_{yu}\boldsymbol{r}_{yu}^H/r_{uu}$ (respectively), provided that $R_{yy} - \boldsymbol{r}_{yu}\boldsymbol{r}_{yu}^H/r_{uu}$ is a positive definite matrix, see e.g. [26] and [74, Th. 10.1.1]. (These expressions follow from the multivariate analysis of variance (MANOVA) model in multivariate statistical analysis, see [26] and [74].) Hence, the M step is obtained by replacing $\boldsymbol{r}_{yu}$ and r_{uu} in $\boldsymbol{r}_{yu}/r_{uu}$ and $R_{yy} - \boldsymbol{r}_{yu}\boldsymbol{r}_{yu}^H/r_{uu}$ with their conditional expectations and the EM iteration follows:

Step 1:

$$\boldsymbol{h}^{(k+1)} = \frac{1}{N+N_T}\Big\{\sum_{t=1}^{N}\Big[\boldsymbol{y}(t)\sum_{m=1}^{M}u_m^*\cdot\rho_m^{(k)}(t)\Big] + \sum_{\tau=1}^{N_T}\boldsymbol{y}_T(\tau)u_T(\tau)^*\Big\}\Big/ r_{uu}^{(k)}, \tag{2.39}$$

where

$$r_{uu}^{(k)} = \frac{1}{N+N_T}\Big\{\sum_{t=1}^{N}\sum_{m=1}^{M}[|u_m|^2\cdot\rho_m^{(k)}(t)] + \sum_{\tau=1}^{N_T}|u_T(\tau)|^2\Big\}. \tag{2.39}$$

Step 2:

$$\Sigma^{(k+1)} = R_{yy} - r_{uu}^{(k)}\cdot\boldsymbol{h}^{(k+1)}(\boldsymbol{h}^{(k+1)})^H, \tag{2.40}$$

where $\rho_m^{(k)}(t)$ is computed using (2.11). Note that (2.39) and (2.40) each incorporate both E and M steps. The condition (2.14) is needed to ensure that $\Sigma^{(k+1)}$ is a positive definite matrix with probability one, which follows using arguments similar to those in [74, Th. 3.1.4], see also [26, eq. (4)] and [74, Th. 10.1.1].

In the constant-modulus scenario (2.3), we have that $r_{uu}^{(k)} \equiv 1$ for all k. Hence, setting $r_{uu}^{(k)} = 1$ in (2.39) and (2.40) yields the EM iteration (2.10)–(2.12).

2.9 Appendix 2.B Cramér-Rao Bound

We present the expression for the complete-data score vector $\boldsymbol{s}_{\mathrm{c}}(\boldsymbol{\upsilon}, \boldsymbol{u}; \boldsymbol{\zeta})$ under the measurement model (2.1)–(2.4) and discuss evaluating the expectations in (2.21) and (2.22), needed for computing the CRB matrix. The complete-data score vector $\boldsymbol{s}_{\mathrm{c}}(\boldsymbol{\upsilon}, \boldsymbol{u}; \boldsymbol{\zeta})$ for this measurement model is obtained by differentiating the complete-data log-likelihood function (2.33) with respect to $\boldsymbol{\zeta}$ (see [56, App. 15C]) and setting $r_{\mathrm{uu}} = 1$:

$$\begin{aligned}
&\boldsymbol{s}_{\mathrm{c}}(\boldsymbol{\upsilon}, \boldsymbol{u}; \boldsymbol{\zeta}) \\
&= [\mathrm{Re}\{\boldsymbol{s}_{\mathrm{c},h}(\boldsymbol{\upsilon}, \boldsymbol{u}; \boldsymbol{\zeta})\}^T, \mathrm{Im}\{\boldsymbol{s}_{\mathrm{c},h}(\boldsymbol{\upsilon}, \boldsymbol{u}; \boldsymbol{\zeta})\}^T, \boldsymbol{s}_{\mathrm{c},\psi}(\boldsymbol{\upsilon}, \boldsymbol{u}; \boldsymbol{\zeta})^T]^T,
\end{aligned} \tag{2.41}$$

where $\boldsymbol{s}_{\mathrm{c},h}(\boldsymbol{\upsilon}, \boldsymbol{u}; \boldsymbol{\zeta})$ and $\boldsymbol{s}_{\mathrm{c},\psi}(\boldsymbol{\upsilon}, \boldsymbol{u}; \boldsymbol{\zeta})$ are given in (2.42) and (2.43), respectively.

$$\begin{aligned}
\boldsymbol{s}_{\mathrm{c},h}(\boldsymbol{\upsilon}, \boldsymbol{u}; \boldsymbol{\zeta}) &= 2 \cdot \Sigma^{-1} \cdot \Big\{ \sum_{t=1}^{N} [\boldsymbol{y}(t) u(t)^* - \boldsymbol{h}] + \sum_{\tau=1}^{N_T} [\boldsymbol{y}_T(\tau) u_T(\tau)^* - \boldsymbol{h}] \Big\} \\
&= 2 \cdot (N + N_T) \cdot \Sigma^{-1} \cdot (\boldsymbol{r}_{yu} - \boldsymbol{h}),
\end{aligned} \tag{2.42}$$

$$\begin{aligned}
[\boldsymbol{s}_{\mathrm{c},\psi}(\boldsymbol{\upsilon}, \boldsymbol{u}; \boldsymbol{\zeta})]_i = &- (N + N_T) \cdot \mathrm{tr}\left(\Sigma^{-1} \frac{\partial \Sigma}{\partial \psi_i} \right) + (N + N_T) \cdot \boldsymbol{h}^H \Sigma^{-1} \frac{\partial \Sigma}{\partial \psi_i} \Sigma^{-1} \boldsymbol{h} \\
&+ \sum_{t=1}^{N} \boldsymbol{y}(t)^H \Sigma^{-1} \frac{\partial \Sigma}{\partial \psi_i} \Sigma^{-1} \boldsymbol{y}(t) + \sum_{\tau=1}^{N_T} \boldsymbol{y}_T(\tau)^H \Sigma^{-1} \frac{\partial \Sigma}{\partial \psi_i} \Sigma^{-1} \boldsymbol{y}_T(\tau) \\
&- \boldsymbol{h}^H \Sigma^{-1} \frac{\partial \Sigma}{\partial \psi_i} \Sigma^{-1} \cdot \sum_{t=1}^{N} [\boldsymbol{y}(t) u(t)^*] - \sum_{t=1}^{N} [\boldsymbol{y}(t)^H u(t)] \cdot \Sigma^{-1} \frac{\partial \Sigma}{\partial \psi_i} \Sigma^{-1} \boldsymbol{h} \\
&- \boldsymbol{h}^H \Sigma^{-1} \frac{\partial \Sigma}{\partial \psi_i} \Sigma^{-1} \cdot \sum_{\tau=1}^{N_T} [\boldsymbol{y}_T(\tau) u_T(\tau)^*] - \sum_{\tau=1}^{N_T} [\boldsymbol{y}_T(\tau)^H u_T(\tau)] \cdot \Sigma^{-1} \frac{\partial \Sigma}{\partial \psi_i} \Sigma^{-1} \boldsymbol{h} \\
= &(N + N_T) \cdot \Big\{ - \mathrm{tr}\left(\Sigma^{-1} \frac{\partial \Sigma}{\partial \psi_i} \right) + \mathrm{tr}\left(\Sigma^{-1} \boldsymbol{h} \boldsymbol{h}^H \Sigma^{-1} \frac{\partial \Sigma}{\partial \psi_i} \right) + \mathrm{tr}\left(\Sigma^{-1} R_{yy} \Sigma^{-1} \frac{\partial \Sigma}{\partial \psi_i} \right) \\
&- \mathrm{tr}\left[(\Sigma^{-1} \boldsymbol{r}_{yu} \boldsymbol{h}^H \Sigma^{-1} + \Sigma^{-1} \boldsymbol{h} \boldsymbol{r}_{yu}^H \Sigma^{-1}) \cdot \frac{\partial \Sigma}{\partial \psi_i} \right] \Big\}, \quad i = 1, 2, \ldots, n_R^2.
\end{aligned} \tag{2.43}$$

To compute (2.43), the following identities can be utilized:

$$\mathrm{tr}\left(A \cdot \frac{\partial \Sigma}{\partial \Sigma_{p,p}} \right) = A_{p,p}, \quad p = 1, 2, \ldots, n_R, \tag{2.45}$$

and

$$\mathrm{tr}\left(A \cdot \frac{\partial \Sigma}{\partial \,\mathrm{Re}\{\Sigma\}_{p,q}}\right) = 2\,\mathrm{Re}\{A_{p,q}\}, \tag{2.45}$$

$$\mathrm{tr}\left(A \cdot \frac{\partial \Sigma}{\partial \,\mathrm{Im}\{\Sigma\}_{p,q}}\right) = 2\,\mathrm{Im}\{A_{p,q}\}, \quad 1 \le q < p \le n_R, \tag{2.46}$$

where A is an arbitrary $n_R \times n_R$ Hermitian matrix. It follows from (2.42) and (2.43) that computing the observed-data score vector $\boldsymbol{s}(\boldsymbol{\upsilon};\boldsymbol{\zeta})$ in (2.22) reduces to replacing $\boldsymbol{r}_{y\mathrm{u}}$ in (2.42) and (2.43) with its conditional expectation given $\boldsymbol{\upsilon}$:

$$\mathrm{E}_{\mathrm{u}|\boldsymbol{\upsilon}}[\boldsymbol{r}_{y\mathrm{u}}|\boldsymbol{\upsilon}] = \frac{1}{N+N_T}\Big\{\sum_{t=1}^{N}\Big[\boldsymbol{y}(t)\sum_{m=1}^{M} u_m^* \cdot \rho_m(t)\Big] \tag{2.47}$$

$$+\sum_{\tau=1}^{N_T}\boldsymbol{y}_T(\tau)u_T(\tau)^*\Big\}, \tag{2.48}$$

where

$$\rho_m(t) = \frac{\exp\{-[\boldsymbol{y}(t)-\boldsymbol{h}u_m]^H \Sigma^{-1}[\boldsymbol{y}(t)-\boldsymbol{h}u_m]\}}{\sum_{n=1}^{M}\exp\{-[\boldsymbol{y}(t)-\boldsymbol{h}u_n]^H \Sigma^{-1}[\boldsymbol{y}(t)-\boldsymbol{h}u_n]\}}. \tag{2.48}$$

Finally, the CRB matrix is computed using (2.21), which requires multidimensional integration to evaluate the expectation with respect to the distribution of $\boldsymbol{\upsilon}$; this can be performed using Monte Carlo integration, i.e. by averaging $\boldsymbol{s}(\boldsymbol{\upsilon};\boldsymbol{\zeta})\boldsymbol{s}(\boldsymbol{\upsilon};\boldsymbol{\zeta})^T$ over many realizations of $\boldsymbol{\upsilon}$.

CHAPTER 3. MAXIMUM LIKELIHOOD CHANNEL AND NOISE ESTIMATION FOR CODED MIMO SYSTEMS

3.1 Introduction

Multi-input multi-output (MIMO) fading channel estimation is a major challenge for multiple antenna systems because the detection of information symbols depends critically on the availability of full or partial channel state information. Recently, there has been an increasing interest in iterative channel estimation and data decoding [38, 7, 89], where data decision obtained from the decoding, either hard or soft, is used as additional information to refine the channel estimation. In [38] and [7], maximum likelihood (ML) and *maximum a posteriori* (MAP) methods are used to estimate the channel via expectation-maximization (EM) algorithms [22]. EM algorithms have also been applied for symbol detection, see [20] and [65]. Least-squares (LS) estimation together with hard and soft decision feedback is studied in [89]. All of these methods assume that the additive noise is both temporally and spatially white. Channel estimation for MIMO systems in spatially correlated noise has been studied in [25] and [63], where deterministic ML and simple non-iterative data decoding methods were proposed.

In this chapter, we propose an iterative channel estimation (via EM algorithm) and decoding scheme for spatially correlated noise with unknown covariance matrix. Instead of MAP estimation in [7] which requires knowledge of second-order statistical properties of the channel at the receiver, we estimate both the channel and the spatial noise covariance without prior knowledge of the channel statistical properties. This work generalizes our results for single-input multi-output (SIMO) systems in Chapter 2 to the coded MIMO scenario. For comparison, we also develop an iterative receiver which alternates between deterministic ML channel estimation [63, 25, 12] with soft decision feedback and error-control decoding.

The system model is introduced in Section 3.2. In Section 3.3, we derive the EM algorithm for estimating the unknown channel and noise parameters. Section 3.4 discussed the design of the iterative space-time receiver. We discuss the initial values and Cramér-Rao bounds of the channel estimation in Section 3.5. Simulation results are presented in Section 3.6 and Section 3.7 concludes this chapter.

3.2 System Modeling

We consider a coded MIMO system having n_T transmit and n_R receive antennas in a frequency-flat block fading environment. We will use turbo code as an example of the error control code. Other codes, such as low-density parity-check (LDPC) codes, can also be used. The discrete-time transmitter model is shown in Fig. 3.1.

Figure 3.1 Discrete-time transmitter model

Suppose that a block of L space-time codewords $\boldsymbol{X}$ of size $n_T \times K$ each are transmitted. The lth received *space-time data matrix* $\boldsymbol{Y}_l$ can be modeled as

$$\boldsymbol{Y}_l = \boldsymbol{H} \cdot \boldsymbol{X}_l + \boldsymbol{E}_l, \quad l = 1, 2, \ldots, L, \tag{3.1}$$

where $\boldsymbol{H}$ is an unknown $n_R \times n_T$ channel response matrix; $\boldsymbol{X}_l$ is the lth transmitted space-time codeword; $\boldsymbol{E}_l = [\boldsymbol{e}_l(1) \cdots \boldsymbol{e}_l(K)]$ is the lth noise matrix, where $\boldsymbol{e}_l(k)$ is temporally white and circularly symmetric zero-mean complex Gaussian noise vector with unknown spatial covariance matrix $\boldsymbol{\Sigma}$. It models co-channel interference (CCI) and receiver noise. This is a standard model for a communication channel, subject to (unstructured) interference and jamming, see e.g., [23, 25, 63].

We assume that M-ary phase shift keying (PSK) modulation and space-time orthogonal design (cf [3, 101, 33]) are used. However, after minor modifications, the proposed method can also be applied to other modulation schemes and general space-time codes. In Appendix 2.A, we discuss similar modifications for the SIMO case; the extension to the MIMO case is straight-

forward, leading to algorithms with higher computational complexity compared with those presented herein. Without loss of generality, assume that each space-time codeword $\boldsymbol{X}_l$ is a linear function of K' transmitted symbols $\mathcal{S}_l = \{s_1^{(l)}, \ldots, s_{K'}^{(l)}\}$:

$$\boldsymbol{X}_l = \sum_{k=1}^{K'} \left(\mathrm{Re}\{s_k^{(l)}\} \boldsymbol{A}_k + j \cdot \mathrm{Im}\{s_k^{(l)}\} \boldsymbol{B}_k \right), \tag{3.2}$$

where $\mathrm{Re}\{\cdot\}$ and $\mathrm{Im}\{\cdot\}$ denote the real and imaginary parts, and $\boldsymbol{A}_k$ and $\boldsymbol{B}_k$ are fixed real-valued $n_T \times K$ "elementary" code matrices, satisfying the orthogonality conditions as follows[101, 33] :

$$\begin{aligned} \boldsymbol{A}_k \boldsymbol{A}_k^T = \boldsymbol{I}_{n_T}, \quad \boldsymbol{B}_k \boldsymbol{B}_k^T = \boldsymbol{I}_{n_T}, \quad \boldsymbol{A}_k \boldsymbol{B}_t^T = \boldsymbol{B}_t \boldsymbol{A}_k^T \\ \boldsymbol{A}_k \boldsymbol{A}_t^T = -\boldsymbol{A}_t \boldsymbol{A}_k^T, \quad \boldsymbol{B}_k \boldsymbol{B}_t^T = -\boldsymbol{B}_t \boldsymbol{B}_k^T, \quad k \neq t \end{aligned} \tag{3.3}$$

so that

$$\boldsymbol{X}_l \boldsymbol{X}_l^H = \sum_{k=1}^{K'} |s_k^{(l)}|^2 \cdot \boldsymbol{I}_{n_T} = K' \boldsymbol{I}_{n_T}, \tag{3.4}$$

where $(\cdot)^T$ and $(\cdot)^H$ denote the transpose and the conjugate transpose, respectively, and symbols $s_k^{(l)}$ from M-ary PSK constellation are assumed to have unit energy. The number of transmitted symbols K' represented by one space-time codeword is usually less than the codeword length K when $n_T > 2$, and is equal to K when $n_T = 2$.

To allow unique estimation of the channel $\boldsymbol{H}$ (i.e., to resolve the phase ambiguity associated with PSK modulation), we further assume that L_p known pilot space-time codewords $\boldsymbol{X}_{\mathrm{p},\ell}$, $\ell = 1, \ldots, L_\mathrm{p}$, are inserted at the beginning of the block, and denote the corresponding data matrices received by the array as $\boldsymbol{Y}_{\mathrm{p},\ell}$. Usually, L_p is a small number (say 2) and the pilot symbols alone do not provide good channel estimation. We adopt the block fading assumption implying that the channel $\boldsymbol{H}$ and noise covariance matrix $\boldsymbol{\Sigma}$ remain constant within each *block* of $(L + L_\mathrm{p})$ codewords, i.e., $K(L + L_\mathrm{p})$ time intervals, and change from one block to another independently.

Since turbo codes need long *frame length* to achieve good error performance, and the length of one block is limited by the coherent time of the fading channel, the turbo encoder implements coding *across* R blocks. Therefore, one turbo code frame is composed of $R(L + L_\mathrm{p})$ space-time

codewords. At the receiver, the turbo decoder needs the estimates of the channels and the noise covariance matrices for all R blocks. A channel interleaver is used to spread the effect of imperfect channel estimates across the whole R blocks.

3.3 EM Algorithm for Channel Estimation

In this section, we derive an EM-based channel and noise covariance estimator from one block. The proposed method incorporates extrinsic information about the transmitted symbols from the turbo decoder through prior symbol probabilities. The estimates of the channel and noise covariance matrix will be used to update the extrinsic information about the transmitted symbols used by the turbo decoder.

Given a block of received data $[\boldsymbol{Y}_{\mathrm{p},1},\ldots,\boldsymbol{Y}_{\mathrm{p},L_\mathrm{p}},\boldsymbol{Y}_1,\ldots,\boldsymbol{Y}_L]$, the pilot space-time codewords $[\boldsymbol{X}_{\mathrm{p},1},\ldots,\boldsymbol{X}_{\mathrm{p},L_\mathrm{p}}]$, and the prior probabilities of the space-time codewords $\boldsymbol{X}_1,\ldots,\boldsymbol{X}_L$, we wish to find the ML estimates of the channel $\boldsymbol{H}$ and the noise covariance matrix $\boldsymbol{\Sigma}$ for this block.

The EM algorithm is a general iterative method for computing ML estimates in the scenarios where ML estimation cannot be easily performed by directly maximizing the likelihood function for the observed data [22]. Each EM iteration consists of maximizing the expected complete-data log-likelihood function, where the expectation is computed with respect to the conditional distribution of the unobserved data given the observed data. A good choice of unobserved data allows easy maximization of the expected complete-data log-likelihood.

For our channel estimation problem, the unknown space-time codewords $\{\boldsymbol{X}_l\}_{l=1}^{L}$ are modeled as the unobserved (or missing) data. By generalizing our results for SIMO systems in Chapter 2, we obtain the following EM iteration:

Step I:

$$\boldsymbol{H}^{(i+1)} = \frac{1}{(L+L_\mathrm{p})K'}\left[\sum_{l=1}^{L}\boldsymbol{Y}_l \mathrm{E}_{\boldsymbol{X}_l|\boldsymbol{Y}_l}(\boldsymbol{X}_l^H;\boldsymbol{H}^{(i)},\boldsymbol{\Sigma}^{(i)}) + \sum_{\ell=1}^{L_\mathrm{p}}\boldsymbol{Y}_{\mathrm{p},\ell}\boldsymbol{X}_{\mathrm{p},\ell}^H\right] \tag{3.5}$$

Step II:

$$\boldsymbol{\Sigma}^{(i+1)} = \boldsymbol{R}_{yy} - \frac{K'}{K} \cdot \boldsymbol{H}^{(i+1)} (\boldsymbol{H}^{(i+1)})^H \tag{3.6}$$

where

$$\boldsymbol{R}_{yy} = \frac{1}{(L + L_{\mathrm{p}})K} \left[\sum_{l=1}^{L} \boldsymbol{Y}_l \boldsymbol{Y}_l^H + \sum_{\ell=1}^{L_p} \boldsymbol{Y}_{\mathrm{p},\ell} \boldsymbol{Y}_{\mathrm{p},\ell}^H \right]. \tag{3.7}$$

Note that both Steps I and II contain both the expectation and maximization steps. To ensure positive definiteness (with probability one) of the estimates of $\boldsymbol{\Sigma}$, the following condition needs to be satisfied:

$$(L + L_{\mathrm{p}})K \geq (n_T + n_R), \tag{3.8}$$

see e.g., [74, Theorems 10.1.1 and 3.1.4]. Since there is a one-to-one mapping between the set of information symbols $\mathcal{S}_l$ and the codeword $\boldsymbol{X}_l$, conditioning on $\mathcal{S}_l$ is equivalent to conditioning on $\boldsymbol{X}_l$. Following a derivation similar to [63, eq. 7], the likelihood function of $\boldsymbol{X}_l$, $\boldsymbol{H}$ and $\boldsymbol{\Sigma}$ can then be written as

$$\begin{aligned} f(\boldsymbol{Y}_l | \boldsymbol{X}_l; \boldsymbol{H}, \boldsymbol{\Sigma}) &= f(\boldsymbol{Y}_l | \mathcal{S}_l; \boldsymbol{H}, \boldsymbol{\Sigma}) \\ &= \text{const} \cdot \prod_{k=1}^{K'} \exp \Big\{ 2\mathrm{Re} \Big(\big(\mathrm{Re} \left(\mathrm{Tr} \left[\boldsymbol{Y}_l^H \boldsymbol{\Sigma}^{-1} \boldsymbol{H} \boldsymbol{A}_k \right] \right) \\ &\qquad + j \cdot \mathrm{Im} \left(\mathrm{Tr} \left[\boldsymbol{Y}_l^H \boldsymbol{\Sigma}^{-1} \boldsymbol{H} \boldsymbol{B}_k \right] \right) \big) s_k^{(l)} \Big) \Big\} \\ &= \text{const} \cdot \prod_{k=1}^{K'} f_k(\boldsymbol{Y}_l | s_k^{(l)}; \boldsymbol{H}, \boldsymbol{\Sigma}) \end{aligned} \tag{3.9}$$

where const denotes the terms that do not depend on $s_k^{(l)}$. The second equality in the above expression follows by applying the orthogonality conditions in (3.3) which leads to the decoupling of the likelihood function for the space-time codeword into the product of the likelihood functions $f_k(\boldsymbol{Y}_l | s_k^{(l)}; \boldsymbol{H}, \boldsymbol{\Sigma})$ for the information symbols $s_k^{(l)}$, where the normalizing constants have been omitted. Assume that the information symbols $s_k^{(l)}$, $k = 1, \ldots, K'$, $l = 1, \ldots, L$, are independent and have the prior probability mass functions $p(s_k^{(l)}) = p(s_k^{(l)} = s_m)$, $m = 1, \ldots, M$,

then Step I of the EM iteration can be simplified as

$$\begin{aligned}\boldsymbol{H}^{(i+1)} =& \frac{1}{(L+L_{\mathrm{p}})K'}\left[\sum_{l=1}^{L}\sum_{k=1}^{K'}\boldsymbol{Y}_l\left(\mathrm{Re}\left(\mathrm{E}_{s_k^{(l)}|\boldsymbol{Y}_l}\left[s_k^{(l)};\boldsymbol{H}^{(i)},\boldsymbol{\Sigma}^{(i)}\right]\right)\boldsymbol{A}_k^H\right.\right.\\ &\left.\left.-j\cdot\mathrm{Im}\left(\mathrm{E}_{s_k^{(l)}|\boldsymbol{Y}_l}\left[s_k^{(l)};\boldsymbol{H}^{(i)},\boldsymbol{\Sigma}^{(i)}\right]\right)\boldsymbol{B}_k^H\right)+\sum_{\ell=1}^{L_{\mathrm{p}}}\boldsymbol{Y}_{\mathrm{p},\ell}\boldsymbol{X}_{\mathrm{p},\ell}^H\right],\end{aligned} \tag{3.10}$$

where

$$\mathrm{E}_{s_k^{(l)}|\boldsymbol{Y}_l}\left[s_k^{(l)};\boldsymbol{H}^{(i)},\boldsymbol{\Sigma}^{(i)}\right]=\frac{\sum_{m=1}^{M}s_m\ p(s_k^{(l)}=s_m)\ f_k(\boldsymbol{Y}_l|s_m;\boldsymbol{H}^{(i)},\boldsymbol{\Sigma}^{(i)})}{\sum_{n=1}^{M}p(s_k^{(l)}=s_n)\ f_k(\boldsymbol{Y}_l|s_n;\boldsymbol{H}^{(i)},\boldsymbol{\Sigma}^{(i)})} \tag{3.11}$$

and Step II remains the same. The prior probabilities $p(s_k^{(l)})$ comes from the error control decoder.

Most of the computations are in the calculation of (3.10). Given $\mathrm{E}_{s_k^{(l)}|\boldsymbol{Y}_l}[s_k^{(l)};\boldsymbol{H}^{(i)},\boldsymbol{\Sigma}^{(i)}]$, we need $2n_RK\cdot LK'+2n_Rn_TK\cdot K'$ multiplications to compute $\boldsymbol{H}^{(i+1)}$. According to (3.9), $2n_RK$ multiplications are needed for computing $\mathrm{E}_{s_k^{(l)}|\boldsymbol{Y}_l}[s_k^{(l)};\boldsymbol{H}^{(i)},\boldsymbol{\Sigma}^{(i)}]$. If $K'=K=n_R=n_T\triangleq n$, then the total computational complexity can be expressed as $\mathcal{O}(4n^2)$ per symbol per iteration.

3.4 Iterative Space-Time Receiver

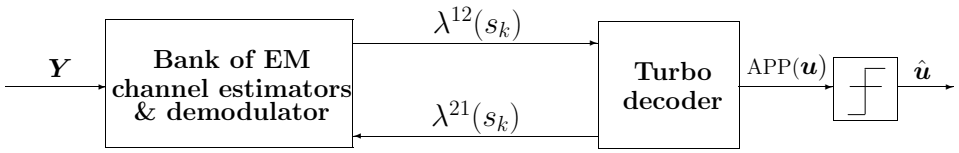

Figure 3.2 The receiver with iterative channel estimation and decoding

The proposed iterative receiver model is shown in Fig. 3.2. It consists of two modules: a bank of R channel estimators and demodulators (developed in the previous section) and a turbo decoder. The soft information about the information symbols is exchanged between them. For simplicity, we have not shown the interleaver and deinterleaver in the diagram. In the following, we also assume that the interleaving and deinterleaving operations are performed as needed.

The received data $\boldsymbol{Y}$ are first divided into R blocks $\left\{[\boldsymbol{Y}^r_{\mathrm{p},1},\ldots,\boldsymbol{Y}^r_{\mathrm{p},L_\mathrm{p}},\boldsymbol{Y}^r_1,\ldots,\boldsymbol{Y}^r_L]\right\}_{r=1}^{R}$ each of length $(L+L_\mathrm{p})K$, and then fed into R channel estimators. Based on the pilot codewords and the prior probabilities of the information symbols, each channel estimator estimates the channel $\widehat{\boldsymbol{H}}_r$ and noise covariance matrix $\widehat{\boldsymbol{\Sigma}}_r$, then computes the posterior log-probabilities of the information symbols as follows

$$\begin{aligned}\Lambda^1_r[s^{(l)}_k] &= \text{const} + \log p(s^{(l)}_k) + \log f_1(\boldsymbol{Y}^r_l | s^{(l)}_k; \widehat{\boldsymbol{H}}_r, \widehat{\boldsymbol{\Sigma}}_r) \\ &= \text{const} + \lambda^{21}_r[s^{(l)}_k] + \lambda^{12}_r[s^{(l)}_k] \\ r = 1,\ldots,R, &\quad l = 1,\ldots,L, \quad k = 1,\ldots,K'.\end{aligned} \tag{3.12}$$

where const denotes the terms independent of $s^{(l)}_k$. The second term $\lambda^{21}_r[s^{(l)}_k]$ represents the prior log-probability of the information symbol $s^{(l)}_k$, which is computed by the turbo decoder in the previous iteration, and then fed back to the channel estimator. For the first iteration, we assume equally likely symbols, i.e., no prior information available. The third term $\lambda^{12}_r[s^{(l)}_k]$ in (3.12) represents the *extrinsic* information produced by the channel estimator and demodulator, based on the received data $\boldsymbol{Y}_r$, pilot codewords, and the prior information of all other symbols in the block. All the extrinsic information metrics $\left\{\lambda^{12}_r[s^{(l)}_k]\right\}_{r=1,k=1,l=1}^{R,K',L}$ are reassembled together, and sent into the turbo decoder, as the prior information for the decoding.

Using the extrinsic information of the information symbols coming from channel estimators and the structure of the turbo codes, the turbo decoder computes the posterior log-probability of each symbol as:

$$\begin{aligned}\Lambda^2_r[s^{(l)}_k] &= \text{const} + \lambda^{12}_r[s^{(l)}_k] + \log p(s^{(l)}_k | \left\{\lambda^{12}_{r'}[s^{(l')}_{k'}]\right\}_{r'=1,k'=1,l'=1,(r',k',l')\neq(r,k,l)}^{R,K',L}; \text{code constraints}) \\ &= \text{const} + \lambda^{12}_r[s^{(l)}_k] + \lambda^{21}_r[s^{(l)}_k]\end{aligned} \tag{3.13}$$

It is seen from (3.13) that the output of the turbo decoder consists of the prior information $\lambda^{12}_r[s^{(l)}_k]$, provided by the channel estimators, and the *extrinsic* information $\lambda^{21}_r[s^{(l)}_k]$ delivered to the channel estimators in the next iteration. This extrinsic information is the information of the symbol $s^{(l)}_k$ in the rth block obtained from the prior information of the other symbols in the

frame and the code constraints. The turbo decoder also outputs the *a posteriori* probability $\mathrm{APP}(u_i)$ of every information bit u_i, which is used to do the decision in the last iteration.

3.5 Discussion

3.5.1 Initialization of the EM algorithm

Although the EM algorithm increases (or at least does not decrease) the likelihood function at each iteration, it may get trapped at the local maximum when the initial values are too far from the true parameters. So we need a more robust method to give good initial estimates of the channel and noise covariance matrices, which are used to initialize our EM algorithm.

For this purpose, we choose the iterative weighted least-squares with projections (ILSP) method for space-time coding systems proposed in [85]. For completeness, we summarize below our implementation of this method:

1. Fix $\boldsymbol{H} = \widehat{\boldsymbol{H}}$ and compute

$$\widehat{\boldsymbol{X}}_l = \mathrm{proj}\left[\boldsymbol{H}^H \boldsymbol{R}_{yy}^{-1} \boldsymbol{Y}_l\right], \quad l = 1, \ldots, L, \tag{3.14}$$

2. Fix $\boldsymbol{X}_1 = \widehat{\boldsymbol{X}}_1, \ldots, \boldsymbol{X}_L = \widehat{\boldsymbol{X}}_L$ and compute

$$\widehat{\boldsymbol{H}} = \frac{1}{(L + L_{\mathrm{p}})K'} \cdot \left[\sum_{l=1}^{L} \boldsymbol{Y}_l \boldsymbol{X}_l^H + \sum_{\ell=1}^{L_{\mathrm{p}}} \boldsymbol{Y}_{\mathrm{p},\ell} \boldsymbol{X}_{\mathrm{p},\ell}^H\right]. \tag{3.15}$$

   Go to step 1 and repeat.

where proj[·] denotes projection onto the nearest (in the Frobenius norm) space-time codeword. This method is initialized with the least-square estimate using the pilot codewords

$$\widehat{\boldsymbol{H}}_{\mathrm{LS}} = \frac{1}{L_{\mathrm{p}} K'} \sum_{\ell=1}^{L_{\mathrm{p}}} \boldsymbol{Y}_{\mathrm{p},\ell} \boldsymbol{X}_{\mathrm{p},\ell}^H \,. \tag{3.16}$$

After several iterations, we obtain a rough estimate of the channel, then the estimate of the noise covariance matrix is computed using (3.6), both of which will be used to initialize the EM algorithm.

3.5.2 Modified Cramér-Rao Bound

The exact Cramér-Rao bound (CRB) for the unknown parameters under the data model in Section 3.2 is difficult to compute. Here, we derive the modified CRB (MCRB) [35], which is a lower bound on the exact CRB. First, we rewrite (3.1) by stacking all K time samples from the lth received space-time data matrix into a single vector:

$$\boldsymbol{y}_l = \boldsymbol{Z}_l \boldsymbol{h}_l + \boldsymbol{e}_l, \tag{3.17}$$

$$\boldsymbol{Z}_l = \boldsymbol{X}_l{}^T \otimes \boldsymbol{I}_{n_R}, \tag{3.18}$$

where $\boldsymbol{y}_l = \mathrm{vec}(\boldsymbol{Y}_l)$, $\boldsymbol{h}_l = \mathrm{vec}\{\boldsymbol{H}_l\}$, $\boldsymbol{e}_k = \mathrm{vec}(\boldsymbol{E}_l)$, $\otimes$ denotes the Kronecker product, and the vec operator stacks the columns of a matrix one below another into a single column vector. Then, (3.17) holds for the pilot data as well, with $\boldsymbol{Y}_l$ and $\boldsymbol{X}_l$ replaced by $\boldsymbol{Y}_{\mathrm{p},\ell}$ and $\boldsymbol{X}_{\mathrm{p},\ell}$, respectively. Define also $\boldsymbol{Z}_{\mathrm{p},\ell} = \boldsymbol{X}_{\mathrm{p},\ell}^T \otimes \boldsymbol{I}_{n_R}$ and the vector of the unknown channel and noise parameters $\boldsymbol{\rho} = [\boldsymbol{\eta}^T, \boldsymbol{\psi}^T]^T$, where $\boldsymbol{\eta} = [\mathrm{Re}(\boldsymbol{h})^T, \mathrm{Im}(\boldsymbol{h})^T]^T$ and $\boldsymbol{\psi} = [\mathrm{Re}\{\mathrm{vech}(\boldsymbol{\Sigma})\}^T, \mathrm{Im}\{\underline{\mathrm{vech}}(\boldsymbol{\Sigma})\}^T]^T$. (The vech and $\underline{\mathrm{vech}}$ operators create a single column vector by stacking elements below the main diagonal columnwise; vech includes the main diagonal, whereas $\underline{\mathrm{vech}}$ omits it.) The MCRB for the unknown parameters $\boldsymbol{\rho}$ is identical to the exact CRB for these parameters when the space-time codewords $\boldsymbol{X}_l$ are *known*, and is equal to:

$$\mathrm{MCRB}_{\boldsymbol{\rho}} = \begin{bmatrix} \mathrm{MCRB}_{\boldsymbol{\eta}} & 0 \\ 0 & \mathrm{MCRB}_{\boldsymbol{\psi}} \end{bmatrix}, \tag{3.19}$$

where

$$\mathrm{MCRB}_{\boldsymbol{\eta}} = \frac{1}{2K'(L+L_{\mathrm{p}})} \cdot \begin{bmatrix} \mathrm{Re}\{\boldsymbol{I}_{n_T} \otimes \boldsymbol{\Sigma}\} & -\mathrm{Im}\{\boldsymbol{I}_{n_T} \otimes \boldsymbol{\Sigma}\} \\ \mathrm{Im}\{\boldsymbol{I}_{n_T} \otimes \boldsymbol{\Sigma}\} & \mathrm{Re}\{\boldsymbol{I}_{n_T} \otimes \boldsymbol{\Sigma}\} \end{bmatrix}, \tag{3.20}$$

$$\mathrm{MCRB}_{\boldsymbol{\psi}} = \frac{1}{K'(L+L_{\mathrm{p}})} \cdot \mathcal{I}_{\boldsymbol{\psi}}^{-1} \tag{3.21}$$

and the (i,k)th element of $\mathcal{I}_{\boldsymbol{\psi}}$ is

$$[\mathcal{I}_{\boldsymbol{\psi}}]_{i,k} = \mathrm{tr}\left\{ \boldsymbol{\Sigma}^{-1} \frac{\partial \boldsymbol{\Sigma}}{\partial \boldsymbol{\psi}_i} \boldsymbol{\Sigma}^{-1} \frac{\partial \boldsymbol{\Sigma}}{\partial \boldsymbol{\psi}_k} \right\} \triangleq \mathcal{I}(\boldsymbol{\psi}_i, \boldsymbol{\psi}_k), \tag{3.22}$$

for $i,k = 1,2,\ldots,n_R^2$. Denote by $\boldsymbol{\Sigma}_{p,q}$ the (p,q) element of $\boldsymbol{\Sigma}$, for $p,q = 1,2,\ldots,n_R$. Using this notation, we further simplify (3.22): for $p_1 > q_1$ and $p_2 > q_2$, we have

$$\begin{aligned}\mathcal{I}(\mathrm{Re}\{\boldsymbol{\Sigma}_{p_1,q_1}\},\mathrm{Re}\{\boldsymbol{\Sigma}_{p_2,q_2}\}) &= \mathcal{I}(\mathrm{Re}\{\boldsymbol{\Sigma}_{p_2,q_2}\},\mathrm{Re}\{\boldsymbol{\Sigma}_{p_1,q_1}\}) \\ &= 2\cdot\mathrm{Re}\big\{[\boldsymbol{\Sigma}^{-1}]_{q_2,p_1}\cdot[\boldsymbol{\Sigma}^{-1}]_{q_1,p_2} + [\boldsymbol{\Sigma}^{-1}]_{q_2,q_1}\cdot[\boldsymbol{\Sigma}^{-1}]_{p_1,p_2}\big\}\end{aligned} \tag{3.23}$$

$$\begin{aligned}\mathcal{I}(\mathrm{Re}\{\boldsymbol{\Sigma}_{p_1,q_1}\},\mathrm{Im}\{\boldsymbol{\Sigma}_{p_2,q_2}\}) &= \mathcal{I}(\mathrm{Im}\{\boldsymbol{\Sigma}_{p_2,q_2}\},\mathrm{Re}\{\boldsymbol{\Sigma}_{p_1,q_1}\}) \\ &= -2\cdot\mathrm{Im}\big\{[\boldsymbol{\Sigma}^{-1}]_{q_2,p_1}\cdot[\boldsymbol{\Sigma}^{-1}]_{q_1,p_2} + [\boldsymbol{\Sigma}^{-1}]_{q_2,q_1}\cdot[\boldsymbol{\Sigma}^{-1}]_{p_1,p_2}\big\}\end{aligned} \tag{3.24}$$

$$\begin{aligned}\mathcal{I}(\mathrm{Im}\{\boldsymbol{\Sigma}_{p_1,q_1}\},\mathrm{Im}\{\boldsymbol{\Sigma}_{p_2,q_2}\}) &= \mathcal{I}(\mathrm{Im}\{\boldsymbol{\Sigma}_{p_2,q_2}\},\mathrm{Im}\{\boldsymbol{\Sigma}_{p_1,q_1}\}) \\ &= 2\cdot\mathrm{Re}\big\{-[\boldsymbol{\Sigma}^{-1}]_{q_2,p_1}\cdot[\boldsymbol{\Sigma}^{-1}]_{q_1,p_2} + [\boldsymbol{\Sigma}^{-1}]_{q_2,q_1}\cdot[\boldsymbol{\Sigma}^{-1}]_{p_1,p_2}\big\},\end{aligned} \tag{3.25}$$

for $p_1 = q_1$ and $p_2 > q_2$,

$$\mathcal{I}(\boldsymbol{\Sigma}_{p_1,p_1},\mathrm{Re}\{\boldsymbol{\Sigma}_{p_2,q_2}\}) = \mathcal{I}(\mathrm{Re}\{\boldsymbol{\Sigma}_{p_2,q_2}\},\boldsymbol{\Sigma}_{p_1,p_1}) = 2\cdot\mathrm{Re}\big\{[\boldsymbol{\Sigma}^{-1}]_{q_2,p_1}\cdot[\boldsymbol{\Sigma}^{-1}]_{p_1,p_2}\big\} \tag{3.26}$$

$$\mathcal{I}(\boldsymbol{\Sigma}_{p_1,q_1},\mathrm{Im}\{\boldsymbol{\Sigma}_{p_2,q_2}\}) = \mathcal{I}(\mathrm{Im}\{\boldsymbol{\Sigma}_{p_2,q_2}\},\boldsymbol{\Sigma}_{p_1,q_1}) = -2\cdot\mathrm{Im}\big\{[\boldsymbol{\Sigma}^{-1}]_{q_2,p_1}\cdot[\boldsymbol{\Sigma}^{-1}]_{p_1,p_2}\big\}, \tag{3.27}$$

and, for $p_1 = q_1$ and $p_2 = q_2$,

$$\mathcal{I}(\boldsymbol{\Sigma}_{p_1,p_1},\boldsymbol{\Sigma}_{p_2,p_2}) = \big|[\boldsymbol{\Sigma}^{-1}]_{p_1,p_2}\big|^2. \tag{3.28}$$

3.6 Simulation Results

We use numerical simulations to evaluate performance of the proposed iterative channel estimation and decoding scheme for a turbo coded MIMO system in a frequency-flat correlated Rayleigh fading environment with $n_T = 2$ transmit and $n_R = 2$ receive antennas. Our performance metrics are the average mean-square error (MSE), bit error rate (BER), and frame error rate (FER), averaged over random channel realizations generated using an independent identically distributed Rayleigh fading model with unit-variance channel coefficients. The Alamouti transmission scheme [3] was used to generate the space-time codewords $\boldsymbol{X}_l$, implying $K' = K = 2$. The transmitted symbols $\{s_k^{(l)}\}$ were generated from a 4-PSK constellation (i.e., $M = 4$) with normalized energy. The space-time codewords were transmitted in R blocks as one frame, and each block consisted of $L_{\mathrm{p}} = 2$ pilot codewords followed by $L = 32$

data codewords. The signal was corrupted by additive complex Gaussian noise with spatial noise covariance matrix $\boldsymbol{\Sigma}$ whose (p,q)th element is

$$\boldsymbol{\Sigma}_{p,q} = \sigma^2 \cdot 0.9^{|p-q|} \cdot \exp[j(\pi/2)(p-q)], \tag{3.29}$$

which is the noise covariance model used in [109] (see also references therein). For simplicity, we assume that $\boldsymbol{\Sigma}$ does not change within the data frame, but this knowledge is not used in the channel and noise covariance estimation. The turbo code consisted of two parallel concatenated $(37, 21)$ recursive systematic convolutional codes connected with a random interleaver. Puncturing was employed to achieve the code rate $R_c = 1/2$. The bit signal-to-noise ratio (SNR) per receive antenna was defined as

$$\text{SNR} = 10\log_{10}\left[\frac{L+L_{\text{p}}}{L} \cdot \frac{n_T K}{K' \log_2(M) \cdot R_c \cdot \sigma^2}\right] = 10\log_{10}\left[\frac{L+L_{\text{p}}}{L} \cdot \frac{n_T}{\sigma^2}\right] \quad \text{(dB)}. \tag{3.30}$$

To initialize the EM algorithm, four iterations of the iterative weighted ILSP method were carried out.

We compare the proposed EM-based scheme with an iterative receiver using deterministic ML channel estimation with soft decision feedback, which is similar to the iterative receiver derived in Section 3.4, but with the channel estimation algorithm replaced by the deterministic ML method [63, 25, 12]. The deterministic ML channel estimator utilizes the expectations of the coded symbols computed from the extrinsic information produced by the decoder. Both methods were initialized using the iterative weighted ILSP method.

Figure 3.3 shows the BER performance versus bit SNR per receive antenna with $R = 16$ blocks. Three iterations have been carried out between the EM channel estimators and the turbo decoder. Clearly, iterating between the channel estimation and turbo decoding can improve the error performance for both EM and deterministic ML methods. As a comparison, we also present the performance of ideal coherent detector for exactly known $\boldsymbol{H}$ and $\boldsymbol{\Sigma}$. After three iterations, our method outperforms the deterministic ML by about 0.6 dB at BER $= 10^{-4}$, and comes within about 2 dB of the performance of the ideal coherent detector.

Next, we study the performance of the proposed EM-based scheme for long frame length, see Figs. 3.4, 3.5 and 3.6. Each data frame consisted of $R = 64$ blocks, and there were 6

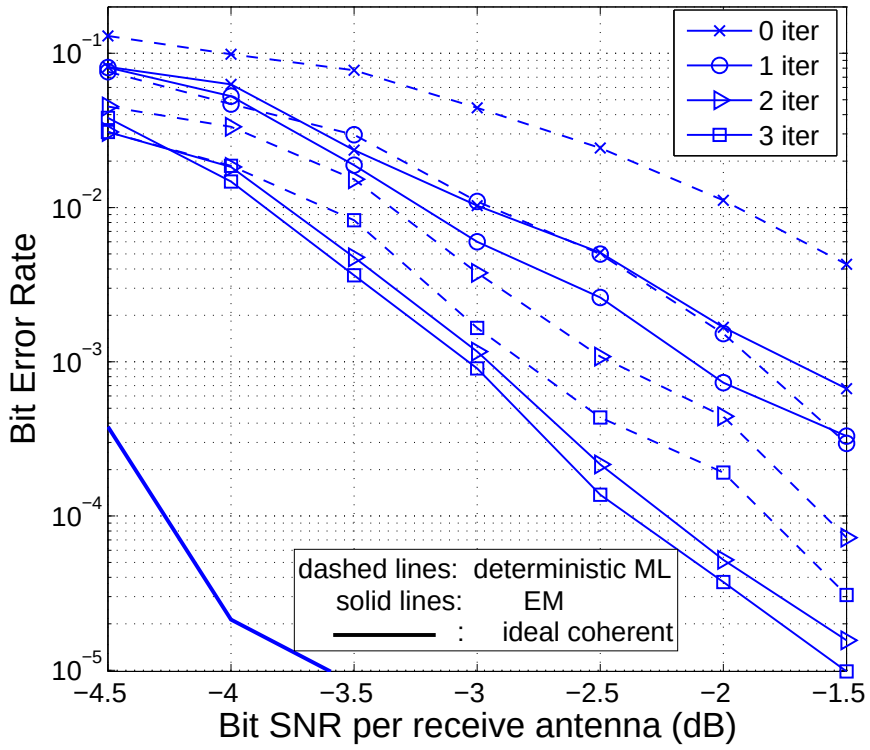

Figure 3.3 BER for EM-based, deterministic ML and ideal coherent detectors with $R = 16$.

iterations between the EM channel estimators and the turbo decoder.

In Fig. 3.4, the average MSE of the channel estimates improves as the number of iterations between the channel estimation and turbo decoding increases, and reaches the MCRB at SNR ≥ -4 dB. Although the MCRB is the CRB assuming known information symbols, and hence a lower bound of the exact CRB, it can be regarded as the exact CRB when SNR ≥ -4 dB since the BER has become very small (see Fig. 3.5) such that almost all the information symbols are correctly decoded.

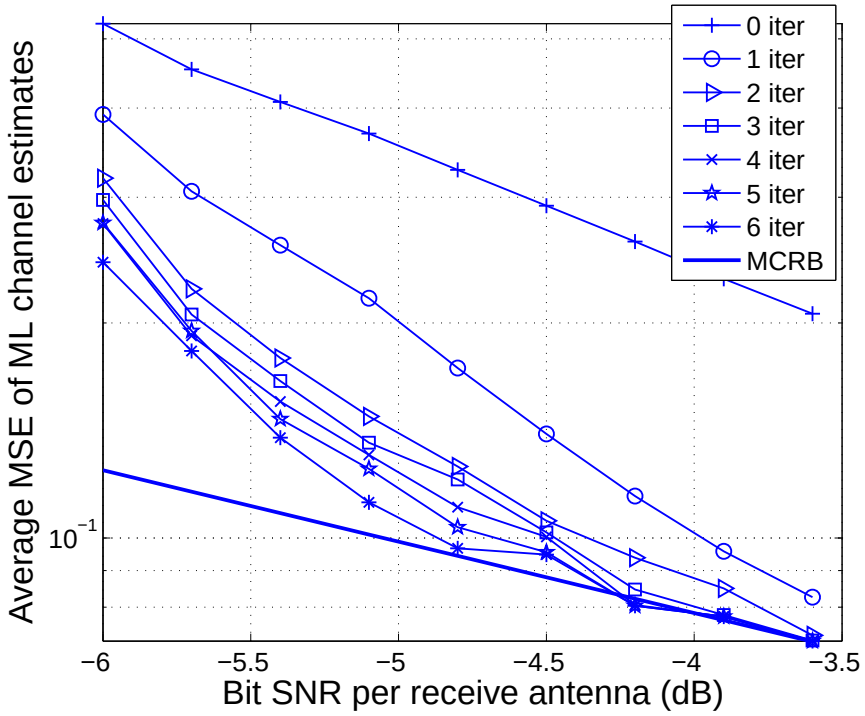

Figure 3.4 MSE of the channel estimates for EM-based method with $R = 64$.

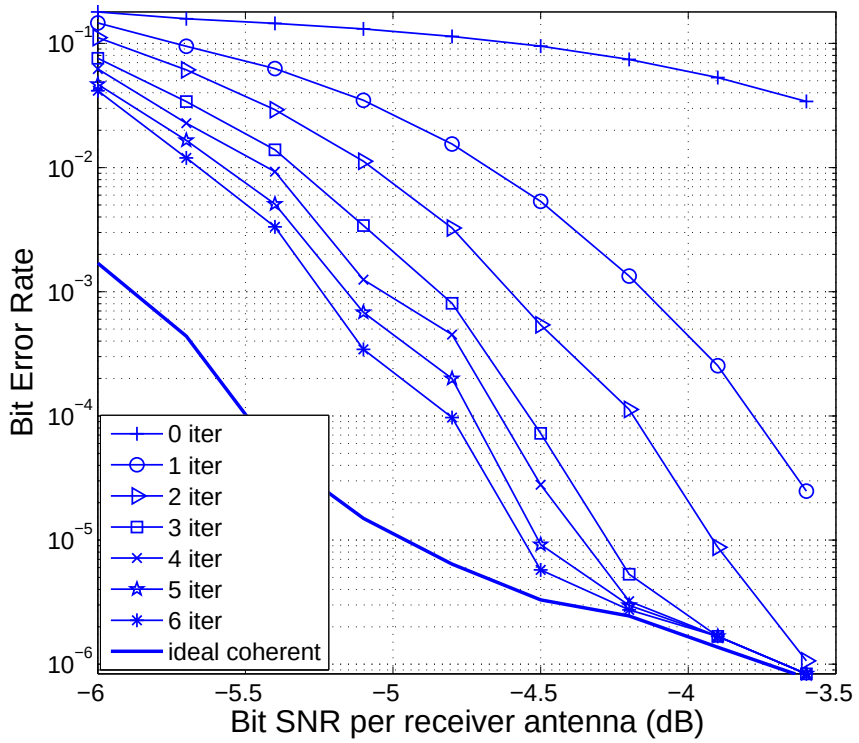

Figure 3.5 BER for EM-based and ideal coherent detectors with $R = 64$.

The BER and FER performances of the proposed scheme are depicted in Figs. 3.5 and 3.6, respectively. After three iterations, the improvement provided by more iterations becomes smaller and smaller: an effect of diminishing returns. Such a saturation effect is more obvious in the Fig. 3.6. The BER performance difference between our method and the ideal coherent detector becomes negligible at a BER level of 10^{-6}, which is achieved after only three iterations. Unlike the BER performance which depends on the specific turbo code used in the system, FER provides a performance measurement of the iterative receiver itself. It is seen from Fig. 3.6 that upon convergence, our method approaches the performance of the ideal coherent detector, which is a lower bound of the performance for such MIMO systems.

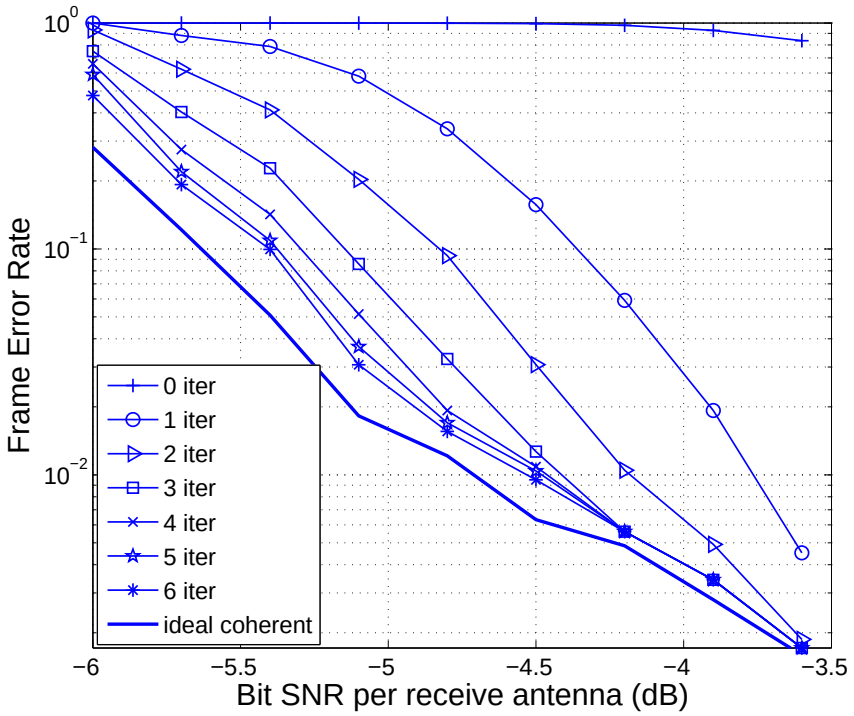

Figure 3.6 FER for EM-based and ideal coherent detectors with $R = 64$.

The proposed method takes into account spatial correlation of the noise. To demonstrate the importance of this factor, we compare the proposed method with another EM-based iterative receiver, termed white-noise EM method, under a spatial correlated noise scenario. The method proposed in Section 3.4 differs from the white-noise EM method by the channel estima-

tion algorithm. The white-noise EM algorithm assumes spatially white noise, i.e., $\boldsymbol{\Sigma} = \sigma^2 \boldsymbol{I}_{n_R}$, where σ^2 is the variance parameter to be estimated. Therefore, the white-noise EM algorithm is a modified version of the EM algorithm proposed in Section 3.3. The only modification is that the Step II, i.e., (3.6), can be simplified as:

$$\boldsymbol{\Sigma}^{(i+1)} = \text{Trace}\Big(\boldsymbol{R}_{yy} - \frac{K'}{K} \cdot \boldsymbol{H}^{(i+1)}(\boldsymbol{H}^{(i+1)})^H\Big) \cdot \boldsymbol{I}_{n_R}. \tag{3.31}$$

A similar algorithm assuming known noise variance is proposed in [38]. Figure 3.7 shows the BER performance of the white-noise EM method after 3 and 6 iterations between channel estimation and turbo decoding. As a comparison, the performance of the ideal coherent detector is also provided. It is seen that the proposed method has a 7 dB advantage over the white-noise EM method at a BER of 10^{-5} after both 3 and 6 iterations.

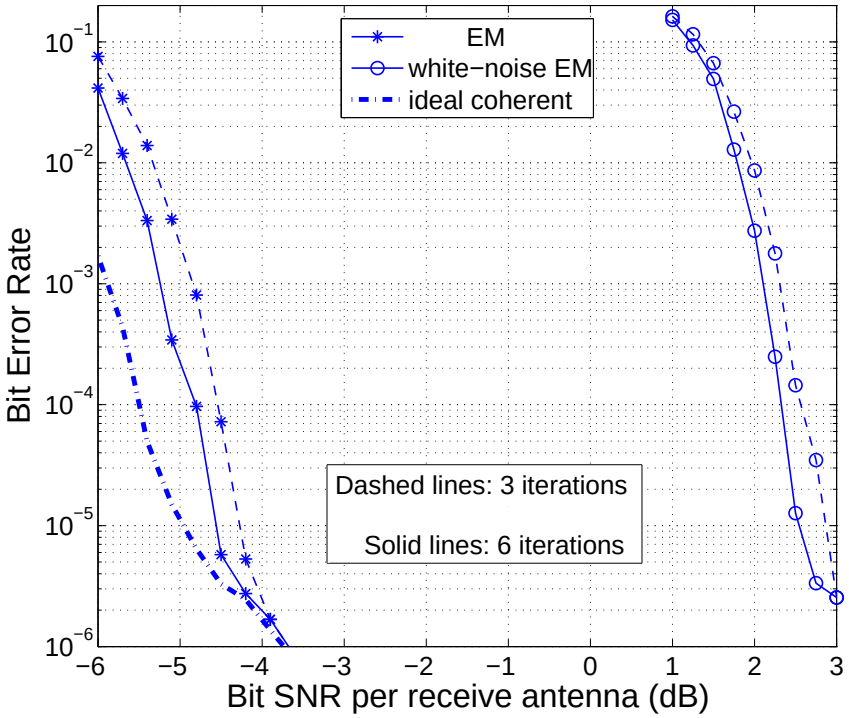

Figure 3.7 BER for EM-based, white-EM based and ideal coherent detectors with $R = 64$.

3.7 Summary

We developed an EM-based iterative channel estimation and decoding scheme for a coded system over MIMO Rayleigh block fading channels in spatially correlated noise. By exchanging the extrinsic information of the transmitted symbols, both the channel estimation and the decoding can be improved. We also presented the modified Cramér-Rao bounds for the unknown parameters. Numerical simulations demonstrated the good performance of the proposed method and other competitive schemes.

One possible extension of this work is to develop and adaptive version of the channel estimation algorithm that can account for continuously varying channels (as opposed to the block-fading scenario considered here) and also reduce the EM algorithm complexity. It is also of interest to adapt the algorithm for frequency-selective MIMO channels, possibly in combination with orthogonal frequency-division multiplexing (OFDM).

CHAPTER 4. LOW-COMPLEXITY NEAR-OPTIMAL DETECTION ALGORITHM FOR CODED MIMO SYSTEMS

4.1 Introduction

The demand of high data rate in wireless systems has been increasing extensively in recent years. Communication systems utilizing multiple antennas at both the transmitter and the receiver have been shown to have much higher spectral efficiency than the conventional single antenna systems [31, 102].

Detection of the transmitted symbols is one fundamental and difficult problem for multiple antenna systems, since the multi-input multi-output (MIMO) channel introduces interference to the received signals. Recently there have been increasing interests in iterative detection and decoding [17, 51, 58, 100], where MIMO detector can incorporate the soft information provided by the channel decoder as *a priori* information to refine the symbol detection. In [17, 100], parallel soft interference cancellation scheme was employed together with channel decoding in an iterative way. However, the cancellation error caused by the bad symbols propagates to other symbols, and can be amplified by the iterative decoding. In [58], a successive soft interference cancellation was proposed, where the cancellation order was based on the estimated signal-to-interference ratio (SIR). In [51], a "list" version of the sphere decoder is proposed, which achieves good performance, but has high computational complexity.

In this chapter, a low-complexity near-optimal detector, namely ordered successive soft interference cancellation (OSSIC), is proposed based on the BLAST (Bell-Labs Layered Space-Time) detection algorithm. The differences from the original nulling-canceling scheme are: i) we incorporate the prior probabilities coming from the error-control decoder into the nulling, ordering and canceling steps, ii) linear minimum mean-square error (LMMSE) filtering in the

nulling step uses the prior information of the transmitted symbols, iii) *a posteriori* probabilities (APP), instead of signal to noise ratios (SNR), are used in the ordering strategy, and iv) soft interferences computed from APP are canceled, instead of the hard interferences. The APP-based ordering strategy was inspired by the work [57].

Another contribution is that we develop a "square-root" algorithm, based on [47], for our proposed MIMO detector which can reduce the complexity to $\mathcal{O}(N^3)$ per iteration, where N is the number of transmit antennas.

Simulation results show that in a 4×4 MIMO system, our proposed low-complexity detector can achieve near-optimal performance for both binary phase-shift keying (BPSK) modulation and 16-quadrature amplitude modulation (QAM).

The remainder of this chapter is organized as follows. Section 4.2 describes the system model and the iterative receiver design. *Maximum a posterior* (MAP) detector and our proposed nulling/canceling detector are presented in Section 4.3. Section 4.4 extends our proposed detector to M-ary modulation cases. Simulation results are presented in Section 4.5. Section 4.6 concludes this chapter.

4.2 System model and receiver structure

We consider a narrow-band, frequency-flat Rayleigh fading, multi-antenna communication system with n_T transmit and $n_R(\geq n_T)$ receive antennas. Let $\boldsymbol{s}$ denotes an $n_T \times 1$ vector of transmitted symbols, whose entries are chosen from BPSK constellation with average energy E_s per symbol. An extension to M-ary modulation will be discussed in Section 4.4. Let $\boldsymbol{y}$ denote an $n_R \times 1$ vector of received signal at each symbol time

$$\boldsymbol{y} = H\boldsymbol{s} + \boldsymbol{n}, \tag{4.1}$$

where $H = [\boldsymbol{h}_1, \ldots, \boldsymbol{h}_{n_T}]$ is the $n_R \times n_T$ channel matrix, known perfectly to the receiver, whose elements are independent identically distributed (i.i.d.) complex Gaussian with zero mean and unit variance, and $\boldsymbol{n}$ is an $n_R \times 1$ vector of independent zero-mean complex Gaussian noise entries with variance $N_0/2$ per real dimension.

In this chapter, we study a coded MIMO system with vertical (V)-BLAST [36] transmission scheme as shown in Fig. 4.1. A frame of information bits u is encoded by a channel encoder into coded bits c, which are interleaved, modulated and divided into blocks of n_T symbols. Each block of symbols $\boldsymbol{s}$ is transmitted simultaneously by n_T transmit antennas. The channel code is chosen to be strong error-control codes, such as Low-Density Parity-Check (LDPC) codes and turbo codes. Since the channel code introduces redundancy and correlation among different blocks, it is sub-optimal for the MIMO detector and channel decoder to operate separately.

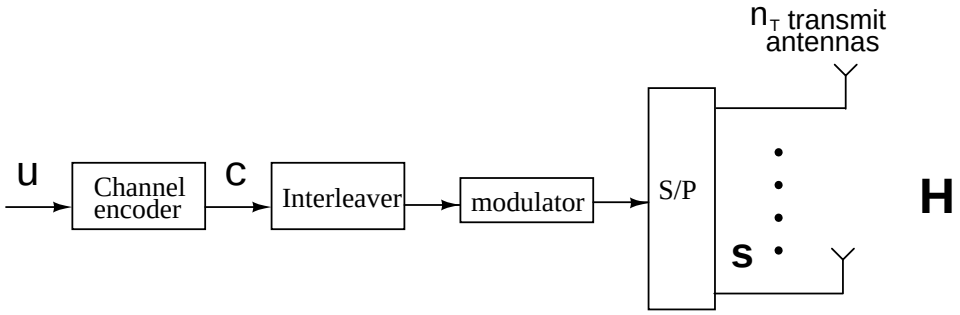

Figure 4.1 Discrete-time transmitter model

The optimal solution is the joint detection and decoding which computes the likelihood of each information bit given the received data $\boldsymbol{y}$'s, and the constraints imposed by the MIMO channel H and the channel code. Unfortunately, it is computationally prohibitive even for codes with reasonable frame length. Therefore, an iterative detection and decoding scheme is employed to simplify the problem. Both the MIMO detector and the channel decoder are soft-input soft-output (SISO) modules, and soft information of coded bits is exchanged between them in an iterative way until desired performance is achieved. It has been shown that such "turbo principle" is very effective and computationally efficient in other joint detection and decoding problems [51, 104]. The iterative receiver structure is shown in Fig. 4.2.

The error-control encoder and decoder are relatively standard. The overall performance and complexity will be determined by the MIMO detector module. We focus in detail on the MIMO detector design in Section 4.3.

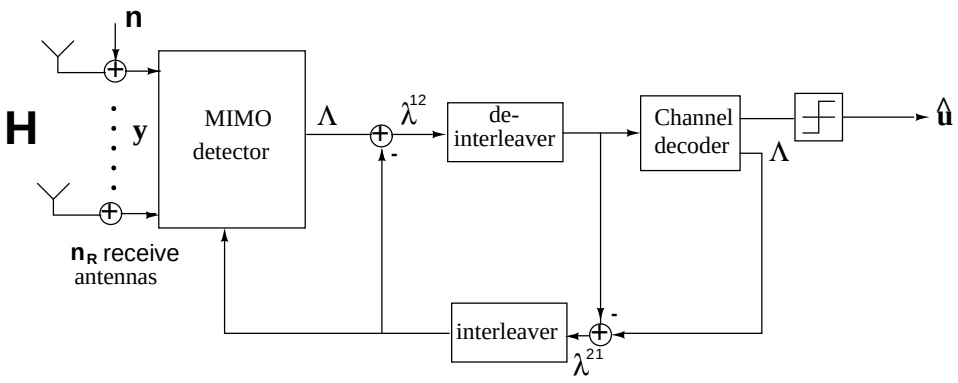

Figure 4.2 Discrete-time receiver model

4.3 MIMO detection

The "best" known detector for the MIMO system (5.1) is the MAP detector which tries to maximize the APP $p(s_k|\boldsymbol{y})$. However, the complexity of this detector grows exponentially with the number of antennas, and becomes computationally infeasible for a system with a large number of antennas. One effective alternative is the V-BLAST nulling/canceling algorithm [36]. The conventional BLAST algorithm does not incorporate the reliability information on symbols provided by the channel decoder and does not output soft information. In this section, we present a nulling/canceling detector, namely ordered successive soft interference cancellation (OSSIC), which i) uses prior information, ii) uses soft inference cancellation, iii) adopts an ordering strategy based on *a posterior* probability [57], and iv) outputs extrinsic information for the error-control decoder.

We will first briefly summarize the MAP detector, which we will compare with, and introduce some standard definitions.

4.3.1 MAP detector

Maximizing the APP of a given symbol minimizes the error probability on that symbol. For BPSK modulation, it is convenient to express the APP in the form of log-probability ratio (LPR). For the MIMO system (5.1), the APP (in LPR form) Λ_k of the symbol $s_k, k = 1, \ldots, n_T$,

conditioned on the received data $\boldsymbol{y}$, is

$$\begin{aligned}\Lambda_k &= \ln \frac{p(s_k = +\sqrt{E_s}|\boldsymbol{y})}{p(s_k = -\sqrt{E_s}|\boldsymbol{y})} \\ &= \ln \frac{p(s_k = +\sqrt{E_s})}{p(s_k = -\sqrt{E_s})} + \ln \frac{p(\boldsymbol{y}|s_k = +\sqrt{E_s})}{p(\boldsymbol{y}|s_k = -\sqrt{E_s})} \\ &= \lambda_k^{21} + \lambda_k^{12},\end{aligned} \tag{4.2}$$

where λ_k^{21} is the *a priori* information on s_k provided by the channel decoder, and λ_k^{12} is the extrinsic information which will be passed to the channel decoder as *a priori* information.

Given the *a priori* information $\lambda_k^{21}, k = 1, \ldots, n_T$, the MAP detector needs to calculate the extrinsic information λ_k^{12}.

$$\lambda_k^{12} = \ln \frac{p(\boldsymbol{y}|s_k = +\sqrt{E_s})}{p(\boldsymbol{y}|s_k = -\sqrt{E_s})} = \ln \frac{\sum_{\boldsymbol{s}\in\mathcal{S}_k^1} p(\boldsymbol{y}|\boldsymbol{s}) \cdot p(\boldsymbol{s})}{\sum_{\boldsymbol{s}\in\mathcal{S}_k^0} p(\boldsymbol{y}|\boldsymbol{s}) \cdot p(\boldsymbol{s})}, \tag{4.3}$$

where

$$\mathcal{S}_k^0 = \{(s_1, \ldots, s_{k-1}, s_k = -\sqrt{E_s}, s_{k+1}, \ldots, s_{n_T})\},$$
$$\mathcal{S}_k^1 = \{(s_1, \ldots, s_{k-1}, s_k = +\sqrt{E_s}, s_{k+1}, \ldots, s_{n_T})\}$$

and

$$p(\boldsymbol{y}|\boldsymbol{s}) = \frac{1}{\pi N_0} \exp \frac{-\|\boldsymbol{y} - H\boldsymbol{s}\|^2}{N_0}.$$

We assume that the interleaver at the transmitter "scrambles" the coded bits so that the transmitted symbols s_k's are approximately statistically independent of one another. Thus, $p(\boldsymbol{s}) = \prod_{k=1}^{n_T} p(s_k)$, where $p(s_k)$ may be easily computed from λ_k^{21}. Since the summation in (4.3) is over all the 2^{n_T-1} possible values of $\boldsymbol{s}$, the complexity of the detector grows exponentially with the number of transmit antennas.

4.3.2 Proposed detector – OSSIC

We propose a nulling/canceling detector using soft inference cancellation and ordering strategy based on APP. We incorporate the *a priori* information into the convention BLAST detection algorithm. The nulling of interferences uses the LMMSE filter with *a priori* probabilities, where the *a priori* probabilities of the transmitted symbols is from error control decoder. The interference cancellation and the ordering are based on the *a posterior* probabilities, which

is inspired by the work in [57], where it proposed to use the log-likelihood ratio (LLR) as the ordering criterion for an uncoded system. Our algorithm consists of three parts: interference nulling, interference canceling, and ordering. In practice, the algorithm proceeds in the order of ordering, nulling, and cancellation.

[Nulling]

Given the received data $\boldsymbol{y} = H\boldsymbol{s} + \boldsymbol{n}$, and *a priori* information $\{\lambda_k^{21}\}_{k=1}^{n_T}$ on $\boldsymbol{s}$ provided by the channel decoder, the linear minimum mean-square error (MMSE) estimate of $\boldsymbol{s}$ is

$$\boldsymbol{x} = \bar{\boldsymbol{s}} + (N_0 D^{-1} + H^H H)^{-1} H^H (\boldsymbol{y} - H\bar{\boldsymbol{s}}), \tag{4.4}$$

where $(\cdot)^H$ denotes complex conjugate transpose, and

$$\begin{aligned} \bar{\boldsymbol{s}} &= [\bar{s}_1, \ldots, \bar{s}_{n_T}], \\ D &= \mathrm{diag}[\bar{\sigma}_1^2, \ldots, \bar{\sigma}_{n_T}^2]\ ^1. \end{aligned} \tag{4.5}$$

For $k = 1, \ldots, n_T$, $\bar{s}_k$ and $\bar{\sigma}_k^2$ are the *a priori* mean and variance of s_k induced from the *a priori* distribution, which are defined as

$$\begin{aligned} \bar{s}_k &= \tanh\{\lambda_k^{21}/2\} \cdot \sqrt{E_s}, \\ \bar{\sigma}_k^2 &= (1 - \tanh^2\{\lambda_k^{21}/2\}) \cdot \sqrt{E_s}. \end{aligned} \tag{4.6}$$

Let

$$W = (N_0 D^{-1} + H^H H)^{-1} H^H = [\boldsymbol{w}_1, \ldots, \boldsymbol{w}_{n_T}]^H, \tag{4.7}$$

where $\boldsymbol{w}_k$ is an $n_R \times 1$ MMSE nulling vector, then

$$x_k = \bar{s}_k + \boldsymbol{w}_k^H (\boldsymbol{y} - H\bar{\boldsymbol{s}}) = \boldsymbol{w}_k^H \boldsymbol{h}_k s_k + (1 - \boldsymbol{w}_k^H \boldsymbol{h}_k)\bar{s}_k + \boldsymbol{w}_k^H \tilde{\boldsymbol{n}}_k, \tag{4.8}$$

where $\tilde{\boldsymbol{n}}_k = \sum_{i=1, i\neq k}^{n_T} \boldsymbol{h}_i (s_i - \bar{s}_i) + \boldsymbol{n}$. It is easy to verify that the covariance matrix of the estimation error $\boldsymbol{s} - \boldsymbol{x}$ is

$$E(\boldsymbol{s} - \boldsymbol{x})(\boldsymbol{s} - \boldsymbol{x})^H = N_0 \cdot (N_0 D^{-1} + H^H H)^{-1} \triangleq \Sigma. \tag{4.9}$$

So the variance of $(x_k - s_k)$ is Σ_{kk}, the k-th diagonal element of Σ. We assume that the residual interference $\boldsymbol{w}_k^H \boldsymbol{h}_i (s_i - \bar{s}_i)$, $i = 1, \ldots, k-1, k+1, \ldots, n_T$ are conditionally independent given

$\boldsymbol{y}$, and are independent of $\boldsymbol{w}_k^H \boldsymbol{n}$. We assume $\boldsymbol{w}_k^H \tilde{\boldsymbol{n}}_k$ is complex Gaussian distributed with zero mean and variance

$$\sigma_k^2 \triangleq \Sigma_{kk} - |1 - \boldsymbol{w}_k^H \boldsymbol{h}_k|^2 \bar{\sigma}_k^2. \tag{4.10}$$

Thus after nulling the interference from all other symbols, except the k-th, we have

$$x_k \sim \mathcal{CN}(\boldsymbol{w}_k^H \boldsymbol{h}_k s_k + (1 - \boldsymbol{w}_k^H \boldsymbol{h}_k)\bar{s}_k,\ \sigma_k^2), \quad k = 1, 2, \ldots, n_T. \tag{4.11}$$

[Canceling]

From (4.11) the APP of s_k in the LPR form is given by

$$\begin{aligned} \Lambda_k &= \ln \frac{p(s_k = +\sqrt{E_s}|x_k)}{p(s_k = -\sqrt{E_s}|x_k)} \\ &= \ln \frac{p(s_k = +\sqrt{E_s})}{p(s_k = -\sqrt{E_s})} + \frac{4\sqrt{E_s}}{\sigma_k^2} \cdot \mathrm{Re}\{\boldsymbol{w}_k^H \boldsymbol{h}_k \cdot x_k^*\} \\ &= \lambda_k^{21} + \lambda_k^{12}, \end{aligned} \tag{4.12}$$

where $(\cdot)^*$ represents complex conjugate, and $\lambda_k^{12} \triangleq 4\sqrt{E_s} \cdot \mathrm{Re}\{\boldsymbol{w}_k^H \boldsymbol{h}_k \cdot x_k^*\}/\sigma_k^2$. Using soft decision of s_k based on APP:

$$\hat{s}_k = \tanh\{\Lambda_k/2\} \cdot \sqrt{E_s} \tag{4.13}$$

and assuming correct detection, we softly cancel the interference caused by s_k from $\boldsymbol{y}$ and obtain a reduced order problem

$$\boldsymbol{y}^{(1)} = \boldsymbol{y} - \boldsymbol{h}_k \hat{s}_k = H^{(1)} \boldsymbol{s}^{(1)} + \boldsymbol{n}, \tag{4.14}$$

where we have defined $H^{(1)}$ and $\boldsymbol{s}^{(1)}$ as

$$H^{(1)} = [\boldsymbol{h}_1, \ldots, \boldsymbol{h}_{k-1}, \boldsymbol{h}_{k+1}, \ldots, \boldsymbol{h}_{n_T}],$$

$$\boldsymbol{s}^{(1)} = [s_1, \ldots, s_{k-1}, s_{k+1}, \ldots, s_{n_T}]^T.$$

The solution to the reduced detection problem in (4.14) requires to compute the corresponding error covariance matrix $N_0(N_0 D_{(1)}^{-1} + {H^{(1)}}^H H^{(1)})^{-1} \triangleq \Sigma^{(1)}$, where

$$D_{(1)} = \mathrm{diag}[\bar{\sigma}_1^2, \ldots, \bar{\sigma}_{k-1}^2, \bar{\sigma}_{k+1}^2, \ldots, \bar{\sigma}_{n_T}^2].$$

[Ordering]

For nulling/canceling detection algorithm, the order in which the components of $\boldsymbol{s}$ are detected and canceled is important to the overall system performance [30]. In general, the conditional bit error probability $P_{e,k} = P(\hat{s}_k \neq s_k | x_k)$ and the APP Λ_k are related by [57]

$$P_{e,k} = \frac{1}{1 + e^{|\Lambda_k|}}. \tag{4.15}$$

Thus, we detect and cancel the component of $\boldsymbol{s}$ that provides the largest $|\Lambda_k|$ first. Since the magnitude of Λ_k is the reliability information of the corresponding bit, the proposed ordering strategy is equivalent to canceling the most reliable bit first.

4.3.3 Modified square-root algorithm

Assuming $n_T = n_R = N$, the proposed detector has the same order of computational complexity $\mathcal{O}(N^4)$ as the conventional BLAST algorithm [36], since both of them have the same nulling step, which accounts for the majority of the computational cost due to the calculation of matrix inverse. Next, we adapt the square-root algorithm proposed by Hassibi [47] to our proposed detector such that the computational cost can be reduced from $\mathcal{O}(N^4)$ to $\mathcal{O}(N^3)$.

The QR decomposition of the augmented channel matrix [47] can be defined as

$$\begin{bmatrix} H \\ \sqrt{N_0} D^{-1/2} \end{bmatrix} = Q_1 R = \begin{bmatrix} Q \\ Q_2 \end{bmatrix} R, \tag{4.16}$$

where Q_1 is an $(n_R + n_T) \times n_T$ matrix with orthonormal columns, Q is $n_R \times n_T$ sub-matrix, and R is $n_T \times n_T$ upper triangular matrix and nonsingular. Define $P^{1/2}$ to be such that $P^{1/2} P^{H/2} = \Sigma / N_0$. It is easy to verify that

$$P^{1/2} = R^{-1} \quad \text{and} \quad W = P^{1/2} Q^H,$$

where W and Σ are defined in (4.7) and (4.9) respectively. Let $P_k^{1/2}$ denote the k-th row of $P^{1/2}$ and $V \triangleq Q^H H = [\boldsymbol{v}_1, \ldots, \boldsymbol{v}_{n_T}]$, then

$$\begin{aligned} \boldsymbol{w}_k^H &= P_k^{1/2} Q^H, \\ \Sigma_{kk} &= N_0 \cdot \| P_k^{1/2} \|, \\ z_k &\triangleq \boldsymbol{w}_k^H \boldsymbol{h}_k = P_k^{1/2} \boldsymbol{v}_k, \end{aligned} \tag{4.17}$$

where $\|\cdot\|$ denotes the ℓ^2 norm. Thus, given $P^{1/2}$ and V, we may compute APP Λ_k of s_k using (4.12) and (4.10).

In order to proceed with the nulling/canceling procedure, we need to find $P^{(1)/2}$ and $V^{(1)}$ for the reduced order problem (4.14) from $P^{1/2}$ and V. Similar to [47], we have the following claims.

Claim 1: *Reorder the entries of* $\boldsymbol{s}$ *and rows of* P *so that the* $|\Lambda_{n_T}|$ *is the largest. Consider any unitary transformation* U *that rotates the* n_T*-th row* $P_{n_T}^{1/2}$ *of* $P^{1/2}$ *to lie along the direction of the* n_T*-th unit vector. In other words,*

$$P^{1/2}U = \begin{bmatrix} P^{(1)/2} & A \\ \mathbf{0} & p_{n_T}^{1/2} \end{bmatrix}, \tag{4.18}$$

where $p_{n_T}^{1/2}$ *is a scalar. Then* $P^{(1)/2}$ *is a square-root of* $P^{(1)}$.

Claim 2: *Using the unitary transformation* U *obtained in Claim 1, rotate the columns of* V *such that*

$$UV = \begin{bmatrix} V^{(1)} & B \\ \boldsymbol{c} & d \end{bmatrix}, \tag{4.19}$$

where d *is a scalar. Then* $V^{(1)}$ *is the matrix* V *needed for the reduced order problem.*

We can now summarize the proposed detector using modified square-root algorithm as follows:

1. Compute $P^{1/2}$ and V by QR decomposition of the augmented channel matrix.
2. Find the largest $|\Lambda_k|$ using (4.12), (4.10), (4.17) and permute $P_k^{1/2}$ and $P_{n_T}^{1/2}$. Permute $\boldsymbol{s}$ accordingly.
3. Find a unitary transformation U such that $P^{1/2}U$ is block upper triangular:
$$P^{1/2}U = \begin{bmatrix} P^{(1)/2} & A \\ \mathbf{0} & p_{n_T}^{1/2} \end{bmatrix}.$$
4. Update V using U such that
$$UV = \begin{bmatrix} V^{(1)} & B \\ \boldsymbol{c} & d \end{bmatrix}.$$

5. Obtain soft estimate of s_{n_T} based on APP Λ_{n_T} as $\hat{s}_{n_T} = \tanh\{\Lambda_{n_T}/2\} \cdot \sqrt{E_s}$.

6. Cancel the effect of s_{n_T}, output the extrinsic information $\lambda_{n_T}^{12}$, and consider the reduced order problem (4.14).

7. Go back to step 2, but now with $P^{(1)/2}$ and $V^{(1)}$.

In contrast to the MAP detector which has exponential complexity, our proposed algorithm has $\mathcal{O}(N^3)$ complexity. Such low complexity makes it more attractive for systems with moderate number of antennas.

4.4 Extension to M-ary modulation

In this section, we extend the proposed MIMO detector to M-ary modulated signals. Assume the transmitted symbol s_k is chosen from the set $\{\alpha_1, \alpha_2, \ldots, \alpha_M\}$, then the APP of $s_k = \alpha_m$ may be obtained from (4.11) as

$$p(s_k = \alpha_m | x_k) = \frac{1}{\pi\sigma_k^2} \exp \frac{-|x_k - \boldsymbol{w}_k^H \boldsymbol{h}_k \cdot \alpha_m|^2}{\sigma_k^2} \cdot \frac{p(s_k = \alpha_m)}{p(x_k)}, \tag{4.20}$$

where $p(s_k = \alpha_m)$ is the *a priori* information of symbol s_k, which may be calculated from the *a priori* information of the corresponding coded bits provided by the channel decoder. (Here, we assume that the coded bits within one transmitted symbol are independent due to the interleaver at the transmitter.) Let

$$\tilde{s}_k = \arg\max_{\alpha_m} p(s_k = \alpha_m | x_k) \tag{4.21}$$

be the MAP decision for the k-th symbol, and

$$\begin{aligned} \Lambda_{k,m} &= \ln \frac{p(s_k = \alpha_m | x_k)}{p(s_k = \tilde{s}_k | x_k)} \\ &= \frac{|x_k - \boldsymbol{w}_k^H \boldsymbol{h}_k \cdot \tilde{s}_k|^2 - |x_k - \boldsymbol{w}_k^H \boldsymbol{h}_k \cdot \alpha_m|^2}{\sigma_k^2} + \ln \frac{p(s_k = \alpha_m)}{p(s_k = \tilde{s}_k)} \end{aligned} \tag{4.22}$$

be the APP of $s_k = \alpha_m$ in the LPR form. Then the conditional probability of symbol error given x_k is [57]

$$\begin{aligned} P(\tilde{s}_k \neq s_k | x_k) &= 1 - P(\tilde{s}_k = s_k | x_k) \\ &= 1 - \frac{1}{\sum_{m=1}^{M} \exp(\Lambda_{k,m})}. \end{aligned} \tag{4.23}$$

Thus, the symbol minimizing $\sum_{m=1}^{M} \exp(\Lambda_{k,m})$, i.e., with the smallest conditional probability of symbol error, is canceled first. The soft decision of s_k is also computed based on the APP

$$\hat{s}_k = \sum_{m=1}^{M} \alpha_m \cdot p(s_k = \alpha_m | x_k). \tag{4.24}$$

Since the nulling step is the same for BPSK and M-ary modulation, the computational complexities of two cases are roughly at the same order for large systems. The square-root algorithm can also be modified for the M-ary modulation. The details are omitted here.

4.5 Simulation Results

Using numerical simulations, we evaluated the performance of the proposed iterative detection and decoding scheme for a coded MIMO system in a frequency-flat Rayleigh fading environment, with $n_T = 4$ transmit and $n_R = 4$ receive antennas. BPSK and 16-QAM were employed with average energy E_s per symbol. The rate $R = 1/2$ channel code was chosen to be a turbo code with 9216 information bits, whose component encoders are $(7, 5)$ convolutional encoder. The signal was corrupted by additive complex Gaussian noise with zero mean and spatial noise covariance matrix $N_0 I_{n_R}$. The signal energy per transmitted information bit at the receiver was defined as $E_b = (N_R/R) \cdot E_s$, therefore the bit SNR at the receiver was

$$SNR = 10 \log_{10} \frac{E_b}{N_0} = 10 \log_{10} \frac{n_R \cdot E_s}{R \cdot N_0} \quad \text{(dB)} \tag{4.25}$$

We compared our proposed detector with the MAP detector, which is optimal but with exponential computational complexity. For the 16-QAM case, a list sphere decoder (LSD) [51] was used to approximate the MAP detector, which also has much higher computational complexity compared with our proposed detector. There were 6 iterations between MIMO detectors and channel decoder. As a reference, we also presented the performance of another well-known MIMO detection algorithm, soft interference cancellation with linear MMSE filtering (SIC+MMSE) [111], which has $\mathcal{O}(N^3)$ complexity as our proposed detector. For completeness, we summarize below our implementation of this method (c.f. [111]). Here, we assume the BPSK modulation, and the extension to 16-QAM modulation is straightforward.

[SIC+MMSE]

For the detection of s_k, $k = 1, \ldots, n_T$

1. Soft interference cancellation (SIC):

$$\boldsymbol{y}_k = \boldsymbol{y} - \sum_{i=1,\ i\neq k}^{n_T} \boldsymbol{h}_i \bar{s}_i. \tag{4.26}$$

where $\bar{s}_i$ is the soft decision of s_i based on the *a priori* probability, and defined in (4.6).

2. Linear MMSE filtering:

$$z_k = \boldsymbol{m}_k^H \boldsymbol{y}_k, \tag{4.27}$$

where $\boldsymbol{m}_k = P_k^{-1}\boldsymbol{h}_k$ is the linear MMSE filter, and

$$P_k = HDH^H + N_0 I_{n_R} + \bar{s}_k^2 \boldsymbol{h}_k \boldsymbol{h}_k^H,$$

where I_{n_R} is $n_R \times n_R$ identity matrix, and D is defined in (4.5).

3. Extrinsic information calculation:

$$\lambda_k^{12} = \frac{4 \cdot \mathrm{Re}\{z_k\}}{1 - \boldsymbol{m}_k^H \boldsymbol{h}_k}. \tag{4.28}$$

Fig. 4.3 shows the bit-error-rate (BER) performance versus bit SNR for BPSK modulation. It is seen that the proposed OSSIC detector has the same performance as the MAP detector and comes within about 0.6 dB of the Shannon limit at BER of 10^{-4}. Such remarkable result tells us that together with very strong error-control codes, our proposed detector can achieve the "optimal" performance with low computational complexity at the order of $\mathcal{O}(N^3)$. An intuitive explanation is as follows. Strong error-control codes make the symbol error probability drop so quickly that the soft information of coded bits provided by the channel decoder is almost all correct, and the proposed detector can use this *a priori* information together with the likelihood information from received data to almost perfectly cancel the interferences. Compared with SIC+MMSE method, the proposed OSSIC detector has about 0.2 dB advantage at BER of 10^{-4} with the same computational complexity.

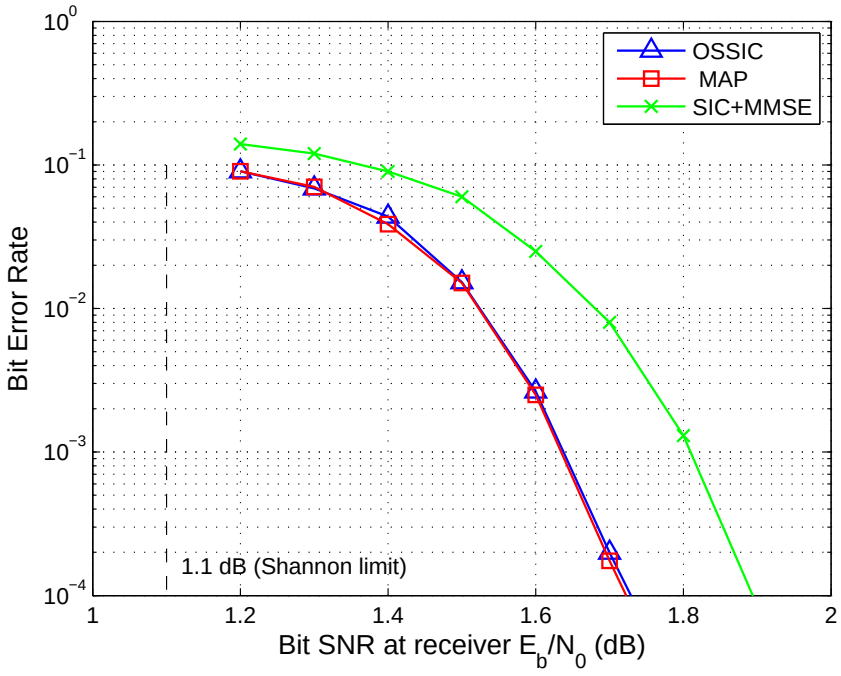

Figure 4.3 BER of the iterative detection and decoding using proposed OSSIC detector, MAP detector and SIC+MMSE detector for MIMO systems with BPSK modulation.

The BER performance for 16-QAM modulation is shown in Fig. 4.4. We observe that the proposed OSSIC detector comes within 2.2 dB of the Shannon limit, and even 0.1 dB better than the LSD detector at BER of 10^{-4}. Compared with SIC+MMSE detector, the advantage of the proposed detector can reach 0.5 dB. Since the LSD detector's performance is close to the one of the MAP detector, we conclude that our proposed OSSIC detector can achieve near-optimal performance with much lower complexity for 16-QAM modulation.

4.6 Summary

In this paper, we studied an iterative detection and decoding scheme for coded MIMO systems. We proposed a low-complexity nulling/ canceling detector using soft interference cancellation and ordering strategy based on *a posteriori* probability. Using the modified square-root algorithm, the complexity of the proposed detector was reduced to $\mathcal{O}(N^3)$ per iteration.

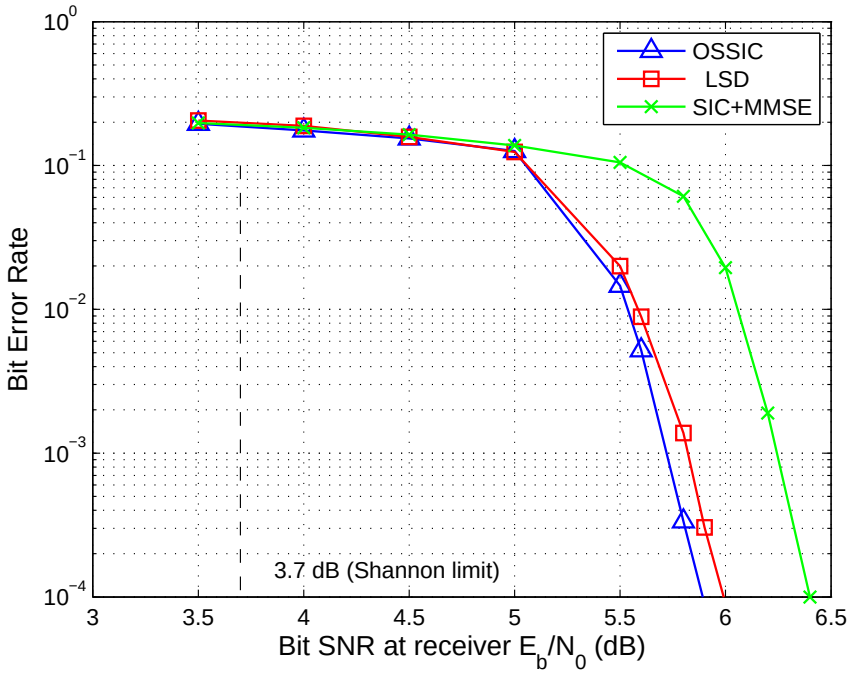

Figure 4.4 BER of the iterative detection and decoding using proposed OSSIC detector, LSD detector and SIC+MMSE detector for MIMO systems with 16-QAM modulation.

Computer simulation results show that for a 4×4 system our proposed detector had the same performance as the MAP detector for BPSK modulation, and 0.1 dB advantage over the approximated MAP detector (LSD detector) for 16-QAM modulation at BER $= 10^{-4}$.

CHAPTER 5. DIVERSITY AND MULTIPLEXING TRADEOFF IN GENERAL FADING CHANNELS

5.1 Introduction

For a wireless link, multiple antennas at both transmitter and receiver can be used to increase the amount of diversity or the number of degrees of freedom. In a seminal work by Zheng and Tse [124], it is shown that the two gains, namely, diversity gain and multiplexing gain, can be simultaneously obtained for a given multi-input multi-output (MIMO) channel, but there is a fundamental tradeoff between them.

Previous works [124, 122, 103] employed the assumption of independent and identically distributed (i.i.d) Rayleigh fading condition to derive the optimal tradeoff result. In practical MIMO communication scenarios, there exist many channel conditions that cannot be accurately modelled by Rayleigh fading. For example, the line-of-sight (LOS) micro-cellular communication channels can be modelled by the Rician distribution [99, 82, 97]. A large number of indoor and outdoor mobile communication channels have been modelled by the Nakagami-m distribution [75, 99, 82, 97]. The Weibull distribution also has gained popularity as a versatile channel model for both indoor and outdoor digital communications [96, 43, 105, 16]. Furthermore, due to the size-limitation at the transmit and/or receive antenna arrays the fading correlation arises [1], which substantially affects the achievable performance of MIMO and space-time coded systems [18, 54, 37]. Therefore, it is of theoretical interest and practical importance to develop a technique to enable the calculation of optimal tradeoff in general fading channel cases. In this work, we extend the previous results to more general fading channel conditions, which includes Rayleigh, Rician, Nakagami-m, Weibull and Nakagami-q fading distributions as special cases. The effects of correlation and non-identical distribution among the

MIMO channel elements, and the non-zero channel mean are also included.

Our technique for this generalization is based on the intuition that the optimal tradeoff performance is determined by the joint probability density function (pdf) of the eigenvalues of the Gram matrix of the MIMO channel, especially the eigenvalue behavior near zeros. Roughly speaking, if the joint pdf of the eigenvalues near zeros can be well approximated by a polynomial, the optimal tradeoff curve (or bounds) can be computed explicitly. This polynomial approximation of the joint pdf becomes accurate for high average signal-to-noise ratios (ASNRs), which is considered here to derive new tradeoff result for generalized fading channels.

Notations: Bold letters denote random variables, vectors, or matrices; plain letters denote the corresponding realizations or constants; I_m denotes $m \times m$ identity matrix; superscripts $(\cdot)^*$, $(\cdot)^T$, and $(\cdot)^\dagger$ denote scalar complex conjugate, vector and matrix transpose and conjugate transpose, respectively. $||\cdot||_F$ denotes the Frobenius norm. Unless otherwise indicated, the (i,j)th entry of matrix H is denoted by h_{ij}. As in [124, 103], we use bold-faced symbols to denote random variables and matrices.

5.2 System Model

We consider a wireless link with n_T transmit and n_R receive antennas. The fading coefficient $\boldsymbol{h}_{ij}$ is the complex path gain from transmit antenna j to receive antenna i. We assume that the coefficients are i.i.d random variables, and write $\boldsymbol{H} = [\boldsymbol{h}_{ij}] \in \mathcal{C}^{n_R \times n_T}$. More general cases (non-i.i.d fading) will be explored in Section 5.6. $\boldsymbol{H}$ is assumed to be known at the receiver, but unknown at the transmitter. We also assume that $\boldsymbol{H}$ remains constant within a block of l symbols, then the received data within one block can be written as

$$\boldsymbol{Y} = \sqrt{\frac{\rho}{n_T}}\boldsymbol{H}\,\boldsymbol{X} + \boldsymbol{W}, \tag{5.1}$$

where $\boldsymbol{X} \in \mathcal{C}^{n_T \times l}$ is the transmitted codeword, the additive noise matrix $\boldsymbol{W}$ has independent circular symmetric complex Gaussian distributed entries $\boldsymbol{w}_{ij} \sim \mathcal{CN}(0,1)$, and ρ controls the signal-to-noise ratio (SNR).

	pdf	a	b	c	t	β
Rayleigh	$\frac{1}{\pi\Omega}e^{-\frac{\lvert h\rvert^2}{\Omega}}$	$\frac{1}{\pi\Omega}$	$\frac{1}{\Omega}$	0	0	2
Rician	$\frac{1}{\pi\Omega}e^{-\frac{\lvert h-\mu\rvert^2}{\Omega}}$	$\frac{1}{\pi\Omega}$	$\frac{1}{\Omega}$	μ	0	2
Nakagami-m	$\frac{m^m\lvert h\rvert^{2m-2}}{\pi\Omega^m\Gamma(m)}e^{-\frac{m\lvert h\rvert^2}{\Omega}}$	$\frac{m^m}{\pi\Omega^m\Gamma(m)}$	$\frac{m}{\Omega}$	0	$2m-2$	2
Weibull	$\frac{\alpha\Omega^{-\alpha}}{2\pi}\lvert h\rvert^{\alpha-2}e^{-(\frac{\lvert h\rvert}{\Omega})^\alpha}$	$\frac{\alpha\Omega^{-\alpha}}{2\pi}$	$\Omega^{-\alpha}$	0	$\alpha-2$	α
Nakagami-q	$\frac{(1+q^2)}{2\pi q\Omega}I_0(\frac{(1-q^4)\lvert h\rvert^2}{4q^2\Omega})e^{-\frac{(1+q^2)^2}{4q^2\Omega}\lvert h\rvert^2}$	See Section 5.6.1				

Table 5.1 Pdf of different fading channels.

We find that the pdf of the complex-valued fading coefficient $\boldsymbol{h}_{ij}$ for many fading types may be written as

$$p_{\boldsymbol{h}}(h) = a|h|^t e^{-b|h-c|^\beta}, \tag{5.2}$$

where $a > 0$, $b > 0$, $\beta > 0$, $t \in \mathcal{R}$, and $c \in \mathcal{C}$ are constants. This model is valid for many frequently used fading channels, including Rayleigh, Rician, Nakagami-m, Weibull, and Nakagami-q distribution. The corresponding parameters a, b, c, t and β are listed in Table 5.1.

We also make the following assumptions:

- For Nakagami-m, Weibull and Nakagami-q fading channels, the amplitude and the phase of fading coefficients are independent, and the phase is uniformly distributed over $[0, 2\pi)$;
- The average power of fading channel coefficients is normalized to 1, i.e., $\mathrm{E}\{\mathrm{tr}[\boldsymbol{H}^\dagger\boldsymbol{H}]\} = n_R n_T$;
- $t \geqslant 0$, i.e., $m \geqslant 1$ for the Nakagami-m fading channel, $\alpha \geqslant 2$ for Weibull fading channel, and $0 < q \leqslant 1$ for the Nakagami-q fading channel.

Since $\boldsymbol{H}$ has i.i.d elements, the pdf of $\boldsymbol{H}$ can be written as

$$p_{\boldsymbol{H}}(H) = \prod_{i=1}^{n_R}\prod_{j=1}^{n_T} a|h_{ij}|^t \cdot \exp\big(-b|h_{ij}-c|^\beta\big). \tag{5.3}$$

A codebook $\mathcal{C}$ of rate R bits per channel use (bpcu) has $|\mathcal{C}| = \lfloor 2^{Rl} \rfloor$ codewords $\{X(1), ..., X(|\mathcal{C}|)\}$. We further assume a power constraint on the codebook $\mathcal{C}$:

$$\frac{1}{|\mathcal{C}|}\sum_{i=1}^{|\mathcal{C}|} ||X(i)||_F^2 \leqslant n_T l, \tag{5.4}$$

so that ρ in (5.1) is the average transmit power, regardless of the value of n_T.

The following definitions were introduced in [124]:

Definition 1: The special symbol $\doteq$ denotes *exponential equality*, i.e., we write $f(\rho) \doteq \rho^b$ to denote

$$\lim_{\rho\to\infty} \frac{\log f(\rho)}{\log \rho} = b, \tag{5.5}$$

and $\dot{\geqslant}$, $\dot{\leqslant}$ are similarly defined.

Definition 2: A *scheme* is a family of codes $\{\mathcal{C}(\rho)\}$ of block length l, one at each transmit power level. $R(\rho)$ is the rate of the code $\mathcal{C}(\rho)$.

Definition 3: A scheme $\{\mathcal{C}(\rho)\}$ is said to achieve *spatial multiplexing gain* r and *diversity gain* d if the data rate $R(\rho)$ and the average error probability $P_e(\rho)$ satisfy the following equalities, respectively,

$$\lim_{\rho\to\infty} \frac{R(\rho)}{\log \rho} = r, \tag{5.6}$$

$$P_e(\rho) \doteq \rho^{-d}. \tag{5.7}$$

For each r, we define $d^*(r)$ as the supremum of the diversity gain achieved over all schemes.

5.3 Mathematical Prerequisite on Random Matrices

In this section, we present some important results on random matrices without proof. Interested readers can refer to [74] and [27].

For a nonsingular matrix $\boldsymbol{H} \in \mathcal{C}^{m\times n}$ $(m \leqslant n)$ with pdf $p_{\boldsymbol{H}}(H)$, there is a unique LQ factorization

$$\boldsymbol{H} = \boldsymbol{L}\boldsymbol{Q}, \tag{5.8}$$

where $\boldsymbol{L} \in \mathcal{C}^{m\times m}$ is upper-triangular with positive diagonal elements and $\boldsymbol{Q} \in \mathcal{C}^{m\times n}$ with $\boldsymbol{Q}\boldsymbol{Q}^\dagger = I_m$. If $\boldsymbol{H}$ is random, the pdf of $\boldsymbol{L}$ can be written as

$$p_{\boldsymbol{L}}(L) = \prod_{i=1}^{m} l_{ii}^{2n-2i+1} \cdot \int_{V_{m,n}} p_{\boldsymbol{H}}(LQ)dQ, \tag{5.9}$$

where $V_{m,n}$ is the complex Stiefel manifold, i.e., a sub-manifold of m by n complex matrices $\boldsymbol{Q}$ such that $\boldsymbol{Q}\boldsymbol{Q}^\dagger = I_m$, and the dimension of $V_{m,n}$ is $2mn - m^2$.

Let

$$\boldsymbol{W} \equiv \boldsymbol{H}\boldsymbol{H}^{\dagger} = \boldsymbol{L}\boldsymbol{L}^{\dagger}, \tag{5.10}$$

then the pdf of $\boldsymbol{W}$ is

$$\begin{aligned} p_{\boldsymbol{W}}(W) &= \left(2^{-m} \prod_{i=1}^{m} l_{ii}^{2i-2m-1} p_{\boldsymbol{L}}(L) \right) \Bigg|_{LL^{\dagger}=W} \\ &= \left(2^{-m} |\det W|^{n-m} \cdot \int_{V_{m,n}} p_H(LQ) dQ \right) \Bigg|_{LL^{\dagger}=W}. \end{aligned} \tag{5.11}$$

Since $\boldsymbol{H}$ is nonsingular, $\boldsymbol{W} \in \mathcal{C}^{m\times m}$ has full rank of m. Thus, there is a unique eigenvalue decomposition of $\boldsymbol{W}$ as

$$\boldsymbol{W} = \boldsymbol{U}\boldsymbol{\Lambda}\boldsymbol{U}^{\dagger}, \tag{5.12}$$

if we assume the diagonal elements of $\boldsymbol{\Lambda}$ are ordered non-decreasingly and the first row of the unitary matrix $\boldsymbol{U}$ is real and non-negative. Then, we have the pdf of $\boldsymbol{\Lambda}$ as

$$p_{\boldsymbol{\Lambda}}(\Lambda) = \frac{1}{(2\pi)^m} \prod_{i<j} (\lambda_i - \lambda_j)^2 \cdot \int_{V_{m,m}} p_{\boldsymbol{W}}(U\Lambda U^{\dagger}) dU. \tag{5.13}$$

The factor $\frac{1}{(2\pi)^m}$ comes from the fact that we assume the first row of U is non-negative and integrate U over the whole manifold $V_{m,m}$.

We know that

$$\boldsymbol{L}\boldsymbol{L}^{\dagger} = \left(\boldsymbol{U}\boldsymbol{\Lambda}^{1/2}\right)\left(\boldsymbol{U}\boldsymbol{\Lambda}^{1/2}\right)^{\dagger},$$

and $\boldsymbol{L}$ is unique for a given $\boldsymbol{H}$, hence there is a unique unitary matrix $\boldsymbol{Q}_1 \in \mathcal{C}^{m\times m}$ for the given $\boldsymbol{H}$ such that

$$\boldsymbol{L} = \boldsymbol{U}\boldsymbol{\Lambda}^{1/2}\boldsymbol{Q}_1. \tag{5.14}$$

Combining (5.11), (5.13) and (5.14), we obtain

$$\begin{aligned} p_{\boldsymbol{\Lambda}}(\Lambda) &= \frac{1}{(4\pi)^m} \left(\prod_{i=1}^{m} \lambda_i^{n-m} \right) \cdot \prod_{i<j} (\lambda_i - \lambda_j)^2 \cdot \int_{V_{m,m}} \int_{V_{m,n}} p_H(U\Lambda^{1/2} Q_1 Q) dQ dU \\ &= \frac{1}{(4\pi)^m} \left(\prod_{i=1}^{m} \lambda_i^{n-m} \right) \cdot \prod_{i<j} (\lambda_i - \lambda_j)^2 \cdot \int_{V_{m,m}} \int_{V_{m,n}} p_H(U\Lambda^{1/2} Q) dQ dU, \end{aligned} \tag{5.15}$$

the second equality follows from the fact that the measure defined by dQ is invariant under unitary transformations.

5.4 Outage Formulation

Consider a non-ergodic fading channel model

$$\boldsymbol{y}_i = \sqrt{\frac{\rho}{n_T}}\boldsymbol{H}\boldsymbol{x}_i + \boldsymbol{w}_i, \quad \text{for } i = 1, 2, \ldots, \infty, \tag{5.16}$$

where $\boldsymbol{x}_i \in \mathcal{C}^{n_T}$, $\boldsymbol{y}_i \in \mathcal{C}^{n_R}$, and $\boldsymbol{w}_i \in \mathcal{C}^{n_R}$ are the transmitted data, received data, and additive white Gaussian noise at time i. The channel matrix $\boldsymbol{H}$ is chosen randomly but is held fixed for all time.

An *outage* is defined as the event that the mutual information of this channel does not support a target data rate R [102]. Without loss of optimality, the input distribution can be taken to be complex Gaussian with a covariance matrix C_{xx}, then

$$I(\boldsymbol{x}_i; \boldsymbol{y}_i | \boldsymbol{H} = H) = \log\det\left(I_{n_R} + \frac{\rho}{n_T} H C_{xx} H^\dagger\right). \tag{5.17}$$

Optimizing over all input distributions that satisfy the average power constraint, the outage probability is

$$P_{\text{out}}(R) = \inf_{C_{xx} \succcurlyeq 0, \mathrm{Tr}(C_{xx}) \leqslant n_T} P\left[\log\det\left(I_{n_R} + \frac{\rho}{n_T}\boldsymbol{H} C_{xx} \boldsymbol{H}^\dagger\right) < R\right], \tag{5.18}$$

where the probability is taken over the random channel matrix $\boldsymbol{H}$. It is shown in [124] that

$$P_{\text{out}}(R) \doteq P\left[\log\det(I_{n_R} + \rho \boldsymbol{H}\boldsymbol{H}^\dagger) < R\right]. \tag{5.19}$$

We assume, without loss of generality, that $n_R \leqslant n_T$. This is because

$$\log\det\left(I_{n_R} + \frac{\rho}{n_T}\boldsymbol{H}\boldsymbol{H}^\dagger\right) = \log\det\left(I_{n_T} + \frac{\rho}{n_T}\boldsymbol{H}^\dagger\boldsymbol{H}\right).$$

hence, swapping n_R and n_T has no effect on the mutual information, except a scaling factor of n_T/n_R on ρ, which can be ignored on the scale of interest.

Since the elements of $\boldsymbol{H}$ are independent, $\boldsymbol{H}$ has full rank of n_R with probability one. Let $\lambda_1 \leqslant \lambda_2 \leqslant \ldots \leqslant \lambda_{n_R}$ be the nonzero eigenvalues of $\boldsymbol{H}\boldsymbol{H}^\dagger$ and $R = r\log\rho$, we have

$$P_{\text{out}}(r\log\rho) \doteq P\left[\log\det(I_{n_R} + \rho\boldsymbol{H}\boldsymbol{H}^\dagger) < R\right] = P\left[\prod_{i=1}^{n_R}(1+\rho\lambda_i) < \rho^r\right].$$

Let $\lambda_i = \rho^{-\alpha_i}$ and $\alpha = [\alpha_1, \ldots, \alpha_{n_R}]$. It is proved in [124] that

$$P_{\text{out}}(r \log \rho) \doteq P\left[\sum_i (1-\alpha_i)^+ < r\right] = \int_{\mathcal{A}} p_{\boldsymbol{\alpha}}(\alpha) d\alpha, \tag{5.20}$$

where $(x)^+$ denotes $\max\{0, x\}$ and $\mathcal{A} = \{\alpha : \sum_i (1-\alpha_i)^+ < r\}$.

Using (5.15) and change of variables, we obtain the joint pdf of $\boldsymbol{\alpha}$ as

$$p_{\boldsymbol{\alpha}}(\alpha) = \left(\frac{\log \rho}{4\pi}\right)^{n_R} \left(\prod_{i=1}^{n_R} \rho^{-(n_T - n_R + 1)\alpha_i}\right) \cdot \prod_{i<j} (\rho^{-\alpha_i} - \rho^{-\alpha_j})^2 \cdot \int_{V_{n_R, n_R}} \int_{V_{n_R, n_T}} p_{\boldsymbol{H}}(UDQ) dQ dU, \tag{5.21}$$

where $D = \text{diag}[\rho^{-\alpha_1/2}, \ldots, \rho^{-\alpha_{n_R}/2}]$ and

$$p_{\boldsymbol{H}}(UDQ) = \left(\sum_{|\kappa| = 2n_R n_T} c(\kappa, U, Q) [\rho^{-\alpha_1/2}, ..., \rho^{-\alpha_{n_R}/2}]^\kappa\right)^{t/2} a^{n_R n_T} \cdot \exp\Big(-b \sum_{i=1}^{n_R} \sum_{j=1}^{n_T} |h_{ij} - c|^\beta\Big), \tag{5.22}$$

where

- $\kappa = [k_1, ..., k_{n_R}]$ is a partition of $2n_R n_T$, i.e., $|\kappa| = \sum_{i=1}^{n_R} k_i = 2n_R n_T$, and k_i is a non-negative integer for all i;
- $[\rho^{-\alpha_1/2}, ..., \rho^{-\alpha_{n_R}/2}]^\kappa \equiv \prod_{i=1}^{n_R} \rho^{-\alpha_i k_i/2}$;
- $c(\kappa, U, Q)$ is the coefficient of the item $[\rho^{-\alpha_1/2}, ..., \rho^{-\alpha_{n_R}/2}]^\kappa$ in the expansion of $\prod_{i=1}^{n_R} \prod_{j=1}^{n_T} |h_{ij}|^2$, where $H = [h_{ij}] = UDQ$. It is easy to check that all $c(\kappa, U, Q)$'s are real and bounded.

Define

$$g(\rho, U, Q, \alpha) \equiv \sum_{|\kappa| = 2n_R n_T} c(\kappa, U, Q) [\rho^{-\alpha_1/2}, ..., \rho^{-\alpha_{n_R}/2}]^\kappa. \tag{5.23}$$

Combining (5.20), (5.21), and (5.22), we have

$$P_{\text{out}}(r \log \rho) \doteq \int_{\mathcal{A}} \left(\frac{\log \rho}{4\pi}\right)^{n_R} \left(\prod_{i=1}^{n_R} \rho^{-(n_T - n_R + 1)\alpha_i}\right) \cdot \prod_{i<j} (\rho^{-\alpha_i} - \rho^{-\alpha_j})^2 \cdot \left[\int_{V_{n_R, n_R}} \int_{V_{n_R, n_T}} a^{n_R n_T} \left(g(\rho, U, Q, \alpha)\right)^{t/2} \cdot \exp\Big(-b \sum_{i=1}^{n_R} \sum_{j=1}^{n_T} |h_{ij} - c|^\beta\Big) dQ dU\right] d\alpha. \tag{5.24}$$

Since $P_{\text{out}}(r\log\rho) \to 0$ as $\rho \to \infty$, and we are only interested in the ρ exponent of P_{out}, i.e.,

$$\lim_{\rho\to\infty} \frac{\log P_{\text{out}}(r\log\rho)}{\log\rho}, \tag{5.25}$$

thus we can make some approximations to simplify the integral. First, the term $\left(\frac{\log\rho}{4\pi}\right)^{n_R}$ has no effect on the ρ exponent, since

$$\lim_{\rho\to\infty} \frac{\log\left(\frac{\log\rho}{4\pi}\right)^{n_R}}{\log\rho} = 0. \tag{5.26}$$

Secondly, we can ignore the outer integral over the range with any $\alpha_i < 0$ when $\rho \to \infty$, and replace the outer integral range $\mathcal{A}$ with $\mathcal{A}' = \mathcal{A} \bigcap \mathcal{R}^{n^+}$, where $\mathcal{R}^{n^+}$ is the set of real n-vectors with nonnegative elements. Similar intuitive argument is stated in [124]. We give the rigorous proof in Appendix 5.A.

For $\alpha \in \mathcal{A}'$ and $\rho \to \infty$, $|h_{ij}|$ approaches 0, and $\exp(-b|h_{ij}-c|^{\beta})$ approaches a constant, which is independent of ρ for given Q and U. $(g(U,Q,D))^{t/2}$ is a polynomial of ρ, where the coefficients are functions of Q and U. The term with the highest order is $\rho^{-n_R n_T t \alpha_{n_R}/2}$, and the corresponding coefficient is nonzero almost everywhere. Thus, the outage probability can be approximated as

$$P_{\text{out}}(r\log\rho) \doteq \int_{\mathcal{A}'} \prod_{i=1}^{n_R} \rho^{-(n_T-n_R+1)\alpha_i} \cdot \prod_{i<j} (\rho^{-\alpha_i} - \rho^{-\alpha_j})^2 \rho^{-\frac{t}{2} n_R n_T \alpha_{n_R}} d\alpha. \tag{5.27}$$

When $\alpha_i = \alpha_j$ for some i and j, the integrand is zero, so we only need to consider the case that α_i's are distinct. In this case, $|\rho^{-\alpha_i} - \rho^{-\alpha_j}|$ is dominated by $\rho^{-\alpha_j}$ for any $i < j$. Therefore,

$$P_{\text{out}}(r\log\rho) \doteq \int_{\mathcal{A}'} \rho^{-\{\sum_{i=1}^{n_R}(n_T-n_R+2i-1)\alpha_i + \frac{t}{2} n_R n_T \alpha_{n_R}\}} d\alpha. \tag{5.28}$$

Finally, as $\rho \to \infty$, the integral is dominated by the term with the largest ρ exponent. This heuristic calculation is made rigorous in Appendix 5.A and the result is stated in the following theorem.

Theorem 1 *(Outage Probability) For the MIMO channel defined in* (5.1) *and* (5.3)*, let* $n = \min\{n_R, n_T\}$*, and the data rate be* $R = r\log\rho$ *(bpcu), with* $0 \leqslant r \leqslant n$*. The outage probability satisfies*

$$P_{out}(R) \doteq \rho^{-d_{out}(r)}, \tag{5.29}$$

where

$$d_{out}(r) = f(\alpha^*) = \inf_{\alpha \in \mathcal{A}'} f(\alpha), \tag{5.30}$$

and

$$\begin{aligned} f(\alpha) &= \sum_{i=1}^{n_R} (|n_T - n_R| + 2i - 1)\alpha_i + \frac{t}{2} n_R n_T \alpha_{n_R}, \\ \mathcal{A}' &= \Big\{ \alpha : \alpha_1 \geqslant \cdots \geqslant \alpha_n \geqslant 0, \sum_{i=1}^{n} (1 - \alpha_i)^+ < r \Big\}. \end{aligned} \tag{5.31}$$

$d_{out}(r)$ *is given by the piecewise-linear function connecting the points* $(k, d^*(k))$, *for* $k = 0, 1, \ldots, n$, *where*

$$d^*(k) = \begin{cases} (n_R - k)(n_T - k) & \text{if } k = 1, \ldots, n, \\ n_R n_T + \frac{t}{2} n_R n_T & \text{if } k = 0. \end{cases} \tag{5.32}$$

Remark: Compared with the outage probability obtained for i.i.d Rayleigh fading channels in [124], the difference arises from the coefficient of $\alpha_{\min\{n_R, n_T\}}$ in $d_{\text{out}}(r)$, which is $n_R + n_T - 1$ for Rayleigh fading channels and $n_R + n_T - 1 + \frac{t}{2} n_R n_T$ for general fading channels.

5.5 Optimal Tradeoff Curve

The outage probability provides a lower bound on the average error probability for channel defined in (5.1), which is proved by [124, Lemma 5] for i.i.d Rayleigh fading case. Based on Theorem 1, this result still holds for the general channel model defined in this chapter. For convenience, we restate it as follows without proof:

Lemma 1 *(Outage Bound) For the channel defined in* (5.1) *and* (5.3), *let the data rate be scaled as* $R = r \log \rho$ *(bpcu). For any coding scheme, the average error probability is lower-bounded as*

$$P_e(\rho) \dot{\geqslant} \rho^{-d_{out}(r)}, \tag{5.33}$$

where $d_{out}(r)$ *is defined in* (5.30).

With Lemma 1 providing a lower bound on the average error probability, to obtain the ρ exponent of P_e, we only need to derive an upper bound on P_e (a lower bound on the optimal diversity gain).

Consider at data rate $R = r\log\rho$ (bpcu),

$$\begin{aligned} P_e(\rho) =& P_{\text{out}}(R)P(\text{error}|\text{outage}) + P(\text{error, no outage}) \\ \leqslant& P_{\text{out}}(R) + P(\text{error, no outage}). \end{aligned} \tag{5.34}$$

By choosing the input to be the random code from the i.i.d Gaussian ensemble, the second term in (5.34) can be upper-bounded via a union bound [124]:

$$P(\text{error, no outage}) \dot{\leqslant} \int_{\mathcal{A}^c} p_{\boldsymbol{\alpha}}(\alpha)\rho^{-l[\sum_{i=1}^{\min\{n_R,n_T\}}(1-\alpha_i)^+ - r]}d\alpha. \tag{5.35}$$

Notice that $\mathcal{A}^c$ as the integral region is more strict than $(\mathcal{A}')^c$ used in [124]. The ρ exponent of the integral is stated in the following lemma and proved in Appendix 5.B.

Lemma 2 *For the MIMO channel defined in* (5.1) *and* (5.3)*, let* $n = \min\{n_R, n_T\}$*, and the data rate be* $R = r\log\rho$ *(bpcu), with* $0 \leqslant r \leqslant n$*. The average error probability when no channel outage occurs satisfies:*

$$P(\textit{error, no outage}) \dot{\leqslant} \rho^{-d_G(r)}, \tag{5.36}$$

where

$$d_G(r) = d_G(r, \alpha^*) = \inf_{\alpha \in \mathcal{A}^c \bigcap \mathcal{R}^{n^+}} d_G(r, \alpha), \tag{5.37}$$

and

$$\begin{aligned} d_G(r,\alpha) &= \sum_{i=1}^{n}(2i - 1 + |n_T - n_R|)\alpha_i + \frac{t}{2}n_R n_T \alpha_n + l\Big(\sum_{i=1}^{n}(1-\alpha_i)^+ - r\Big), \\ \mathcal{A}^c \bigcap \mathcal{R}^{n^+} &= \left\{\alpha : \alpha_1 \geqslant \ldots \geqslant \alpha_n \geqslant 0, \sum_{i=1}^{n}(1-\alpha_i)^+ \geqslant r\right\}. \end{aligned} \tag{5.38}$$

For convenience, we call a system with n_T transmit, n_R receive antennas, and a block length l as an (n_T, n_R, l) system. Combining the results from Theorem 1, Lemma 1, and Lemma 2, we can see that given a multiplexing gain r, the optimal diversity gain is bounded by $\min\{d_G(r), d_{\text{out}}(r)\} \leqslant d^*(r) \leqslant d_{\text{out}}(r)$. Whether the optimal tradeoff curve $d^*(r)$ can be exactly characterized or not wholly depends on the relation among n_T, n_R, l and t as we conclude in Theorem 2 and Theorem 3.

Theorem 2 *For an* (n_T, n_R, l) *system defined by channel model* (5.1) *and* (5.3) *with* $l \geqslant n_T + n_R - 1 + n_T n_R t/2$*, the optimal tradeoff curve* $d^*(r)$ *is given by the piecewise-linear function*

connecting the points $(k, d^*(k))$, $k = 0, 1, ..., \min\{n_R, n_T\}$, *where*

$$d^*(k) = \begin{cases} (n_R - k)(n_T - k) & \text{if } k = 1, \ldots, \min\{n_R, n_T\}, \\ n_R n_T + \frac{t}{2} n_R n_T & \text{if } k = 0. \end{cases} \tag{5.39}$$

In particular, $d^*_{\max} = n_R n_T + \frac{t}{2} n_R n_T$ *and* $r^*_{\max} = \min\{n_R, n_T\}$

Proof: This is a direct result of Theorem 1, Lemma 1, and Lemma 2. □

Theorem 3 *For an* (n_T, n_R, l) *system defined by channel model* (5.1) *and* (5.2) *with* $l < n_T + n_R - 1 + n_T n_R t/2$, *the optimal tradeoff curve* $d^*(r)$ *is upper bounded by* $d_{out}(r)$ *and lower bounded by* $d_G(r)$. *Let*

$$k_1 = \min\left\{ \left\lceil \frac{l - |n_R - n_T| - 1}{2} \right\rceil, \min\{n_R, n_T\} - 1 \right\}. \tag{5.40}$$

For $\min\{n_R, n_T\} - k_1 < r \leqslant \min\{n_R, n_T\}$, $d_G(r)$ *agrees with the upper bound* $d_{out}(r)$ *; For* $0 \leqslant r \leqslant \min\{n_R, n_T\} - k_1$, $d_G(r)$ *is linear with slope* $-l$ *and is strictly below* $d_{out}(r)$.

The proof of Theorem 3 is similar to the one in [124, Section IV-A], and omitted here due to space limitation.

Remark: It is interesting to notice that the optimal tradeoff curve (or bounds) only depends on parameter t and not on a, b, c, β. This statement also holds for non i.i.d cases as discussed in Section 5.6.

As an example, in Figs. 5.1 -5.3, tradeoff curves are plotted for systems with $n_R = n_T = 4$, i.i.d Nakagami-m fading ($m = 1.5$) and block length $l = 1, 10, 15$, compared with the curves for i.i.d Rayleigh case. As indicated by Fig. 5.1, when the block length is short for both Nakagami-m and Rayleigh cases, their lower bounds are the same but Nakagami-m case yields a higher upper bound; When block length is long enough for Rayleigh case but still short for Nakagami-m case, the upper and lower bounds for Rayleigh case are exactly the same while the lower bound of Nakagami-m case is no less than that of Rayleigh case as shown in Fig. 5.2. Fig. 5.3 illustrates the tradeoff curves when the block length is long for both cases. The upper and lower bounds for either of the two channels are identical, thus exactly characterize the channel. We observe that, although the Nakagami-m case has a higher tradeoff curve when

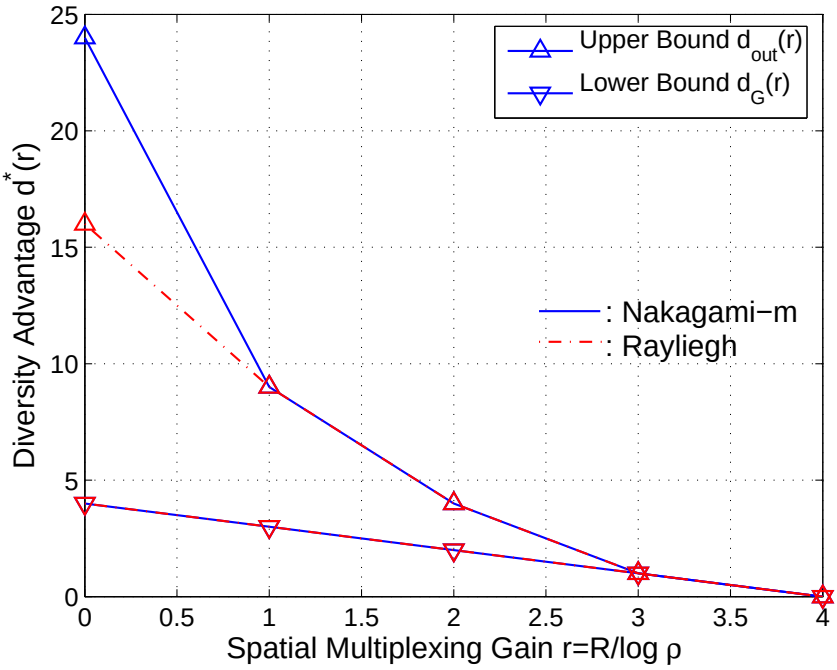

Figure 5.1 The bounds of optimal tradeoff curves for a (4, 4, 1) system over Rayleigh and Nakagami-m ($m = 1.5$) fading channels

$0 < r \leqslant 1$, it yields the same result when $r > 1$ as the Rayleigh case. In general, different fading models only affect the first segment of the optimal tradeoff curve (or bounds), compared with the results in [124].

5.6 Discussion and Extension

As stated in the introduction, the optimal tradeoff curve is determined by the behavior of $p_{\boldsymbol{\Lambda}}(\Lambda)$ near zeros. The i.i.d fading condition assumed in the previous sections is not a necessary condition to have $p_{\boldsymbol{\Lambda}}(\Lambda)$ decrease in a polynomial fashion as $\Lambda \to \mathbf{0}$, which is required to calculate the optimal tradeoff curve explicitly by the technique we developed. In this section, we will extend our result to some more general and practical models.

5.6.1 Nakagami-q Channel

The zeroth-order modified Bessel function of the first kind $I_0(x)$ satisfies:

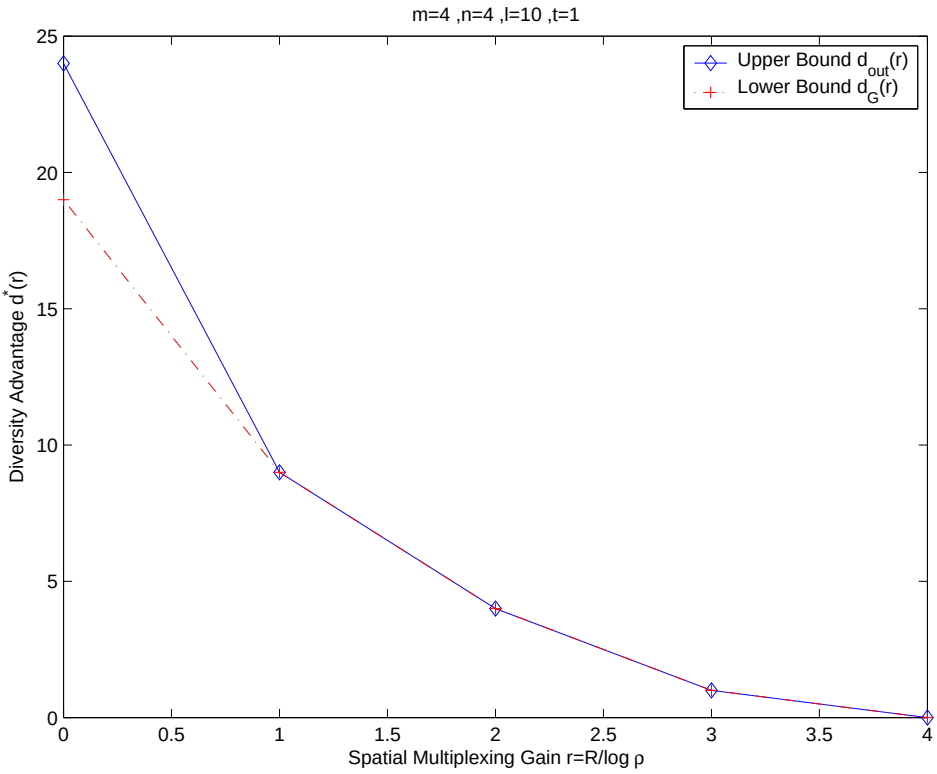

Figure 5.2 The bounds of optimal tradeoff curves for a (4, 4, 10) system over Rayleigh and Nakagami-m ($m = 1.5$) fading channels

$$1 \leqslant I_0(x) = \sum_{k=0}^{\infty} \frac{(x/2)^{2k}}{k!k!} \leqslant \left(\sum_{k=0}^{\infty} \frac{(x/2)^k}{k!} \right)^2 = e^x.$$

Thus for Nakagami-q model, where

$$p_{\boldsymbol{h}}(h) = \frac{(1+q^2)}{2\pi q\Omega} I_0\Big(\frac{(1-q^4)|h|^2}{4q^2\Omega}\Big) e^{-\frac{(1+q^2)^2}{4q^2\Omega}|h|^2},$$

we can use the parameters in Table 5.2 to construct a lower and an upper bounds on $p_{\boldsymbol{h}}(h)$, which are easily integrated into our framework. Therefore, the results obtained in Section 5.5 are also applicable for Nakagami-q fading channels. Note that the optimal tradeoff depends only on the t parameters, which is 0 in this case for both lower and upper bounds. As a result, the optimal tradeoff performance of Nakagami-q channels is the same as that of Rayleigh channels.

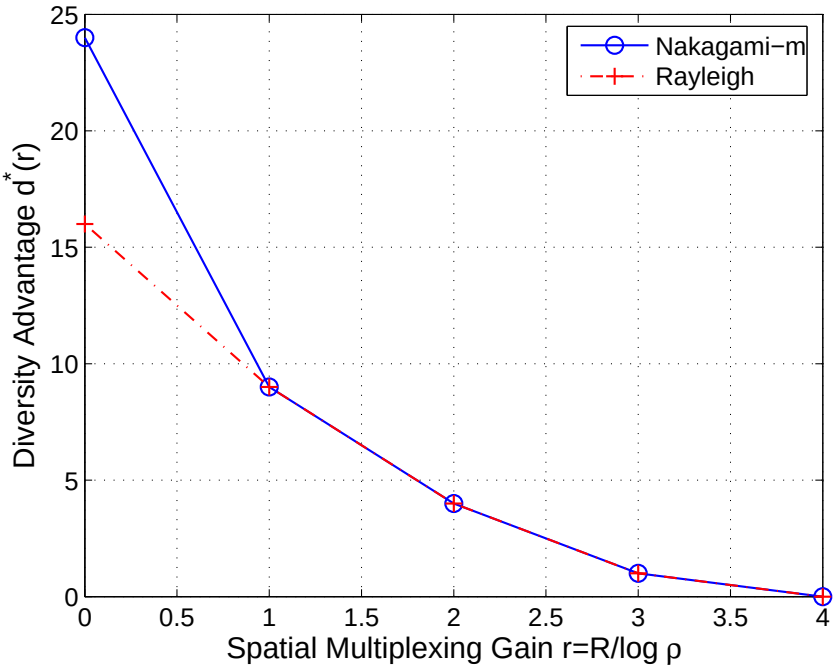

Figure 5.3 Optimal tradeoff curves for a (4, 4, 15) system over Rayleigh and Nakagami-m ($m = 1.5$) fading channels

	pdf	a	b	c	t	β
Lower Bound	$\frac{(1+q^2)^2}{2\pi q\Omega} e^{-\frac{(1+q^2)}{4q^2\Omega}\lvert h\rvert^2}$	$\frac{(1+q^2)}{2q\pi\Omega}$	$\frac{(1+q^2)^2}{4q^2\Omega}$	0	0	2
Upper Bound	$\frac{(1+q^2)}{2\pi q\Omega} e^{-\frac{(1+q^2)}{2\Omega}\lvert h\rvert^2}$	$\frac{(1+q^2)}{2q\pi\Omega}$	$\frac{(1+q^2)}{2\Omega}$	0	0	2

Table 5.2 Lower and Upper bounds on $p_{\boldsymbol{h}}(h)$ for Nakagami-q fading channels.

5.6.2 Independent Non-Identical Distribution

As defined in (5.3), we assume that $\boldsymbol{h}_{ij}$ are i.i.d random variables. In fact, if $\boldsymbol{h}_{ij}$'s are just independent random variables following the same model defined in (5.2), but have different parameters a, b, c, t and β, similar results can be drawn as stated in the following theorem.

Theorem 4 *Suppose that the channel matrix* $\boldsymbol{H}$ *in* (5.1) *has independently non-identically distributed elements* $\boldsymbol{h}_{ij}$*, whose pdf has the form of*

$$p_{\boldsymbol{h}_{ij}}(h) = a_{ij}|h|^{t_{ij}} e^{-b_{ij}|h-c_{ij}|^{\beta_{ij}}}, \tag{5.41}$$

where $a_{ij} > 0$, $b_{ij} > 0$, $\beta_{ij} > 0$, $t_{ij} \geqslant 0$, *and* $c_{ij} \in \mathcal{C}$ *are constants. Then the optimal*

diversity and multiplexing tradeoff curves (or bounds) can be obtained by replacing $\frac{t}{2}n_R n_T$ *with* $\sum_{i=1}^{n_R}\sum_{j=1}^{n_T} t_{ij}/2$ *in Theorems 2 and 3.*

The outline of the proof is given as following:

1. It is easy to check that for the proofs given in the Appendices for the i.i.d case, changing c to c_{ij} for different fading path will not affect the procedure and the result of each proof.

2. Changing a to a_{ij} for different fading path will not affect the result of each proof. When a_{ij}'s are constants, it is obvious. For Nakagami-q model, notice that the constructed lower and upper bounds on $p_{\boldsymbol{h}}(h)$ in Table 5.2 have the same parameter a which is a constant.

3. When changing b to b_{ij}, we can use $\min\{b_{ij}\}$ and $\max\{b_{ij}\}$ to construct the upper and lower bounds on $p_{\boldsymbol{h}}(h)$ which have the same parameter t. Thus the results still hold.

4. When we change t to t_{ij} for different fading path, instead of constructing lower and upper bound on $g(\rho, U, Q, \alpha)$, we can construct those bounds for each $|h_{ij}|^{t_{ij}}$ with the similar method. And this will results in the replacement of $\frac{t}{2}n_R n_T$ by $\sum_{i=1}^{n_R}\sum_{j=1}^{n_T} t_{ij}/2$ in each proof.

5. It is easy to verify that changing β to β_{ij} for different fading path will not alter the proof of ρ exponent of I_1 in Appendix 5.A. For the ρ exponent of I_2 in Appendix 5.A, notice that

$$|h_{ij}|^{\beta_{ij}} \geqslant \begin{cases} |h_{ij}|^{\min_{ij}\beta_{ij}} - 1 & |h_{ij}| < 1 \\ |h_{ij}|^{\min_{ij}\beta_{ij}} & |h_{ij}| \geqslant 1 \end{cases},$$

   so we have

$$\sum_{i,j}\left(\frac{|h_{ij}|}{2}\right)^{\beta_{ij}} \geqslant \sum_{i,j}\left(\frac{|h_{ij}|}{2}\right)^{\min_{i,j}\beta_{ij}} - n_R n_T$$

   Then applying (5.56), the result of I_2 still holds in this case. Similar argument is also applicable for the proof of Lemma 2.

5.6.3 Effect of Correlation

We assume that the correlation can be decoupled as the transmit correlation and receive correlation, i.e. $\boldsymbol{H} = \Sigma_1^{1/2}\widetilde{\boldsymbol{H}}\Sigma_2^{1/2}$, where $\widetilde{\boldsymbol{H}}$ has independent elements with pdf $p_{\widetilde{\boldsymbol{H}}}(\cdot)$, Σ_1 is the receive covariance matrix, and Σ_2 is the transmit covariance matrix. Assume that both covariance matrices are of full rank. Notice

$$p_{\boldsymbol{H}}(H) = (\det \Sigma_1)^{-n_T}(\det \Sigma_2)^{-n_R} p_{\widetilde{\boldsymbol{H}}}(\Sigma_1^{-1/2} H \Sigma_2^{-1/2}), \tag{5.42}$$

then combining (5.42) with (5.15), we have

$$\begin{aligned} p_{\boldsymbol{\Lambda}}(\Lambda) =& \det(\Sigma_1)^{-n_T} \det(\Sigma_2)^{-n_R}(4\pi)^{-n_R} \cdot \prod_{i=1}^{n_R} \lambda_i^{n_T - n_R} \cdot \prod_{i<j}(\lambda_i - \lambda_j)^2 \\ & \cdot \int_{V_{m,m}} \int_{V_{m,n}} p_{\widetilde{\boldsymbol{H}}}(\Sigma_1^{-1/2} U \Lambda^{1/2} Q \Sigma_2^{-1/2}) dQ dU. \end{aligned} \tag{5.43}$$

For $\Sigma_1^{-1/2} U \Lambda^{1/2} Q \Sigma_2^{-1/2}$, each element of it is still a linear combination of $[\rho^{-\alpha_1/2}, ..., \rho^{-\alpha_{n_R}/2}]^\kappa$ and the coefficients are bounded. Thus we expect the optimal tradeoff curve not to change, which is proved in Appendix 5.C. The result is summarized in the following theorem.

Theorem 5 *Suppose that the channel matrix $\boldsymbol{H}$ in (5.1) can be decoupled as $\Sigma_1 \widetilde{\boldsymbol{H}} \Sigma_2$, where $\widetilde{\boldsymbol{H}}$ has independent elements distributed according to (5.41), Σ_1 and Σ_2 are the covariance matrices at the receiver and the transmitter, respectively, both of full rank. Then $d_{out}(r)$ and $d_G(r)$ of this channel are the same as those of a MIMO system with channel $\widetilde{\boldsymbol{H}}$. The optimal diversity and multiplexing tradeoff curve (or bounds) for channel $\boldsymbol{H}$ is the same as that for $\widetilde{\boldsymbol{H}}$, which can be characterized using Theorem 4.*

5.6.4 Effect of Channel Mean

In Table 5.1, the only model with a non-zero channel mean is the Rician channel. For both Rayleigh and Rician channels, the parameter t is 0. Therefore, for a fading coefficient $\boldsymbol{h}_{ij}$ with complex Gaussian distribution, its channel mean will not affect the optimal tradeoff curve of the whole channel.

For other models where $t_{ij} \neq 0$, adding a channel mean $\overline{h}_{ij}$, i.e., $\boldsymbol{h}_{ij} = \widetilde{\boldsymbol{h}}_{ij} + \overline{h}_{ij}$, where $p_{\widetilde{\boldsymbol{h}}_{ij}}(h) = a_{ij}|h|^{t_{ij}} e^{-b_{ij}|h-0|^{\beta_{ij}}}$, results in the pdf of the fading coefficient $\boldsymbol{h}_{ij}$ as

$$p_{\boldsymbol{h}_{ij}}(h) = a_{ij}|h - \overline{h}_{ij}|^{t_{ij}} e^{-b_{ij}|h-\overline{h}_{ij}|^{\beta_{ij}}}.$$

Notice when $|h|$ approaches 0, $p_{\boldsymbol{h}_{ij}}(h)$ will approach a constant instead of $|h|^{t_{ij}}$ in the zero-mean case. Thus this t_{ij} will not be counted in the term $\sum_{i=1}^{n_R}\sum_{j=1}^{n_T} t_{ij}/2$ in the optimal tradeoff as shown in Section 5.6.2. Therefore, for the channel $\boldsymbol{H}$ with a channel mean $\overline{H}$, we should replace $\frac{t}{2}n_R n_T$ in Theorems 2 and 3 by

$$\frac{1}{2}\sum_{(i,j)\in\mathcal{I}} t_{ij}, \tag{5.44}$$

where $\mathcal{I} = \big\{(i,j) : \overline{h}_{ij} = 0\big\}$. In other words, non-zero channel mean of a particular path will degrade this path into a Rayleigh fading path in the calculation of the optimal tradeoff curve (or bounds). The observation here is that the non-zero channel mean will not help improve performance in the sense of optimal diversity-multiplexing tradeoff. We summarize this result in the next theorem and prove it in Appendix 5.D.

Theorem 6 *Suppose that the channel matrix $\boldsymbol{H}$ in (5.1) has the form of $\boldsymbol{H} = \overline{H} + \widetilde{\boldsymbol{H}}$, where $\widetilde{\boldsymbol{H}}$ has independent elements distributed according to (5.41), and $E\{\widetilde{\boldsymbol{H}}\} = 0_{n_R\times n_T}$. Then $d_{out}(r)$ and $d_G(r)$ of channel $\boldsymbol{H}$ are the same as those of a MIMO system with channel matrix $\boldsymbol{B}$ with independent elements such that:*

- *If $\overline{H}_{ij} \neq 0$, $\boldsymbol{B}_{ij}$ has a zero mean complex Gaussian distribution;*
- *if $\overline{H}_{ij} = 0$, $\boldsymbol{B}_{ij}$ has the same distribution as $\widetilde{\boldsymbol{H}}_{ij}$.*

The optimal diversity and multiplexing tradeoff (or bounds) for channel $\boldsymbol{H}$ is the same as that for $\boldsymbol{B}$, which can be characterized using Theorem 4.

5.6.5 Effect of Combination of Channel Mean and Channel Correlation

In fact we can generalize the result in Section 5.6.3 and Section 5.6.4 in one theorem. The proof is similar thus omitted here.

Theorem 7 *Suppose that the channel matrix* $\boldsymbol{H}$ *in* (5.1) *has the form of* $\boldsymbol{H} = \overline{H} + \Sigma_1 \widetilde{\boldsymbol{H}} \Sigma_2$, *where* $\overline{H}$ *is the channel mean;* Σ_1 *and* Σ_2 *are the covariance matrices at the receiver and the transmitter, respectively, both of full rank;* $\widetilde{\boldsymbol{H}}$ *has independent elements distributed according to* (5.41), *and* $E\{\widetilde{\boldsymbol{H}}\} = 0_{n_R \times n_T}$. *Then* $d_{out}(r)$ *and* $d_G(r)$ *of channel* $\boldsymbol{H}$ *are the same as those of a MIMO system with channel matrix* $\boldsymbol{B}$ *with independent elements such that:*

- *If* $\left[\Sigma_1^{-1} \overline{H} \Sigma_2^{-1}\right]_{ij} \neq 0$, $\boldsymbol{B}_{ij}$ *has a zero mean complex Gaussian distribution;*
- *if* $\left[\Sigma_1^{-1} \overline{H} \Sigma_2^{-1}\right]_{ij} = 0$, $\boldsymbol{B}_{ij}$ *has the same distribution as* $\widetilde{\boldsymbol{H}}_{ij}$.

The optimal diversity and multiplexing tradeoff curve (or bounds) for channel $\boldsymbol{H}$ *is the same as that for* $\boldsymbol{B}$, *which can be characterized using Theorem 4.*

5.7 Summary

In this chapter, we derived the optimal multiplexing-diversity tradeoff for general MIMO fading channels, which include different fading types as special cases. We also treated channels with non-identical fading distributions, spatial correlation, and non-zero channel means. We showed that for a (n_R, n_T, l) system with n_R receive antennas, n_T transmit antennas, and encoding block length l, the optimal tradeoff is determined by a set of parameters t_{ij}, $i \in [1, n_R]$, $j \in [1, n_T]$, one for each fading path, describing the near-zero (or deep-fade) behavior of the probability density function of the fading path. The i.i.d Rayleigh fading case considered in [124] corresponds to $t_{ij} = 0$, $\forall i, j$. Compared with the results in [124] for i.i.d. Rayleigh channels, the optimal tradeoff in the general case may be different only on first segment, i.e. for multiplexing gain $r \in [0, 1)$, which suggests that for $r \geq 1$, the optimal tradeoff depends only on the MIMO system array structure, rather than the channel fading types. We proved that under certain full-rank assumptions spatial correlation has no effect on the the optimal tradeoff. We also argued that non-zero channel means in general are not beneficial for multiplexing-diversity tradeoff. These results could facilitate a more comprehensive understanding of the limiting performance of MIMO systems under generalized fading conditions. The techniques

we developed can also be used to analyze the diversity-multiplexing tradeoff in multiple-access and broadcast channels [103] [115].

5.8 Appendix 5.A Proof of Theorem 1

Let $\mathcal{A}' = \mathcal{A} \bigcap \mathcal{R}^{n^+}$ and $\mathcal{A}'' = \mathcal{A} \bigcap \left(\mathcal{R}^{n^+}\right)^c$, where $\left(\mathcal{R}^{n^+}\right)^c$ denotes the compliment of $\mathcal{R}^{n^+}$. Without loss of generality, we assume that $n_R \leqslant n_T$. Then,

$$P_{\text{out}}(r \log \rho) \doteq \int_{\mathcal{A}} p_{\boldsymbol{\alpha}}(\alpha) d\alpha \doteq I_1 + I_2 \doteq \rho^{-d_{\text{out}}(r)}, \tag{5.45}$$

where

$$I_1 = \int_{\mathcal{A}'} p_{\boldsymbol{\alpha}}(\alpha) d\alpha, \qquad I_2 = \int_{\mathcal{A}''} p_{\boldsymbol{\alpha}}(\alpha) d\alpha,$$

and

$$p_{\boldsymbol{\alpha}}(\alpha) = \left(\frac{\log \rho}{4\pi}\right)^{n_R} \prod_{i=1}^{n_R} \rho^{-(n_T - n_R + 1)\alpha_i} \cdot \prod_{i<j} (\rho^{-\alpha_i} - \rho^{-\alpha_j})^2 \cdot \left[\int_{V_{n_R, n_R}} \int_{V_{n_R, n_T}} (g(\rho, U, Q, \alpha))^{t/2} \cdot a^{n_R n_T} \cdot \exp\Big(- b \sum_{i=1}^{n_R} \sum_{j=1}^{n_T} |h_{ij} - c|^{\beta} \Big) dQ dU \right]. \tag{5.46}$$

I. ρ exponent of I_1

First, we study the ρ exponent of I_1. We will construct an upper bound and a lower bound on I_1, and show that they have the same ρ exponents.

Upper bound

Notice that

1. $\exp(-b \sum_{i=1}^{n_R} \sum_{j=1}^{n_T} |h_{ij} - c|^{\beta}) \leqslant 1$.

2. Since $UU^{\dagger} = I$ and $QQ^{\dagger} = I$, it is clear that, $\exists\ 0 < N_2 < \infty$ (independent of Q and U when n_R and n_T are fixed), such that $\sum_{|\kappa| = 2n_R n_T} |c(\kappa, U, Q)| < N_2$. Using the fact that $\sum_{i=1}^{n_R} k_i = 2n_R n_T$ and $\alpha_1 \geqslant \alpha_2 \geqslant \ldots \geqslant \alpha_{n_R}$, we have

$$[\rho^{-\alpha_1/2}, \ldots, \rho^{-\alpha_{n_R}/2}]^{\kappa} = \rho^{-\sum_{i=1}^{n_R} \alpha_i k_i/2} \leqslant \rho^{-n_R n_T \alpha_{n_R}}.$$

Then

$$\begin{aligned} g(\rho, U, Q, \alpha) &= \sum_{|\kappa|=2n_R n_T} c(\kappa, U, Q)[\rho^{-\alpha_1/2}, ..., \rho^{-\alpha_{n_R}/2}]^\kappa \\ &\leqslant \rho^{-n_R n_T \alpha_{n_R}} \cdot \sum_{|\kappa|=2n_R n_T} |c(\kappa, U, Q)| \\ &< N_2 \cdot \rho^{-n_R n_T \alpha_{n_R}}. \end{aligned} \tag{5.47}$$

Based on these observations, the upper bound can be constructed as

$$\begin{aligned} I_1 &\dot{\leqslant} \int_{\mathcal{A}'} \prod_{i=1}^{n_R} \rho^{-(n_T - n_R + 1)\alpha_i} \prod_{i<j} (\rho^{-\alpha_i} - \rho^{-\alpha_j})^2 \rho^{-\frac{t}{2} n_R n_T \alpha_{n_R}} \left(\int_{V_{n_R, n_R}} \int_{V_{n_T, n_R}} dQ dU \right) d\alpha \\ &\dot{\leqslant} \int_{\mathcal{A}'} \prod_{i=1}^{n_R} \rho^{-(n_T - n_R + 1)\alpha_i} \prod_{i<j} (\rho^{-\alpha_j} - 0)^2 \rho^{-\frac{t}{2} n_R n_T \alpha_{n_R}} d\alpha \\ &\doteq \int_{\mathcal{A}'} \rho^{-f(\alpha)} d\alpha, \end{aligned} \tag{5.48}$$

where

$$f(\alpha) = \sum_{i=1}^{n_R} (n_T - n_R + 2i - 1)\alpha_i + \frac{t}{2} n_R n_T \alpha_{n_R}. \tag{5.49}$$

Following the same method used to prove [124, (44)], we obtain

$$\int_{\mathcal{A}'} \rho^{-f(\alpha)} d\alpha \doteq \rho^{-f(\alpha^*)}, \tag{5.50}$$

where $\alpha^* = \arg\inf_{\mathcal{A}'} f(\alpha)$.

Lower bound

Notice that

1. Since $H = UDQ$, $\alpha_1 \geqslant \alpha_2 \geqslant \ldots \geqslant \alpha_{n_R}$, and U,Q are unitary matrices, $\exists\ 0 < M < \infty$ (independent of U and Q when n_R, n_T are fixed), such that $|h|_{ij}^\beta = \left| \sum_{l=1}^{n_R} u_{il} q_{lj} \rho^{-\alpha_l/2} \right|^\beta \leqslant M \cdot \rho^{-\alpha_{n_R}\beta/2}$. Notice

$$|h_{ij} - c|^\beta \leqslant (|h_{ij}| + |c|)^\beta \leqslant 2^\beta (|h_{ij}|^\beta + |c|^\beta),$$

then, the third term in the double integral of (5.46) can be lower bounded as

$$\begin{aligned} \exp(-b \sum_{i=1}^{n_R} \sum_{j=1}^{n_T} |h_{ij} - c|^\beta) &\geqslant \exp(-b 2^\beta \sum_{i=1}^{n_R} \sum_{j=1}^{n_T} |h_{ij}|^\beta - b 2^\beta n_R n_T |c|^\beta) \\ &\geqslant \exp\left(-bMn_r n_t \rho^{-\alpha_{n_R}\beta/2}\right) \exp(-b 2^\beta n_R n_T |c|^\beta). \end{aligned}$$

For $\alpha \in \mathcal{A}'$, $\rho^{-\alpha_i \beta/2} \leqslant 1$ when $\rho > 1$, thus

$$\exp(-b\sum_{i=1}^{n_R}\sum_{j=1}^{n_T}|h_{ij}-c|^{\beta}) \geqslant \exp(-bMn_rn_t)\exp(-b2^{\beta}n_Rn_T|c|^{\beta}). \tag{5.51}$$

2. For any $\delta > 0$, define

$$\mathcal{S}(\delta) \equiv \{\alpha : |\alpha_i - \alpha_j| > \delta, \forall i \neq j\}, \tag{5.52}$$

then $\mathcal{A}' \bigcap \mathcal{S}(\delta) \uparrow \mathcal{A}'$ as $\delta \to 0$.

3. For some $0 < \epsilon < \frac{1}{n_R n_T}$, define

$$\begin{aligned} V'_{n_R,n_T}(\epsilon) &= \left\{ Q \in \mathcal{C}^{n_R \times n_T} : QQ^{\dagger} = I_{n_R}, \quad |q_{n_R j}| \geqslant \epsilon, j = 1, ..., n_T \right\}, \\ V''_{n_R,n_R}(\epsilon) &= \left\{ U \in \mathcal{C}^{n_R \times n_R} : UU^{\dagger} = I_{n_R}, \quad |u_{in_R}| \geqslant \epsilon, i = 1, ..., n_R \right\}, \end{aligned} \tag{5.53}$$

and $\kappa_0 = [0, ..., 0, 2n_Rn_T]$. Given $Q \in V'_{n_R,n_T}(\epsilon)$ and $U \in V''_{n_R,n_R}(\epsilon)$, the coefficient of $\rho^{-n_Rn_T\alpha_{n_R}}$ in the expansion of $g(\rho, U, Q, \alpha)$ can be expressed as

$$c(\kappa_0, U, Q) = \prod_{j=1}^{n_T}\prod_{i=1}^{n_R}|q_{n_R j}|^2|u_{in_T}|^2 \geqslant \epsilon^{4n_Rn_T}.$$

For given $\alpha \in \mathcal{S}(\delta)$, $\exists\ 0 < N_3 < \infty$ (independent of Q and U when n_R and n_T are fixed) such that

$$\begin{aligned} &\Big| \sum_{|\kappa|=2n_Rn_T, \kappa \neq \kappa_0} c(\kappa, U, Q)[\rho^{-\alpha_1/2}, \ldots, \rho^{-\alpha_{n_R}/2}]^{\kappa} \Big| \\ \leqslant &\sum_{|\kappa|=2n_Rn_T, \kappa \neq \kappa_0} \Big| c(\kappa, U, Q) \Big| \cdot [\rho^{-\alpha_1/2}, \ldots, \rho^{-\alpha_{n_R}/2}]^{\kappa} \\ \leqslant &N_3 \cdot \rho^{-n_Rn_T\alpha_{n_R}} \cdot \rho^{-\delta/2}. \end{aligned}$$

Then, we obtain a lower bound on $g(\rho, U, Q, \alpha)$ for given $Q \in V'_{n_R,n_T}(\epsilon)$ and $U \in V''_{n_R,n_R}(\epsilon)$ as

$$\begin{aligned} g(\rho, U, Q, \alpha) =& c(\kappa_0, U, Q)\rho^{-n_Rn_T\alpha_{n_R}} + \sum_{|\kappa|=2n_Rn_T, \kappa \neq \kappa_0} c(\kappa, U, Q)[\rho^{-\alpha_1/2}, \ldots, \rho^{-\alpha_{n_R}/2}]^{\kappa} \\ \geqslant& c(\kappa_0, U, Q)\rho^{-n_Rn_T\alpha_{n_R}} - \Big| \sum_{|\kappa|=2n_Rn_T, \kappa \neq \kappa_0} c(\kappa, U, Q)[\rho^{-\alpha_1/2}, \ldots, \rho^{-\alpha_{n_R}/2}]^{\kappa} \Big| \\ \geqslant& \rho^{-n_Rn_T\alpha_{n_R}} \left(\epsilon^{4n_Rn_T} - N_3 \cdot \rho^{-\delta/2} \right) \qquad \text{when } \rho > 1. \end{aligned} \tag{5.54}$$

It is true that $\forall \delta > 0$, $\epsilon^{4n_R n_T} - N_3 \cdot \rho^{-\delta/2} > 0$, when $\rho > \left(\frac{N_3}{\epsilon^{4n_R n_T}}\right)^{2/\delta}$.

Lemma 3 *Define the topological metric/distance in the complex Stiefel manifold $V_{m,n}$ as*

$$d(Q_1, Q_2) = ||Q_1 - Q_2||_F, \quad \textit{for } Q_1, Q_2 \in V_{m,n}.$$

$\forall Q_0 \in V_{m,n}$ and $\forall r > 0$, the volume of a ball centered at Q_0 with radius r is always positive. i.e.,

$$\int_{d(Q,Q_0) \leqslant r} dQ > 0$$

Proof: First, due to the invariant property of dQ, the volume does not depend on the center of the ball. Second, when the distance is defined as the geodesic distance instead, a positive lower bound of the volume of a ball is given in [50, (42)–(46)]. Finally, the distances under these two definitions are locally equivalent [50, (21)], which completes the proof. □

With the assistance of Lemma 3, next we show that both $V'_{n_R,n_T}(\epsilon)$ and $V''_{n_R,n_R}(\epsilon)$ have positive volumes. We can find a $U_0 \in V_{n_R,n_R}$ with non-zero elements on its last column, and set ϵ_1 half the minimum modulus of the elements of the last column of U_0. Similarly we can find a $Q_0 \in V_{n_R,n_T}$ with non-zero elements on its last row, and set ϵ_2 half the minimum modulus of the elements of the last row of Q_0. Let $\epsilon = \min\{\epsilon_1, \epsilon_2, 1/(n_R n_T)\}$. Then, we can construct a ball B_u centered at U_0 with sufficient small radius $0 < r \leqslant \epsilon$, such that B_u is a subset of $V''_{n_R,n_R}(\epsilon)$. To see this, $\forall U \in B_u$, $\|U_0 - U\|_F \leqslant r$. Thus,for $0 < r \leqslant \epsilon$, $\forall 1 \leqslant i \leqslant n_R$

$$r \geqslant \left|[u_0]_{in_R} - u_{in_R}\right| \geqslant \left|[u_0]_{in_R}\right| - |u_{in_R}| \geqslant 2\epsilon - |u_{in_R}|,$$

then we have $|u_{in_R}| \geqslant 2\epsilon - r \geqslant \epsilon$, i.e., $U \in V''_{n_R,n_R}(\epsilon)$. Since $B_u \subseteq V''_{n_R,n_R}(\epsilon)$, by Lemma 3, $\mathrm{Vol}(V''_{n_R,n_R}(\epsilon)) \geqslant \mathrm{Vol}(B_u) > 0$. Similarly $\mathrm{Vol}(V'_{n_R,n_T}(\epsilon)) > 0$.

Using (5.51), (5.52), (5.53) and (5.54), we obtain a lower bound on I_1as

$$
\begin{aligned}
I_1 \dot{\geqslant} & \int_{\mathcal{A}' \bigcap \mathcal{S}(\delta)} \prod_{i=1}^{n_R} \rho^{-(n_T-n_R+1)\alpha_i} \prod_{i<j} (\rho^{-\alpha_i} - \rho^{-\alpha_j})^2 \Big[\int_{V''_{n_R,n_R}(\epsilon)} \int_{V'_{n_R,n_T}(\epsilon)} (g(\rho,U,Q,\alpha))^{t/2} \, dQdU \Big] d\alpha \\
\dot{\geqslant} & \int_{\mathcal{A}' \bigcap \mathcal{S}(\delta)} \prod_{i=1}^{n_R} \rho^{-(n_T-n_R+1)\alpha_i} \prod_{i<j} ((1-\rho^{-\delta})\rho^{-\alpha_j})^2 \cdot \rho^{-\frac{tn_Rn_T}{2}\alpha_{n_R}} \left(\epsilon^{4n_Rn_T} - N_3 \cdot \rho^{-\delta/2} \right)^{t/2} \\
& \cdot \Big[\int_{V''_{n_R,n_R}(\epsilon)} dU \cdot \int_{V'_{n_R,n_T}(\epsilon)} dQ \Big] d\alpha \\
\doteq & (1-\rho^{-\delta})^{{n_R}^2-n_R} \left(\epsilon^{4n_Rn_T} - N_3 \cdot \rho^{-\delta/2} \right)^{t/2} \int_{\mathcal{A}' \bigcap \mathcal{S}(\delta)} \rho^{-f(\alpha)} d\alpha \\
\doteq & \int_{\mathcal{A}' \bigcap \mathcal{S}(\delta)} \rho^{-f(\alpha)} d\alpha \\
\doteq & \rho^{-\inf_{\mathcal{A}' \bigcap \mathcal{S}(\delta)} f(\alpha)}.
\end{aligned}
$$

By the continuity of f, $\inf_{\mathcal{A}' \bigcap \mathcal{S}(\delta)} f(\alpha)$ approaches $f(\alpha^*)$ as $\delta \to 0$. Therefore, we have

$$
I_1 \doteq \rho^{-d_{\text{out}}(r)}, \tag{5.55}
$$

where

$$
d_{\text{out}}(r) = \inf_{\alpha \in \mathcal{A}'} \left[\sum_{i=1}^{\min\{n_R,n_T\}} (|n_T - n_R| + 2i - 1)\alpha_i + \frac{n_Rn_Tt}{2} \alpha_{\min\{n_R,n_T\}} \right],
$$

and

$$
\mathcal{A}' = \left\{ \alpha : \alpha_1 \geqslant \cdots \geqslant \alpha_{\min\{n_R,n_T\}} \geqslant 0, \sum_i (1-\alpha_i)^+ < r \right\}.
$$

II. ρ exponent of I_2

Next, we prove that the ρ exponent of I_2 is no less than the one of I_1. The range of r we need to consider is $0 \leqslant r \leqslant n_R$. Since α_i are arranged in non-increasing order, we can partition $\mathcal{A}''$ as

$$
\mathcal{A}'' = \bigcup_{q=1}^{n_R-1} \left(\mathcal{A} \bigcap \mathcal{B}_q \right),
$$

where $\mathcal{B}_q = \{\alpha : \alpha_1, ..., \alpha_q \geqslant 0, \alpha_{q+1}, ..., \alpha_{n_R} < 0\}$. Notice that $\mathcal{B}_0$ is the set in which $\forall i, \alpha_i < 0$, then $\mathcal{A} \bigcap \mathcal{B}_0 = \emptyset$. Therefore,

$$
I_2 = \sum_{q=1}^{n_R-1} I_{2,q},
$$

where $I_{2,q} = \int_{\mathcal{A}\bigcap\mathcal{B}_q} p_{\boldsymbol{\alpha}}(\alpha)d\alpha$.

Notice that:

1.
$$|h_{ij} - c|^\beta \geqslant 2^{-\beta}|h_{ij}|^\beta - |c|^\beta,$$

Further,

$$\sum_{i,j}|h_{ij}|^\beta = \sum_{i,j}(|h_{ij}|^2)^{\beta/2} \geqslant \begin{cases} (\sum_{i,j}|h_{ij}|^2)^{\beta/2} & 0<\beta<2 \\ n_R n_T\big(\sum_{i,j}\frac{|h_{ij}|^2}{n_R n_T}\big)^{\beta/2} & \beta \geqslant 2 \end{cases}, \tag{5.56}$$

and

$$\Big(\sum_{i,j}|h_{ij}|^2\Big)^{\beta/2} = \big[\operatorname{tr}(HH^\dagger)\big]^{\beta/2} = \Big(\sum_{i=1}^{n_R}\rho^{-\alpha_i}\Big)^{\beta/2} \geqslant \frac{1}{n_R}\sum_{i=1}^{n_R}\rho^{-\alpha_i\beta/2}, \tag{5.57}$$

Thus $\exists\ 0 < N_1 < \infty$, such that

$$\exp\Big(-b\sum_{i=1}^{n_R}\sum_{j=1}^{n_T}|h_{ij}-c|^2\Big) \leqslant \exp\Big(-bN_1\sum_{i=1}^{n_R}\rho^{-\alpha_i\beta/2}\Big)\exp(bn_Rn_T|c|^\beta).$$

2. By (5.47), $\exists\ 0 < N_2 < \infty$ such that $g(\rho, U, Q, \alpha) < N_2 \cdot \rho^{-n_R n_T \alpha_{n_R}}$

3. N_1 and N_2 are independent of Q and U when n_R ,n_T and β are fixed.

4. when $r \leqslant n_R - q$, $\mathcal{A}\bigcap\mathcal{B}_q = \emptyset$

Let $\alpha_1^q = \{\alpha_1, \ldots, \alpha_q\}$ and $d\alpha_1^q = d\alpha_1 \ldots d\alpha_q$. Based the above observations, when $r > n_R - q$, set $\delta = r - n_R + q$, then $I_{2,q}$ can be upper bounded as

$$\begin{aligned} I_{2,q} &= \int_{\mathcal{A}\bigcap\mathcal{B}_q} p_{\boldsymbol{\alpha}}(\alpha)d\alpha \\ &\dot{\leqslant} \int_{\mathcal{A}\bigcap\mathcal{B}_q}\Big[\prod_{i=1}^{n_R}\rho^{-(n_T-n_R+1)\alpha_i}\cdot e^{-bN_1\rho^{-\alpha_i\beta/2}}\Big]\cdot\prod_{i<j}(\rho^{-\alpha_j}-0)^2\cdot\rho^{-\frac{t}{2}n_Rn_T\alpha_{n_R}}d\alpha \\ &\doteq \int_{\mathcal{A}\bigcap\mathcal{B}_q}\prod_{i=1}^{n_R}\Big[\rho^{-(n_T-n_R+2i-1)\alpha_i+\frac{t}{2}n_Rn_T\alpha_{n_R}}\cdot e^{-bN_1\rho^{-\alpha_i\beta/2}}\Big]d\alpha. \end{aligned}$$

For $\alpha_i \geqslant 0$, $e^{-bN_1\rho^{-\alpha_i\beta/2}} \leqslant 1$. Since

$$\begin{aligned} \mathcal{A}\bigcap\mathcal{B}_q &= \Big\{\alpha : \alpha_1, \ldots, \alpha_q \geqslant 0, \alpha_{q+1}, \ldots, \alpha_{n_R} < 0, \sum_{i=1}^{q}(1-\alpha_i)^+ < \delta + \sum_{i=q+1}^{n_R}\alpha_i\Big\} \\ &\subseteq \mathcal{B}_q\bigcap\Big\{\alpha : \sum_{i=1}^{q}(1-\alpha_i)^+ < \delta\Big\}, \end{aligned}$$

then

$$I_{2,q} \dot{\leqslant} C(q) \int_{\mathcal{A}_q^1(\delta)} \rho^{-\sum_{i=1}^{q}(n_T-n_R+2i-1)\alpha_i} d\alpha_1^q, \tag{5.58}$$

where

$$\begin{aligned} C(q) = & \int_{-\infty}^{0} \rho^{-(n_R+n_T-1+\frac{t}{2}n_R n_T)\alpha_{n_R}} \cdot e^{-bN_1\rho^{-\alpha_{n_R}\beta/2}} d\alpha_{n_R} \\ & \cdot \prod_{i=q+1}^{n_R-1} \int_{-\infty}^{0} \rho^{-(n_T-n_R+2i-1)\alpha_i} e^{-bN_1\rho^{-\alpha_i\beta/2}} d\alpha_i, \end{aligned} \tag{5.59}$$

and

$$\mathcal{A}_q^1(\delta) = \{\alpha_1^q : \alpha_1 \geqslant \ldots \alpha_q \geqslant 0, \sum_{i=1}^{q}(1-\alpha_i)^+ < \delta\}. \tag{5.60}$$

Changing the integral variables α_i to $\lambda_i = \rho^{-\alpha_i}$, it turns out that $C(q)$ does not affect the ρ exponent of $I_{2,q}$.

Lemma 4 *Without loss of generality, we assume that $n_R \leqslant n_T$. $\forall \delta > 0$ and $\forall q \in \{1, 2, ..., n_R - 1\}$, the following two inequalities hold:*

$$\int_{\mathcal{A}_q^1(\delta)} \rho^{-\sum_{i=1}^{q}(n_T-n_R+2i-1)\alpha_i} d\alpha_1^q \quad \dot{\leqslant} \quad \rho^{-d_{out}(n_R-q+\delta)}, \tag{5.61}$$

$$\int_{\mathcal{A}_q^2(\delta)} \rho^{-\sum_{i=1}^{q}(n_T-n_R+2i-1)\alpha_i} \rho^{-l[\sum_{i=1}^{q}(1-\alpha_i)^+-\delta]} d\alpha_1^q \quad \dot{\leqslant} \quad \rho^{-d_G(n_R-q+\delta)}, \tag{5.62}$$

where $d_{out}(\cdot)$, $d_G(\cdot)$, $\mathcal{A}_q^1(\delta)$ and $\mathcal{A}_q^2(\delta)$ are defined in (5.31), (5.38), (5.60) *and* (5.66) *respectively.*

Proof:

1. Define

$$f_q(\alpha_1^q) = \sum_{i=1}^{q}(n_T - n_R + 2i - 1)\alpha_i = f(\alpha)|_{\alpha_{q+1}=\ldots=\alpha_{n_R}=0},$$

where $f(\alpha)$ is defined in (5.31). Using the fact that

$$\begin{aligned} & \{\alpha : \alpha_1^q \in \mathcal{A}_q^1(\delta), \alpha_{q+1} = \ldots = \alpha_{n_R} = 0\} \\ \subseteq & \{\alpha : \alpha_1 \geqslant \ldots \geqslant \alpha_{n_R} \geqslant 0, \sum_i (1-\alpha_i)^+ < n_R - q + \delta\} \\ = & \mathcal{A}' \qquad \text{with } r = n_R - q + \delta, \end{aligned}$$

where $\mathcal{A}'$ is defined in (5.31), we have

$$\inf_{\mathcal{A}_q^1(\delta)} f_q(\alpha) \geqslant \inf_{\mathcal{A}'} f(\alpha) = d_{\text{out}}(n_R - q + \delta).$$

Thus

$$\int_{\mathcal{A}_q^1(\delta)} \rho^{-\sum_{i=1}^q (n_T - n_R + 2i - 1)\alpha_i} d\alpha_1^q \doteq \rho^{-\inf_{\mathcal{A}_q^1(\delta)} f_q(\alpha)} \dot{\leqslant} \rho^{-d_{\text{out}}(n_R - q + \delta)}.$$

2. Define

$$\begin{aligned} d_{G,q}(r, \alpha_1^q) &= \sum_{i=1}^q (n_T - n_R + 2i - 1)\alpha_i + l\Big(\sum_{i=1}^q (1 - \alpha_i)^+ - r + n_R - q\Big) \\ &= d_G(r, \alpha)|_{\alpha_{q+1} = \ldots = \alpha_{n_R} = 0}, \end{aligned}$$

where $d_G(r, \alpha)$ is defined in (5.38). Using the fact that

$$\begin{aligned} &\{\alpha : \alpha_1^q \in \mathcal{A}_q^2(\delta), \alpha_{q+1} = \ldots = \alpha_{n_R} = 0\} \\ \subseteq &\{\alpha : \alpha_1 \geqslant \ldots \geqslant \alpha_{n_R} \geqslant 0, \sum_i (1 - \alpha_i)^+ > n_R - q + \delta\} \\ = &\mathcal{A}^c \bigcap \mathcal{R}^{n_R^+} \qquad \text{with } r = n_R - q + \delta, \end{aligned}$$

we have

$$\inf_{\mathcal{A}_q^2(\delta)} d_{G,q}(n_R - q + \delta, \alpha_1^q) \geqslant \inf_{\mathcal{A}^c \bigcap \mathcal{R}^{n_R^+}} d_G(n_R - q + \delta, \alpha) = d_G(n_R - q + \delta).$$

Thus

$$\int_{\mathcal{A}_q^2(\delta)} \rho^{-\sum_{i=1}^q (n_T - n_R + 2i - 1)\alpha_i} \rho^{-l[\sum_{i=1}^q (1 - \alpha_i)^+ - \delta]} d\alpha_1^q \doteq \rho^{-\inf_{\mathcal{A}_q^2(\delta)} d_{G,q}(n_R - q + \delta, \alpha_1^q)} \dot{\leqslant} \rho^{-d_G(n_R - q + \delta)}.$$

□

With the assistance of Lemma 4, we obtain

$$I_{2,q} \dot{\leqslant} \begin{cases} \rho^{-\infty} & r \leqslant n_R - q, \\ \rho^{-d_{\text{out}}(r)} & r > n_R - q\ . \end{cases}$$

Now, we can conclude that the ρ exponent of $I_{2,q}$ is no less than the ρ exponent of I_1, and therefore the ρ exponent of I_2 is no less than the one of I_1.

5.9 Appendix 5.B Proof of Lemma 2

Without loss of generality, we assume that $n_R \leqslant n_T$. The range of r we need to consider is $0 \leqslant r \leqslant n_R$. Since α_i are arranged in non-increasing order, we can partition $\mathcal{A}^c$ as

$$\mathcal{A}^c = \left(\mathcal{A}^c \bigcap \mathcal{R}^{n_R^+}\right) \bigcup \left\{ \bigcup_{q=0}^{n_R-1} \left(\mathcal{A}^c \bigcap \mathcal{B}_q\right) \right\},$$

where $\mathcal{B}_q = \{\alpha : \alpha_1, ..., \alpha_q \geqslant 0, \alpha_{q+1}, ..., \alpha_{n_R} < 0\}$, then [cf. (5.35)]

$$P(\text{error,no outage}) \dot{\leqslant} \int_{\mathcal{A}^c} p_{\boldsymbol{\alpha}}(\alpha) \rho^{-l[\sum_{i=1}^{n_R}(1-\alpha_i)^+ - r]} d\alpha, = J_1 + \sum_{q=0}^{n_R-1} J_{2,q},$$

where

$$J_1 = \int_{\mathcal{A}^c \bigcap \mathcal{R}^{n_R^+}} p_{\boldsymbol{\alpha}}(\alpha) \rho^{-l[\sum_{i=1}^{n_R}(1-\alpha_i)^+ - r]} d\alpha,$$
$$J_{2,q} = \int_{\mathcal{A}^c \bigcap \mathcal{B}_q} p_{\boldsymbol{\alpha}}(\alpha) \rho^{-l[\sum_{i=1}^{n_R}(1-\alpha_i)^+ - r]} d\alpha.$$

Using the similar method in Appendix 5.A, it is easy to check that:

$$J_1 \doteq \rho^{-d_G(r)},$$

where $d_G(r)$ is defined in Lemma 2. Next we will show that $\forall q \in \{0, 1, ..., n_R - 1\}$, the ρ exponent of $J_{2,q}$ is no less than that of J_1. To be more specific:

$$J_{2,q} \dot{\leqslant} \begin{cases} \rho^{-l(n_R-q-r)-d_G(n_R-q)} & r \leqslant n_R - q, \\ \rho^{-d_G(r)} & r > n_R - q\ . \end{cases} \tag{5.63}$$

We use the observations obtained in Appendix 5.A to construct the upper bound of $J_{2,q}$ as follows.

- When $r \leqslant n_R - q$,

$$\mathcal{A}^c \bigcap \mathcal{B}_q = \left\{\alpha : \alpha_1, \ldots, \alpha_q \geqslant 0, \alpha_{q+1}, \ldots, \alpha_{n_R} < 0, \sum_{i=1}^{q}(1-\alpha_i)^+ \geqslant r - (n_R - q) + \sum_{i=q+1}^{n_R} \alpha_i \right\}$$
$$\subseteq \mathcal{B}_q \bigcap \left\{\alpha : \sum_{i=1}^{q}(1-\alpha_i)^+ \geqslant 0\right\},$$

(5.64)

then following the same procedure to obtain (5.58) in Appendix 5.A, we can upper bound $J_{2,q}$ as

$$J_{2,q} \dot{\leqslant} \rho^{-l(n_R-q-r)} C(q) \cdot \int_{\mathcal{A}_q^2(0)} \rho^{-\sum_{i=1}^{n_R}(n_T-n_R+2i-1)\alpha_i} \rho^{-l[\sum_{i=1}^{q}(1-\alpha_i)^+-0]} d\alpha_1^q, \tag{5.65}$$

where $C(q)$ is defined in (5.59) and $\mathcal{A}_q^2(\delta)$is defined as

$$\mathcal{A}_q^2(\delta) = \{\alpha_1^q : \alpha_1 \geqslant \ldots \alpha_q \geqslant 0, \sum_{i=1}^{q}(1-\alpha_i)^+ \geqslant \delta\}. \tag{5.66}$$

Here, we have used the fact that for $\alpha_i < 0$ and $\rho > 1$, $\rho^{l\alpha_i} \leqslant 1$. For $q = 0$, we set the integral in (5.65) to be 1.

As shown before, $C(q)$ does not affect the ρ exponent. For the integral in (5.65), it is exponentially less than or equal to $\rho^{-d_G(n_R-q)}$ by Lemma 4. This completes the proof of the first part in (5.63).

- When $r > n_R - q$, set $\delta = r - n_R - q$. Using (5.64), we have

$$\begin{aligned}
\mathcal{A}^c \bigcap \mathcal{B}_q &= (\mathcal{A}^c \bigcap \mathcal{B}_q) \bigcap \{\alpha : \sum_{i=1}^{q}(1-\alpha_i)^+ \geqslant 0\} \\
&= (\mathcal{A}^c \bigcap \mathcal{B}_q) \bigcap \Big[\{\alpha : \sum_{i=1}^{q}(1-\alpha_i)^+ \geqslant \delta\} \bigcup \{\alpha : \sum_{i=1}^{q}(1-\alpha_i)^+ < \delta\}\Big] \\
&= \Big[\mathcal{A}^c \bigcap \mathcal{B}_q \bigcap \mathcal{D}_{q,\delta}\Big] \bigcup \Big[\mathcal{A}^c \bigcap \mathcal{B}_q \bigcap \mathcal{D}_{q,\delta}^c\Big],
\end{aligned}$$

where $\mathcal{D}_{q,\delta} = \big\{\alpha : \sum_{i=1}^{q}(1-\alpha_i)^+ < \delta\big\}$. For $\alpha \in \mathcal{A}^c \bigcap \mathcal{B}_q \bigcap \mathcal{D}_{q,\delta}$, use the following upper bound:

$$\rho^{-l[\sum_{i=1}^{n_R}(1-\alpha_i)^+-r]} \leqslant 1$$

For $\alpha \in \mathcal{A}^c \bigcap \mathcal{B}_q \bigcap \mathcal{D}_{q,\delta}^c$, use the following upper bound:

$$\rho^{-l[\sum_{i=1}^{n_R}(1-\alpha_i)^+-r]} \leqslant \rho^{-l[\sum_{i=1}^{q}(1-\alpha_i)^+-\delta]}$$

then we can upper bound $J_{2,q}$ as

$$\begin{aligned}
J_{2,q} \leqslant & \int_{\mathcal{A}^c \bigcap \mathcal{B}_q \bigcap \mathcal{D}_{q,\delta}} p_{\boldsymbol{\alpha}}(\alpha) d\alpha + \int_{\mathcal{A}^c \bigcap \mathcal{B}_q \bigcap \mathcal{D}^c_{q,\delta}} p_{\boldsymbol{\alpha}}(\alpha) \rho^{-l[\sum_{i=1}^{n_R}(1-\alpha_i)^+ - r]} d\alpha \\
\dot{\leqslant} & C(q) \int_{\mathcal{A}_q^1(\delta)} \rho^{-\sum_{i=1}^{q}(n_T - n_R + 2i - 1)\alpha_i} d\alpha_1^q \\
& + C(q) \int_{\mathcal{A}_q^2(\delta)} \rho^{-\sum_{i=1}^{q}(n_T - n_R + 2i - 1)\alpha_i} \rho^{-l[\sum_{i=1}^{q}(1-\alpha_i)^+ - \delta]} d\alpha_1^q \\
\doteq & \int_{\mathcal{A}_q^1(\delta)} \rho^{-\sum_{i=1}^{q}(n_T - n_R + 2i - 1)\alpha_i} d\alpha_1^q \\
& + \int_{\mathcal{A}_q^2(\delta)} \rho^{-\sum_{i=1}^{q}(n_T - n_R + 2i - 1)\alpha_i} \rho^{-l[\sum_{i=1}^{q}(1-\alpha_i)^+ - \delta]} d\alpha_1^q \\
\dot{\leqslant} & \rho^{-d_{\text{out}}(n_R - q + \delta)} + \rho^{-d_G(n_R - q + \delta)} \quad \text{by Lemma 4} \\
\doteq & \rho^{-d_{\text{out}}(r)} + \rho^{-d_G(r)} \\
\doteq & \rho^{-d_G(r)} \qquad\qquad \text{since } d_G(r) \leqslant d_{\text{out}}(r).
\end{aligned}$$

where $C(q)$, $\mathcal{A}_q^1(\delta)$, and $\mathcal{A}_q^2(\delta)$ are defined in (5.59), (5.60) and (5.66), respectively. This completes the proof of the second part in (5.63).

5.10 Appendix 5.C Proof of Theorem 5

Without loss of generality, we assume that $n_R \leqslant n_T$. Recall that

$$\begin{aligned}
p_{\boldsymbol{\Lambda}}(\Lambda) = & \det(\Sigma_1)^{-n_T} \det(\Sigma_2)^{-n_R} (4\pi)^{-n_R} \cdot \prod_{i=1}^{n_R} \lambda_i^{n_T - n_R} \cdot \prod_{i<j} (\lambda_i - \lambda_j)^2 \\
& \cdot \int_{V_{n_R, n_R}} \int_{V_{n_R, n_T}} p_{\widetilde{\boldsymbol{H}}}(\Sigma_1^{-1/2} U \Lambda^{1/2} Q \Sigma_2^{-1/2}) dQ dU.
\end{aligned}$$

Since each element of $(\Sigma_1^{-1/2} U \Lambda^{1/2} Q \Sigma_2^{-1/2})$ is a linear combination of $[\rho^{-\alpha_1/2}, ..., \rho^{-\alpha_{n_R}/2}]^\kappa$, and the corresponding coefficients are bounded, little modification is needed for the proof of the upper bound of I_1 in Appendix 5.A to be applicable for the correlated case.

For the lower bound of I_1, we only need to prove that the observation 3) in Appendix 5.A still holds. For some $0 < \epsilon < \frac{1}{n_R n_T}$, define

$$\mathcal{Q}(\epsilon) = \left\{ Q \in \mathcal{C}^{n_R \times n_T} : QQ^\dagger = I_{n_R}, \quad \left| [Q \Sigma_2^{-1/2}]_{n_R j} \right| \geqslant \epsilon, j = 1, ..., n_T \right\},$$

$$\mathcal{U}(\epsilon) = \left\{ U \in \mathcal{C}^{n_R \times n_R} : UU^\dagger = I_{n_R}, \quad \left| [\Sigma_1^{-1/2} U]_{i n_R} \right| \geqslant \epsilon, i = 1, ..., n_R \right\},$$

then it is enough to show that $\mathrm{Vol}(\mathcal{Q}(\epsilon)) > 0$ and $\mathrm{Vol}(\mathcal{U}(\epsilon)) > 0$.

Consider a particular U_0 in V_{n_R,n_R}, whose last column is parallel to $\Sigma_1^{1/2}(1,1,...,1)^T$, then each element of the last column of $(\Sigma_1^{-1/2}U_0)$ is non-zero. Set ϵ_1 half the minimum modulus of the elements of the last column of $\Sigma_1^{-1/2}U_0$. Similarly, we can find a Q_0 such that each element of the last raw of $Q\Sigma_2^{-1/2}$ is non-zero, and set ϵ_2 half the minimum modulus of the elements of the last row of $Q_0\Sigma_2^{-1/2}$. Let $\epsilon = \min\{\epsilon_1, \epsilon_2, 1/(n_R n_T)\}$. By Lemma 3 and the continuity of the mapping $f_1(U) = \Sigma_1^{-1/2}U$ and $f_2(Q) = Q\Sigma_2^{-1/2}$, we can show that $\mathrm{Vol}(\mathcal{U}(\epsilon)) > 0$ and $\mathrm{Vol}(\mathcal{Q}(\epsilon)) > 0$, following the similar argument in Appendix 5.A.

For the upper bound of I_2 in Appendix 5.A, define the eigenvalue decompositions of Σ_1 and Σ_2 as

$$\Sigma_1 = U_1\Lambda_1 U_1^\dagger \quad \text{and} \quad \Sigma_2 = U_2\Lambda_2 U_2^\dagger.$$

Since both Σ_1 and Σ_2 are of full rank, the diagonal elements of Λ_1 and Λ_2 are all positive. Let x_1 and x_2 denote the largest elements of Λ_1 and Λ_2, respectively. It is easy to show that

$$\sum_{i,j}|h_{ij}|^2 = ||H||_F^2 = ||\Sigma_1^{-1/2}U\Lambda^{1/2}Q\Sigma_2^{-1/2}||_F^2 \geqslant \frac{1}{x_1x_2}||U\Lambda^{1/2}Q||_F^2 = \frac{1}{x_1x_2}\sum_{i=1}^{n_R}\rho^{-\alpha_i}, \quad (5.67)$$

then we have

$$(\sum_{i,j}|h_{ij}|^2)^{\beta/2} \geqslant (\frac{\sum_{i=1}^{n_R}\rho^{-\alpha_i}}{x_1x_2})^{\beta/2} \geqslant \frac{\sum_{i=1}^{n_R}\rho^{-\alpha_i\beta/2}}{(x_1x_2)^{\beta/2}n_R}. \quad (5.68)$$

Using (5.68) instead of (5.57) in the construction of the upper bound of I_2, it turns out that the result in Appendix 5.A still holds. Similar argument is applicable for the proof of Lemma 2. Arguments for the case of independent non-identical distribution in Section 5.6.2 can also be applied here. Thus, the covariance matrices Σ_1 and Σ_2 have no effect on the calculation of $d_{\mathrm{out}}(r)$ and $d_G(r)$, provided that they have full ranks. This completes the proof.

5.11 Appendix 5.D Proof of Theorem 6

The key for this proof is to handle the term $\prod_i\prod_j|h_{ij} - \bar{h}_{ij}|^{t_{ij}}$ properly. Without loss of generality, we assume that $n_R \leqslant n_T$.

For the upper bound of I_1 in Appendix 5.A, notice that $\exists\ 0 < M < \infty$ (independent of U and Q when n_R and n_T are fixed) such that

$$|h_{ij} - \bar{h}_{ij}|^{t_{ij}} \leqslant 2^{t_{ij}}(|h_{ij}|^{t_{ij}} + |\bar{h}_{ij}|^{t_{ij}}) \leqslant M\rho^{-\alpha_{n_R} t_{ij}/2} + 2^{t_{ij}}|\bar{h}_{ij}|^{t_{ij}}.$$

Thus

$$\prod_{i,j} |h_{ij} - \bar{h}_{ij}|^{t_{ij}} \leqslant \prod_{i,j} \left(M\rho^{-\alpha_{n_R} t_{ij}/2} + 2^{t_{ij}}|\bar{h}_{ij}|^{t_{ij}} \right).$$

In the expansion of the right hand side of the above inequality, the term with the lowest order of $(\rho^{-\alpha_{n_R}})$ is $(\rho^{-\alpha_{n_R}})^{\frac{1}{2}\sum_{(i,j\in\mathcal{I})} t_{ij}}$, where $\mathcal{I} = \{(i,j) : \bar{h}_{ij} = 0\}$. This term will determine the diversity result, since integration of it yields the smallest diversity gain.

For the lower bound of I_1 in Appendix 5.A, we use a slightly different definition of $\mathcal{S}(\delta)$ as

$$\mathcal{S}(\delta) \equiv \{\alpha : |\alpha_i - \alpha_j| > \delta, \forall i \neq j \text{ and } \alpha_{n_R} > \delta\},$$

then $\mathcal{A}' \bigcap \mathcal{S}(\delta) \uparrow \mathcal{A}'$ as $\delta \to 0$. Next, we only need to show that for given $Q \in V'_{n_R,n_T}(\epsilon)$, $U \in V''_{n_R,n_R}(\epsilon)$, and $\alpha \in \mathcal{S}(\delta)$,

$$\prod_{i=1}^{n_R}\prod_{j=1}^{n_T} |h_{ij} - \bar{h}_{ij}|^{t_{ij}} \geqslant \rho^{-\sum_{(i,j)\in\mathcal{I}} \frac{t_{ij}}{2}\cdot\alpha_{n_R}} \cdot (\theta + f(\rho,\delta)), \tag{5.69}$$

where $\mathcal{I} = \{(i,j) : \bar{h}_{ij} = 0\}$, $\theta > 0$ is a constant, and $f(\rho,\delta)$ is a function of ρ and δ. We can see that

- if $\bar{h}_{ij} = 0$,

$$|h_{ij} - \bar{h}_{ij}|^{t_{ij}} \geqslant \rho^{-\alpha_{n_R} t_{ij}/2}(\epsilon - N_3\rho^{-\delta/2})^{t_{ij}}, \tag{5.70}$$

  where $0 < N_3 < \infty$ is a constant.

- if $\bar{h}_{ij} \neq 0$,

$$|h_{ij} - \bar{h}_{ij}|^{t_{ij}} \geqslant (|\bar{h}_{ij}| - N_4\rho^{-\delta/2}), \tag{5.71}$$

  where $0 < N_4 < \infty$ is a constant.

Combining (5.70) and (5.71), we obtain (5.69). Then following the same method in Appendix 5.A, we can complete the proof for I_1. The proof for J_1 in Appendix 5.B is similar. The proofs for the upper bound of I_2 in Appendix 5.A and the upper bound of $J_{2,q}$ in Appendix 5.B are similar to the proof of the upper bound of I_1 here. The arguments for the case of independent non-identical distribution in Section 5.6.2 can also be applied here.

Therefore, the results of $d_{\text{out}}(r)$ and $d_G(r)$ in Theorem 1 and Lemma 2 are also applicable for the case of non-zero channel mean $\overline{H}$, with $\frac{t}{2}n_R n_T$ replaced by $\sum_{(i,j)\in\mathcal{I}} t_{ij}/2$. This completes the proof.

CHAPTER 6. CONCLUSIONS AND FUTURE WORK

In this thesis, we studied two important issues in wireless MIMO communication systems: iterative receiver design for coded MIMO systems and diversity-multiplexing tradeoff analysis for general fading channels. We proposed the iterative receiver structure which includes two modules: MIMO demodulator and error-control decoder, and further decoupled the receiver design problem into two sub-problems, MIMO channel estimation and MIMO detection. We developed an EM-based semi-blind channel and noise covariance matrix estimation algorithm for space-time coding systems under spatially correlated noise, and derived the modified Cramér-Rao (MCRB) bounds for unknown parameters. We showed that the proposed channel estimation algorithm can achieve the MCRB after several iterations between MIMO demodulator and error-control decoder. For the MIMO detection problem, we proposed a novel low-complexity MIMO detection algorithm by incorporating the prior information from error-control decoder into BLAST nulling/cancelling algorithm. We demonstrated that this MIMO detection algorithm can achieve near-optimal (MAP detection) performance with only cubic order complexity, which is much lower than the exponential complexity of MAP detection algorithm. Our solutions to the receiver design problem give the wireless communication systems designers an option to approach the goal of reliable high-speed communications over unreliable wireless channels. In the second part of this thesis, we derive the optimal diversity-multiplexing tradeoff for general MIMO fading channels, which include different fading types as special cases. We show that optimal diversity-multiplexing tradeoff can be characterized exactly in a simple piecewise linear function given long enough channel coherent length, where only the first segment is affected by different fading types. When the channel coherent length is short, we only provide lower and upper bounds for the optimal tradeoff curve. We proved that under certain

full-rank assumptions spatial correlation has no effect on the the optimal tradeoff. We also argued that non-zero channel means in general are not beneficial for multiplexing-diversity tradeoff. Our new diversity-multiplexing tradeoff results may facilitate a more comprehensive understanding of the limiting performance of MIMO systems under generalized fading conditions.

We have the following three topics for future research which are closely related to the work in this thesis.

- *Channel estimation for fast fading MIMO systems* The channel estimation algorithm proposed in Chapter 3 are specifically designed for quasi-static fading model. In practice, due to the relative movement between the transmitter and the receiver, the channel coherence time may be much smaller than our frame length. For such fast fading MIMO systems, channel tracking is much more difficult. Most of current channel estimation algorithms for fast fading MIMO systems are based on first-order AR model, and use Kalman filtering method [77, 90]. Finding a better model and more sophisticated estimation algorithms for this problem will be one of our future research topics.

- *Per antenna power and rate control with limited feedback* When perfect MIMO channel estimation is available at the transmitter, higher spectral efficiency and better transmission quality can be achieved. Unfortunately, due to channel estimation errors and non-perfect feedback channels, the transmitter can only access partial channel information through limited feedback. With such limited feedback, we can design per antenna power and rate control algorithm to improve the spectral efficiency and system performance. Most of existing algorithms choose the optimal rate and power for each antenna by maximizing the capacity, or minimizing the error probability for very simple linear receiver (e.g., zero-forcing or LMMSE). For medium-frame transmission, the outage probability is more meaningful than the ergodic capacity. On the other hand, the outage probability can be characterized by diversity gain and coding gain at high SNR [114], which makes it easier to evaluate than the capacity. Therefore, minimizing the outage probability is another possible optimization criterion. Another issue that needs to be considered is the channel

estimation error. The influence of channel estimation error on the performance of per antenna power and rate control schemes is also an interesting topic.

- *Cooperative MIMO networks* In cooperative wireless networks, each user is assumed to transmit its own data as well as act as a cooperative agent for other users such that the average performance (e.g., spectral efficiency for each user) is improved under the total power and bandwidth constraints [78]. With the cooperation from other users, a virtual MIMO channel can be constructed between two single-antenna users without the use of multiple antennas, and the spatial diversity gain can also be obtained. The asymptotic performance of such systems can be analyzed using the method proposed in Appendix A. Given the total power constraint, both amplify-and-forward (AF) cooperative schemes and decode-and-forward (DF) schemes can be studied and compared with each other. Another theoretical problem is to study the optimal diversity-multiplexing tradeoff for such cooperative MIMO systems. Previous work has been done for simple relay channels with AF and DF cooperative schemes [6, 81]. The extension to cooperative MIMO systems with AF and DF schemes over general fading channels will be one of our future research topics.

APPENDIX A. AVERAGE SYMBOL ERROR PROBABILITY AND OUTAGE PROBABILITY ANALYSIS FOR GENERAL COOPERATIVE DIVERSITY SYSTEMS AT HIGH SIGNAL TO NOISE RATIO

A.1 Introduction

Recently, cooperation between wireless communicators has been proposed in wireless and *ad hoc* networks to provide spatial diversity without requiring the use of physical antenna arrays; see e.g., [61]. Such spatial diversity has been termed as *cooperative diversity*. The idea is that there are a number of terminals around a source terminal, which are willing to cooperate and transmit signals for the source as relays so that a virtual (or distributed) multi-antenna system is formed to provide spatial diversity.

Different cooperation schemes have been introduced [60, 61, 62, 91, 92]. Based on the transmission strategy at relays, they can be divided into two categories: *amplify-and-forward* (also known as *non-regenerative*) schemes, and *decode-and-forward* (*regenerative*) schemes. For non-regenerative schemes, the relays simply amplify and re-transmit the received signal; for regenerative schemes, the relay decode, re-encode, and re-transmit the received signal. Space-time coding can be combined with regenerative schemes to boost the performance further [62, 98]. Some adaptive relaying techniques are also proposed in [60].

In this appendix, we will focus on non-regenerative cooperative diversity systems which are appealing from the implementation perspective. We will study the end-to-end performance of such schemes over random fading channels. Similar work so far has dealt with the cooperative systems with two hops [45, 44], multiple hops [13, 46], and multiple branches with multiple hops [87], over some special forms of fading channels. A *hop* is a point-to-point link between a source and a relay, two relays, or a relay and the destination. A *branch* is a single path from

the source to the destination, consisting one or more hops. Most of the work tried to find the closed-form expressions of the error performance and/or outage probability. Relying on high signal-to-noise ratio (SNR) approximation proposed in [114], we aim to analyze the asymptotic error performance and outage probability for a general non-regenerative cooperative diversity system. Using two parameters, namely *diversity gain* and *coding gain*, the system performance can be quantified by a simple expression at high SNR. This simplicity offers useful insight to understanding of the performance limiting factors in cooperative diversity systems.

An outline of this appendix is as follows. Section A.2 reviews an important result for asymptotic error performance analysis for communications over fading channels that we will use in our analysis. Section A.3 analyzes the error performance of a two-hop diversity system, which is generalized to a general cooperative diversity system in Section A.4. Section A.5 present results on the asymptotic outage probability. Simulation results are provided in Section A.6, and Section A.7 concludes this appendix.

A.2 Average error probability

We briefly review in this section some result of [114] that will be used in our subsequent analysis. Consider a communication system over time-flat fading channels. The average symbol error probability (SEP) is given by

$$P_{\mathrm{E}} = \int_0^\infty P_{\mathrm{E}}(\gamma) p(\gamma) d\gamma \tag{A.1}$$

where γ is the instantaneous SNR at the receiver, $P_{\mathrm{E}}(\gamma)$ is the instantaneous SEP, and $p(\gamma)$ is the probability density function (PDF) of γ. In order to study the average SEP at high SNR, we make the following assumptions:

1. The instantaneous SNR is $\gamma = \beta\bar{\gamma}$, where $\bar{\gamma}$ is a positive deterministic quantity, and β is a channel-dependent nonnegative random variable.

2. The β-dependent instantaneous SEP is given by $P_{\mathrm{E}}(\beta) = Q(\sqrt{k\beta\bar{\gamma}})$, where $Q(\cdot)$ is Gaussian Q function, and k is a positive constant depending on the modulation scheme only.

3. The PDF $p(\beta)$ can be approximated as $p(\beta) = a\beta^t + o(\beta^{t+\epsilon})$, for $\beta \to 0^+$, where $\epsilon > 0$ and a is a positive constant. Both a and t are determined by the channel PDF.

Proposition 1 [114] *(Diversity and Coding Gains): At high SNR, the average SEP of a system satisfying the above assumptions i)-iii) depends only on the behavior of $p(\beta)$ at $\beta \to 0^+$. Specifically, it is given by*

$$P_E \approx \frac{2^t a \Gamma(t+\frac{3}{2})}{\sqrt{\pi}(t+1)} \cdot (k\bar{\gamma})^{-(t+1)} = (G_c \cdot \bar{\gamma})^{-G_d} \tag{A.2}$$

where $\Gamma(\cdot)$ is the Gamma function and

$$G_d = t+1, \quad \textit{and} \quad G_c = k\left(\frac{2^t a \Gamma(t+\frac{3}{2})}{\sqrt{\pi}(t+1)}\right)^{-1/(t+1)}. \tag{A.3}$$

In the following table, we list the PDF and parameters t and a as in Proposition 1 for some commonly used fading types.

Channel Type	$p(\beta)$	t	a
Rayleigh	$e^{-\beta}$	$t=0$	$a=1$
Nakagami-n	$p(\beta;n) = (1+n^2)e^{-n^2}\exp(-(1+n^2)\beta)I_0(2n\sqrt{(1+n^2)\beta})$	$t=0$	$a=(1+n^2)e^{-n^2}$
Nakagami-m	$p(\beta;m) = \frac{m^m\beta^{m-1}}{\Gamma(m)}\exp(-m\beta)$	$t=m-1$	$a=m^m/\Gamma(m)$

This proposition implies that the average SEP at high SNR can be quantitatively parameterized with G_d and G_c, termed as *diversity gain* and *coding gain* respectively. The intuition behind Proposition 1 is that the average SEP at high SNR is dominated by the low-probability event that the instantaneous SNR becomes small. The behavior of $p(\beta)$ at $\beta \to 0^+$ determines the high SNR performance. Refer to [114] for consequences of the proposition and more results on diversity combining.

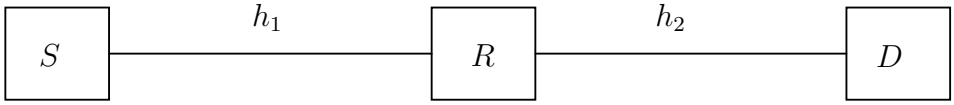

Figure A.1 A cooperative diversity system with two hops

A.3 Performance analysis for two-hop diversity system

A.3.1 System model

We first study a simple cooperative diversity system with two independent hops as depicted in Fig. A.1.

A terminal S is communicating with terminal D through a relay terminal R over time-flat fading channels. The source S transmits a digital symbol x from a finite constellation (e.g., phase-shift keying or quadrature amplitude modulation). The relay receives a noisy copy of x through the fading channel h_1, amplifies the received signal y_1 with amplifying gain A, and forward it to the destination D through the fading channel h_2. We assume that h_1 and h_2 are independent. The received signal y_1 and y_2 at relay R and terminal D can be written as

$$y_1 = h_1 x + n_1, \tag{A.4}$$

$$y_2 = h_2 A(h_1 x + n_1) + n_2 = h_2 A h_1 x + (h_2 A n_1 + n_2). \tag{A.5}$$

Without loss of generality, we assume that the complex additive white Gaussian noises (AWGN), n_1 and n_2, are independent with the same variance N_0. The end-to-end instantaneous SNR is

$$\gamma := \frac{|h_2 A h_1|^2 E[|x|^2]}{|h_2 A|^2 E[|n_1|^2] + E[|n_2|^2]} = \frac{|h_1|^2 |h_2|^2 A^2 E_s}{(|h_2|^2 A^2 + 1) N_0}, \tag{A.6}$$

where $E_s := E[|x^2|]$ is energy per symbol of the digital symbol x from source S.

There are a number of choices for the amplifying gain A, which affects the relay power. One choice as proposed in [61] is

$$A^2 = \frac{E_s}{E_s |h_1|^2 + N_0}, \tag{A.7}$$

which makes the relay power the same as that of the source. With this choice of A, by substituting (A.7) into (A.6), we obtain

$$\frac{1}{\gamma} = \frac{1}{\gamma_1} + \frac{1}{\gamma_2} + \frac{1}{\gamma_1 \gamma_2}, \tag{A.8}$$

where $\gamma_1 := |h_1|^2 E_s/N_0$ and $\gamma_2 := |h_2|^2 E_s/N_0$ are the per-hop instantaneous SNR.

Another choice of the amplification gain is

$$A^2 = \frac{1}{|h_1|^2}, \tag{A.9}$$

which inverts the fading attenuation. With this choice of A, the end-to-end SNR satisfies

$$\frac{1}{\gamma} = \frac{1}{\gamma_1} + \frac{1}{\gamma_2}. \tag{A.10}$$

It turns out that γ in (A.10) is mathematically more tractable than that in (A.8). Although practically less attractive (because it leads to more power at relay R), the choice of γ in (A.9) is a tight upper bound for the one in (A.7) at high SNR, as (A.7) becomes the same as (A.9) when $N_0 \to 0$. Simulation results in [45, 44, 46] also showed that the average SEP and outage probability with (A.7) are tightly lower bounded by those with (A.9). In the following, we will therefore fix A as in (A.9).

A.3.2 Average SEP for a single-branch two-hop system

We define $\gamma := \beta\bar{\gamma}$ as in assumption i) in Section A.2, where $\bar{\gamma} = E_s/N_0$, then (A.10) can be expressed as

$$\frac{1}{\beta} = \frac{1}{\beta_1} + \frac{1}{\beta_2}, \tag{A.11}$$

where $\beta_1 = |h_1|^2$ and $\beta_2 = |h_2|^2$, which are independent. Based on Proposition 1, the average SEP of this two-hop diversity system at high SNR can be analyzed through the behavior of $p(\beta)$ at $\beta \to 0^+$. In particular, we have the following result.

Proposition 2 *(PDF of β for two-hop system): Suppose the PDF $p_1(\beta_1)$ and $p_2(\beta_2)$ can be approximated by $p_1(\beta_1) = a_1\beta_1^{t_1} + o(\beta_1^{t_1+\epsilon_1})$, for $\beta_1 \to 0^+$ and $p_2(\beta_2) = a_2\beta_2^{t_2} + o(\beta_2^{t_2+\epsilon_2})$, for $\beta_2 \to 0^+$, respectively. The PDF $p(\beta)$ of β as in* (A.11) *is approximated as*

$$p(\beta) = a\beta^t + o(\beta^{t+\epsilon}), \quad for \beta \to 0^+,$$

where

$$t = \min(t_1, t_2), \quad \textit{and} \quad a = \begin{cases} a_1 & \textit{if} \quad t_1 < t_2, \\ a_1 + a_2 & \textit{if} \quad t_1 = t_2, \\ a_2 & \textit{if} \quad t_1 > t_2. \end{cases} \tag{A.12}$$

Proof:

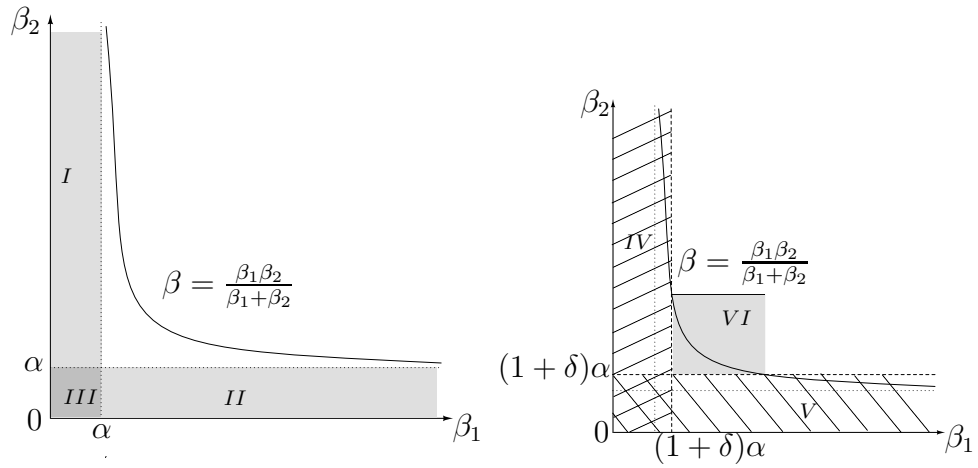

Figure A.2 Decomposition of the event region of $\{\beta < \alpha\}$.

In the (β_1, β_2) two-dimensional space, the probability $\mathrm{P}(\beta < \alpha)$ for a fixed positive α can be written as the integral of the joint PDF $p(\beta_1, \beta_2)$ over the region $\{(\beta_1, \beta_2) : \frac{1}{\beta_1} + \frac{1}{\beta_2} > \frac{1}{\alpha}\}$, which is the region under the hyperbola curve in Fig. A.2. By decomposing the region into smaller pieces, we can upper and lower bound the probability $\mathrm{P}(\beta < \alpha)$. We obtain a lower bound P_L of $P(\beta < \alpha)$ for $\alpha \to 0^+$ as follows:

$$\begin{aligned} P_L \triangleq & P(I) + P(II) - P(III) = P(\beta_1 < \alpha) + P(\beta_2 < \alpha) - P(\beta_1 < \alpha)P(\beta_2 < \alpha) \\ = & \frac{a_1}{t_1+1}\alpha^{t_1+1} + \frac{a_2}{t_2+1}\alpha^{t_2+1} + o_L(\alpha^{t_1+1+\epsilon_1}) + o_L(\alpha^{t_2+1+\epsilon_2}) + o_L(\alpha^{t_1+t_2+2}) \end{aligned}$$

For a fixed small positive number δ, the probability $P(\beta < \alpha)$ can be upper bounded by:

$$\begin{aligned} P_U \triangleq & P(IV) + P(V) + P(VI) \\ = & P\big(\beta_1 < (1+\delta)\alpha\big) + P\big(\beta_2 < (1+\delta)\alpha\big) + \\ & P\big((1+\delta)\alpha < \beta_1 < (1+\delta)\alpha/\delta\big) \cdot P\big((1+\delta)\alpha < \beta_2 < (1+\delta)\alpha/\delta\big) \\ = & \frac{a_1(1+\delta)^{t_1+1}}{t_1+1}\alpha^{t_1+1} + \frac{a_2(1+\delta)^{t_2+1}}{t_2+1}\alpha^{t_2+1} + o_U(\alpha^{t_1+1+\epsilon_1}) + o_U(\alpha^{t_2+1+\epsilon_2}) + o_U(\alpha^{t_1+t_2+2}) \end{aligned}$$

In the above derivation, we have used the fact that $P(\beta_1 < \alpha)P(\beta_2 < \alpha)$ and $P\big((1+\delta)\alpha < \beta_1 < (1+\delta)\alpha/\delta\big)P\big((1+\delta)\alpha < \beta_2 < (1+\delta)\alpha/\delta\big)$ have the order of α as $t_1 + t_2 + 2$ for fixed δ, and all other higher order terms can be omitted. Since the upper bound holds for any $\delta > 0$, we can let $\delta \to 0$ and obtain that

$$P_U = \frac{a_1}{t_1+1}\alpha^{t_1+1} + \frac{a_2}{t_2+1}\alpha^{t_2+1} + o_U(\alpha^{t_1+1+\epsilon_1}) + o_U(\alpha^{t_2+1+\epsilon_2}) + o_U(\alpha^{t_1+t_2+2})$$

Notice that we are studying the behavior of $P(\beta < \alpha)$ for $\alpha \to 0^+$, thus we can always choose α much smaller than δ so that the above expression is valid (for example, take $\alpha = \delta^2/(1+\delta)$). By comparing the corresponding polynomial terms of $P(\beta < \alpha) = a \cdot \alpha^{t+1}/(t+1) + o(\alpha^{t+1+\epsilon})$ with P_L and P_U, , we can reach the final results. □

As stated in Section A.2, the average SEP at high SNR can be characterized by the diversity gain and coding gain, which depend only on the behavior of $p(\beta)$ at β around 0^+. Therefore, combining the results in Propositions 1 and 2, we can obtain the following result about the average SEP of a two-hop relay system.

Proposition 3 *(Average SEP of two-hop diversity system): Consider a two-hop diversity system as specified by* (A.4)–(A.6), (A.9), *and* (A.10), *where the two hops h_1 and h_2 are independent. Let G_{dl} and G_{cl} denote the diversity and coding gains associated with $\gamma_l = \beta_l\bar{\gamma}$, $l = 1, 2$. The average SEP at high SNR can be approximated as*

$$P_E \approx (G_c \cdot \bar{\gamma})^{-G_d}$$

where the diversity gain G_d and the coding gain G_c for γ are given, respectively, by

$$G_d = \min(G_{d1}, G_{d2}), \quad \textit{and} \quad G_c = \begin{cases} G_{c1} & \textit{if} \quad G_{d1} < G_{d2}, \\ \left(G_{c1}^{-G_d} + G_{c2}^{-G_d}\right)^{-1/G_d} & \textit{if} \quad G_{d1} = G_{d2}, \\ G_{c2} & \textit{if} \quad G_{d1} > G_{d2}. \end{cases} \tag{A.13}$$

Notice that the two hops can have not only different SNR's, but also different types of PDF's. However, the end-to-end diversity gain is always determined by the hop with smaller diversity gain, i.e., the weaker hop.

A.4 General cooperative diversity system

A.4.1 Single-Branch Multi-Hop System

Figure A.3 A cooperative diversity system with N hops.

The results in Section A.3 can be generalized to a multi-hop system. As shown in Fig. A.3, the system with L hops is composed of a source terminal S, a destination terminal D, and $(L-1)$ intermediate relay terminals R_1 through R_{L-1}. The fading coefficient for lth hop will be denoted as h_l, the AWGN as n_l, and the amplification coefficient at terminal R_i as A_i. Without loss of generality, we assume all n_l's are independent and have the same variance N_0. Then the received signal y_l at the end of lth hop can be expressed as

$$y_l = h_l A_l y_{l-1} + n_l, \quad l = 1, \ldots, L-1, \tag{A.14}$$

$$y_L = h_L y_{L-1} + n_L, \tag{A.15}$$

where $y_0 = x$, which is the transmitted symbol from terminal S with energy E_s. As stated in Section A.3.1, we choose $A_l^2 = 1/|h_l|^2$. With this simplification we obtain the instantaneous end-to-end SNR γ as

$$\frac{1}{\gamma} = \frac{1}{\gamma_1} + \frac{1}{\gamma_2} + \cdots + \frac{1}{\gamma_L} \tag{A.16}$$

which is equivalent to (cf. assumption i in Section A.2)

$$\frac{1}{\beta} = \frac{1}{\beta_1} + \frac{1}{\beta_2} + \cdots + \frac{1}{\beta_L} \tag{A.17}$$

where $\beta = \gamma/\bar{\gamma}$, $\beta_l = \gamma_l/\bar{\gamma}$, and $\bar{\gamma} = E_s/N_0$. By Proposition 2 and induction on l, we can readily obtain the following result.

Proposition 4 *(Diversity and coding gains of a single-branch multi-hop system): Consider L non-negative independent random variables $\beta_1, \beta_2, \ldots, \beta_L$ with approximated PDFs $p_l(\beta_l) = a_l \beta_l^{t_l} + o(\beta_l^{t_l+\epsilon_l})$, for $\beta_l \to 0^+$ and $l = 1, \ldots, L$. The PDF $p(\beta)$ of β as in* (A.17) *can be*

approximated as

$$p(\beta) = a\beta^t + o(\beta^{t+\epsilon}), \quad \textit{for } \beta \to 0^+,$$

where

$$t = \min_{l=1,\ldots,L}(t_l), \qquad a = \sum_{i=1}^{L_c} a_{l_i}, \tag{A.18}$$

and $\{l_1, \ldots, l_{L_c}\}$ *is the set of indices of* t_l*'s such that* $t_l = t$*. The corresponding diversity and the coding gains are given by*

$$G_d = \min_{l=1,\ldots,L}(G_{d,l}) \quad \textit{and} \quad G_c = \left(\sum_{i=1}^{L_c} G_{c,l_i}^{-G_d}\right)^{-1/G_d} \tag{A.19}$$

where $G_{d,l}$ *and* $G_{c,l}$ *are the diversity and the coding gains of the* l*th hop, respectively.*

This important result reveals that the overall asymptotic performance of a multi-hop system is determined by the weakest hops. Here, the "weakest" hops means the hops with smallest diversity gain.

A.4.2 Multi-branch system

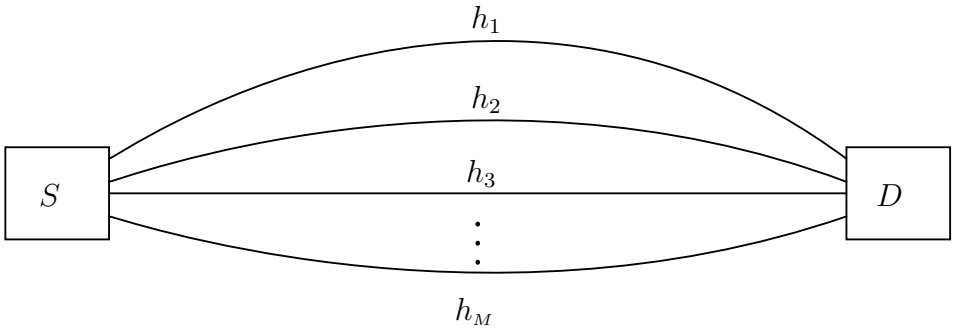

Figure A.4 A cooperative diversity system with M hops.

In addition to the multi-hop system, multi-branch cooperative diversity system is another choice. Consider a diversity system with M branches between terminal S and terminal D as shown in Fig. A.4. We assume that all branches are mutually orthogonal, and *maximum ratio combining* (MRC) is employed at the terminal D. Other combining schemes can also be dealt with. Then the overall end-to-end SNR γ is the sum of the end-to-end SNR's for each branch, i.e., $\gamma = \sum_{m=1}^{M} \gamma_m$.

For such a system, the overall diversity gain and coding gain have been given in [114], which is repeated in the following proposition for completeness.

Proposition 5 [114] *(Diversity combining): Let $\gamma_m = \beta_m \bar{\gamma}$ have diversity gain $G_{d,m}$ and coding gain $G_{c,m}$, for $m = 1, \ldots, M$, and suppose that β_m's are mutually independent. Then, the diversity gain G_d and coding gain G_c for $\gamma = \beta\bar{\gamma}$ are given, respectively, by*

$$\begin{aligned} G_d &= \sum_{m=1}^{M} G_{d,m} \\ G_c &= \left[\frac{2^{M-1}\pi^{(M-1)/2}\Gamma(1/2+G_d)[\prod_m G_{d,m}\Gamma(G_{d,m})]}{\Gamma(1+G_d)[\prod_m G_{c,m}^{G_{d,m}}\Gamma(G_{d,m}+1/2)} \right]^{1/G_d} \end{aligned} \tag{A.20}$$

Notice that each branch can have different fading conditions, and the result only depends on the end-to-end diversity gain and coding gain of each branch.

A.4.3 Multi-branch, multi-hop system

Based on the results in Sections A.4.1 and A.4.2, we can now study the asymptotic performance of a general cooperative diversity system with multi-branch and multi-hop.

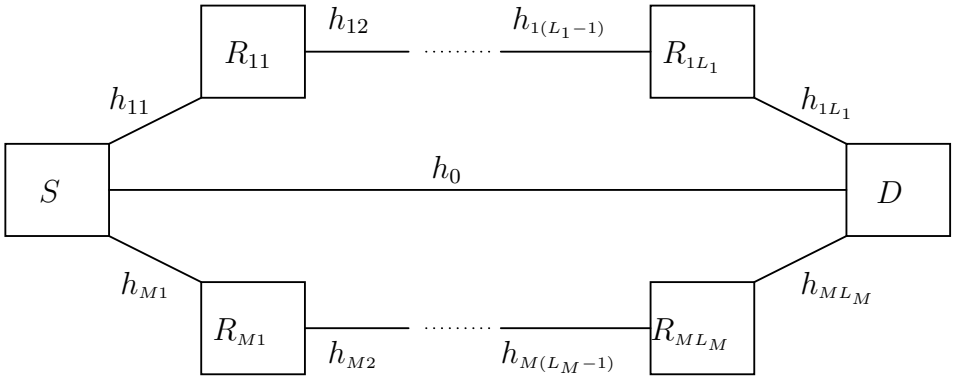

Figure A.5 A cooperative diversity system with multi-hop and multi--branch.

A general cooperative system can be modeled as a system with M branches, the mth of which has L_m hops, as depicted in Fig. A.5. We assume that the fading coefficients are mutually independent, and MRC is employed. Other combining schemes such as equal-gain combining or selection combining can also be dealt with. Since each branch is a multi-hop

diversity system as studied in Section A.4.1, the end-to-end diversity gain $G_{\mathrm{d},m}$ and coding gain $G_{\mathrm{c},m}$ of the mth branch are given by (A.19), for $m = 1, \ldots, M$. Then, such branches can be viewed as non-relay fading channels with the corresponding diversity gains and coding gains. Based on this observation, we have the following result.

Proposition 6 *(Diversity and coding gains for a multi-branch multi-hop system): The overall diversity and coding gains of the multi-branch multi-hop cooperative diversity system are given by:*

$$\begin{aligned} G_d &= \sum_{m=1}^{M} G_{d,m} \\ G_c &= \left[\frac{2^{M-1}\pi^{(M-1)/2}\Gamma(1/2+G_d)[\prod_m G_{d,m}\Gamma(G_{d,m})]}{\Gamma(1+G_d)[\prod_m G_{c,m}^{G_{d,m}}\Gamma(G_{d,m}+1/2)} \right]^{1/G_d} \\ G_{d,m} &= \min_{l=1,\ldots,L_m} G_{d,ml} \\ G_{c,m} &= \left(\sum_{i=1}^{L_{c,m}} G_{c,ml_i}^{-G_{d,m}} \right)^{-1/G_{d,m}} \end{aligned} \tag{A.21}$$

where $G_{d,ml}$ and $G_{c,ml}$ are the diversity gain and coding gain of the lth hop in the mth branch, respectively.

Therefore, the diversity of multi-branch multi-hop cooperative system is the sum of the branch diversities, and the diversity gain of a branch is equal to the least diversity gain among all hops in the branch.

The result is quite general: It applies to many types of fading models, such as Rayleigh, Rician, Nakagami-m, etc.. The only requirement is that the PDF of the fading coefficients can be approximated by a term like β^t, where t does not have to be integer. The hops can also have different fading types.

It can be seen from (A.21) that, in general, the resource is better used to add a cooperative branch than to add a hop in an existing branch.

A.5 Outage probability

In addition to the average SEP, outage probability is another performance criterion for the communication system over fading channels. It is defined as the probability that the instantaneous SNR γ falls below a certain threshold γ_{th} [99]:

$$P_{\text{out}} := P(0 \leqslant \gamma \leqslant \gamma_{\text{th}}) = \int_0^{\gamma_{\text{th}}/\bar{\gamma}} p(\beta)\mathrm{d}\beta. \tag{A.22}$$

where $\gamma = \beta\bar{\gamma}$. If $\bar{\gamma}$ is large enough, then P_{out} depends only on the behavior of $p(\beta)$ at $\beta \to 0^+$.

In a general cooperative diversity system, we define "outage" as the event that the overall end-to-end SNR falls below a certain threshold. The outage probability therefore only depends on the PDF of the end-to-end SNR. It has been shown in [114] that the outage probability and average SEP share the same diversity gain, and their coding gains are different by a constant that is easily computable. Therefore, all the results that we have obtained on average SEP can be suitably modified to deal with outage probability.

A.6 Simulation results

We used Monte Carlo simulations to find the end-to-end performance of cooperative diversity systems, and compared them with the analytical results developed herein. For simplicity, binary phase shift keying (BPSK) modulation was employed. Our performance criteria were bit error rate (BER) and outage probability of the whole system. We define the average SNR as $\bar{\gamma} = E_b/N_0$, where E_b is the energy of the BPSK symbol.

Since the results of two-hop diversity system presented in Section A.3 are important for all other results after that, we first simulated the single-branch two-hop setup. Suppose the first hop is over Rayleigh fading channel, and the second one is over a Nakagami-m channel with parameter m equal to 2, 3, or 4. The amplification coefficient A at the relay has the form of (A.9). For these three different cases, the diversity gain of the first hop $G_{\text{d},1}$ is always 1, and the second hop $G_{\text{d},2} = 2, 3, 4$, respectively. Using Proposition 3 and the argument in Section A.5, we can obtain the analytical expressions of the BER and the outage probability. According to the analysis, the BER performance at high SNR for three different cases are all the same.

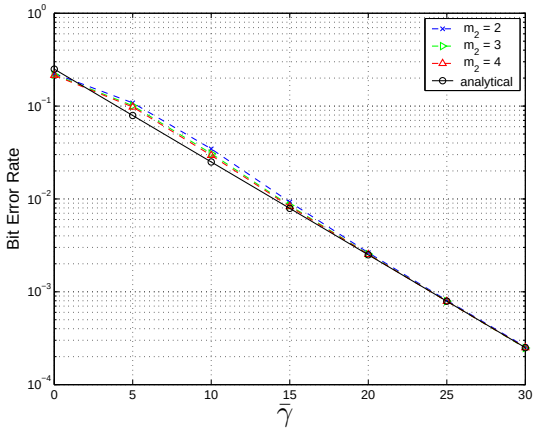

(a) BER versus average SNR $\bar{\gamma} = E_b/N_0$

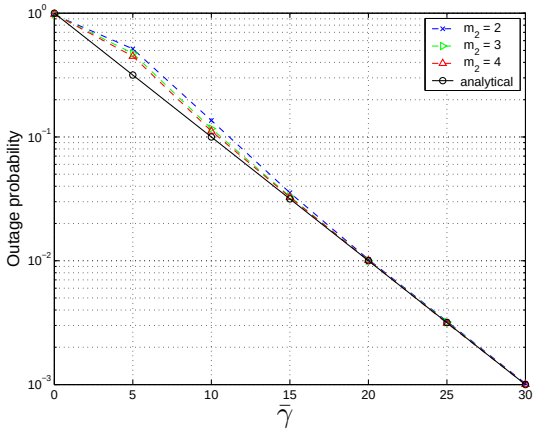

(b) Outage probability versus normalized SNR $\bar{\gamma}/\gamma_{\text{th}}$

Figure A.6 Performance of a two-hop cooperative diversity system. The first hop is over Rayleigh fading channel, and the second hop is over Nakagami-m channels with $m = 2, 3$, or 4.

The simulation results matched well the analytical line predicted by Proposition 3. Similar observations can be drawn from the outage probabilities. Moreover, the analytical results also provide a very good approximation for moderate SNR values. These facts verify the conclusion that the end-to-end performance of a two-hop system is determined by the "weaker" hop. In this case, it corresponds to the first hop, since $G_{\text{d},1} = 1$, which is less than $G_{\text{d},2} = 2, 3, 4$.

We next focus on a general cooperative diversity system with multi-branch and multi-hop. Consider a system with two branches, and each branch has multiple hops. Suppose the first branch has two hops over Rayleigh and Rician ($K = 4$) fading channels, and the second branch has four hops over Nakagami-m fading channels, where $m = 0.5, 1.5, 2, 0.5$ respectively. To justify the choice of amplification coefficients at the relays, simulation results of the systems using (A.7) and (A.9) as amplification coefficients are both depicted in Fig. A.7, together with the analytical lines. It is seen from the above figure that the performance of the system using (A.9) as amplification coefficients is a tight lower bound on that of a system using (A.7), even at the low and moderate SNR values. Another important observation is that, for both BER and outage probability, the analytical lines match the simulation results perfectly at high SNR, and are also good approximations for the moderate SNR. Notice that the analytical results

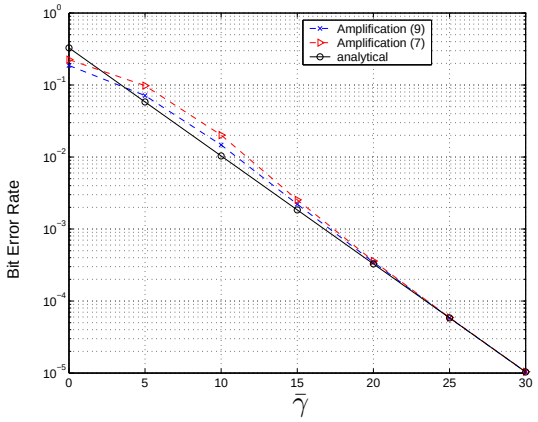

(a) BER versus average SNR $\bar{\gamma} = E_b/N_0$

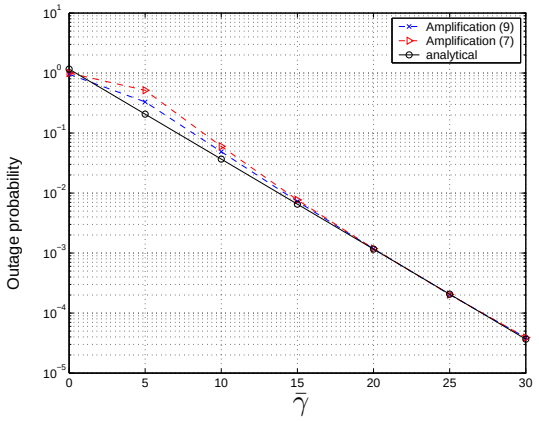

(b) Outage probability versus normalized SNR $\bar{\gamma}/\gamma_{\text{th}}$

Figure A.7 Performance of a general cooperative diversity system with two branches. The first branch has two hops over Rayleigh and Rician ($K = 4$) fading channels, and the second branch has four hops over Nakagami-m fading channels with $m = 0.5, 1.5, 2, 0.5$, respectively. The dotted lines are obtained from Monte-Carlo simulation.

do not predict the true performance behavior at low SNR. This is due to the fact that our approximations are based on the high SNR assumption, which is the focus of this work.

A.7 Summary

We introduced two parameters, diversity gain and coding gain, to characterize the average symbol error probability and outage probability of a cooperative diversity system at high SNR. We analyzed the asymptotic error probability and outage probability for a single-branch two-hop system, a multi-branch system, and a general multi-branch multi-hop system, all with non-regenerative relay policy. Our analysis indicates that the diversity of multi-branch multi-hop cooperative system is the sum of the branch diversities, and the diversity gain of a branch is equal to the least diversity gain among all hops in the branch. We have also obtained coding gain expressions for the general setup. Our analysis is applicable to cooperative systems with any number of branches and hops, and valid for almost all commonly used fading models. Simulations results match well the analytical performance at moderate and high SNR values. Our results are important in providing guidelines for designing a cooperative system. For

example, a simple consequence is the observation that it is better to add a cooperative branch than to add a hop in an existing branch.

APPENDIX B. LIFETIME MAXIMIZATION UNDER CONNECTIVITY AND k-COVERAGE CONSTRAINTS IN WIRELESS SENSOR NETWORKS

B.1 Introduction

Energy conservation is perhaps the most important issue in wireless sensor networks [2, 28]. Most sensor devices are battery-powered and hence have a very limited amount of energy. It is, therefore, very important to extend the battery operation time of individual sensors and, consequently, the network's lifetime. Operating each sensor device in a low duty-cycle has been recognized as an effective way to achieve this goal, where *duty-cycle* is defined as the fraction of time that a sensor device is active. On the other hand, a wireless sensor network typically has two major tasks: *sensing* and *communication*. It is always desirable to have all active sensors connected and, at the same time, to have the entire sensing field k-covered. The connectivity among active sensors is required in order for an active sensor to report its sensing results back to the user, and the reason for requiring k-coverage rather than just 1-coverage is to increase the detection probability and accuracy of tracking. Obviously, the lower the duty-cycles of individual sensors, the longer the wireless sensor network's lifetime, but at the same time, there are a smaller number of active sensors at a given time and, hence, more likely either active sensors are not connected or the k-coverage of the sensing field cannot be guaranteed. So, there are inherent tradeoffs, and the key contribution of our work is to present an integrated study on connectivity, k-coverage, and lifetime of a large-scale wireless sensor network.

B.1.1 Related Work

Several researchers [40, 112, 95, 59] have addressed the coverage and connectivity issues in wireless sensor/ad hoc networks. Gupta et al. [40] studied scaling laws for asymptotic connectivity of sensors placed at random over a unit area, and provided bounds on connectivity probability for finite-size networks. In [112], the authors studied the relation between k-coverage and k-connectivity when the communication radius is at least twice the sensing radius, where the sensing radius is deterministic. However, no statistical properties of either k-coverage or k-connectivity were given. In [95] and [59], the asymptotic coverage problem was addressed for mostly-sleeping (unreliable) wireless sensor networks, where 1-coverage was studied in [95] and k-coverage in [59], but neither one provided the sufficient and necessary condition for asymptotic coverage. Moreover, none of the above work considered the inherent irregularity of sensing radii due to the time-varying environments. In contrast, we model the sensing radius as a random variable.

Recently, research efforts [118, 121] have also been made to analyze the lifetime of a wireless sensor network with coverage requirements. The definitions of network's lifetime in these literature are different from ours. In [118], the lifetime was defined as the time it takes for the coverage — defined as the ratio of the area covered by working sensors to the entire area — to drop below a pre-defined threshold. In [121], the α-lifetime of a wireless sensor network was defined as the interval during which at least α portion of the sensing region is covered by at least one sensor node. Both [118] and [121] only studied the relation between network's lifetime and coverage of the sensing field without, however, considering the connectivity among active sensors, which is another key element for the network to function properly. The above definitions of network's lifetime are all from the deterministic point of view. Considering the fact that the deployment and dynamics of wireless sensor networks are random and, hence, the coverage of the sensing field and the connectivity among active sensors are also random variables, we study network's lifetime from a (different) probabilistic perspective.

B.1.2 Key Contributions

We explore the fundamental limits of a wireless sensor network's lifetime under connectivity and k-coverage constraints, and the contributions are threefold. First, asymptotic results for k-coverage of the sensing field are presented. Under independent sleeping schemes and random sensing radius model, we derive the sufficient and necessary condition on the sensing radius in order to maintain k-coverage with probability one as the number of sensors goes to infinity. Second, we introduce a new definition of network's lifetime from a probabilistic perspective, namely ω-lifetime, which is defined as the expectation of the time interval during which the probability of guaranteeing connectivity and k-coverage simultaneously is at least ω. By solving two convex optimization problems, we obtain a lower bound and an upper bound on the network's maximum ω-lifetime. Third, based on the obtained lower bound, we propose a near-optimal scheduling scheme, called CIS (Coordinated Independent Sleeping), to maximize the network's ω-lifetime, and describe a possible distributed implementation of the CIS scheme.

B.1.3 Organization

The rest of this appendix is organized as follows. Section B.2 describes our network model and gives the problem statement. In Section B.3, we derive the sufficient and necessary condition for maintaining k-coverage with probability one as the number of sensors goes to infinity. Section B.4 describes the details of the proposed CIS scheduling scheme. Section B.5 presents and evaluates the simulation results and, finally, the appendix concludes in Section B.6.

B.2 Network Model and Problem Statement

B.2.1 Network Model

Consider a wireless sensor network of n sensors deployed independently and uniformly within a square sensing field $\mathcal{D}$ of unit area. In order to extend network's lifetime, an appropriate duty cycle and a well-designed sleeping schedule are required, and we propose the following Coordinated Independent Sleeping (CIS) scheme for this purpose: *time is divided*

into rounds, and at the beginning of a round, each alive sensor becomes active with probability p or inactive (sleeping) with probability (1−p), independently from others. The value of p varies with the round and is determined by the performance metric to be optimized. Here, alive sensors refer to the sensors with enough energy to operate. The CIS scheme is based on the Randomized Independent Sleeping (RIS) scheme proposed in [59] and the details of CIS will be discussed in Section B.4.

B.2.1.1 Sensing model

To consider the sensing radii irregularity caused by time-varying environments, we assume a random disc sensing model where (1) each active sensor has a *sensing radius* of r_s; (2) any object within a disc of radius r_s centered at an active sensor can be reliably-detected by the sensor; and (3) r_s's are independently identically distributed (i.i.d) random variables with mean r_0 and variance $r_0^2\sigma_s^2$, and the underlying distribution is assumed unknown. A point in the sensing field $\mathcal{D}$ is said to be *k-covered* if it is within the sensing radius of at least k active sensors. The field $\mathcal{D}$ is said to be *k-covered* if every point in $\mathcal{D}$ is k-covered.

B.2.1.2 Communication model

Two active sensors can communicate directly with each other if and only if the distance between them is no more than r_c. The radius r_c is usually referred to as the *communication radius*. For the purpose of simplicity, we assume that all active sensors have the same and deterministic communication radii. The network is said to be connected if the underlying graph composed of active sensors is connected. Moreover, we assume torus convention (also known as the toroidal model) [41], i.e., each disc (communication or sensing) that protrudes one side of the field $\mathcal{D}$ enters $\mathcal{D}$ again from the opposite side. This eliminates the edge effects and simplifies the problem.

B.2.1.3 ω-lifetime

Due to the randomness in sensor deployment and sleeping schedule, it is impossible to guarantee connectivity and k-coverage with probability one with finite number of sensors, unless the communication disc and the sensing disc of each active sensor can cover the entire field. However, the physical limitations prohibit such large communication radius and sensing radius. In other words, there is no deterministic guarantee of connectivity or k-coverage for randomly-deployed wireless sensor networks in practice. Such facts motivate us to study the network's lifetime from a probabilistic perspective. More specifically, we define the *ω-lifetime* of a randomly-deployed wireless sensor network as the expectation of the time interval during which the probability of guaranteeing k-coverage of field $\mathcal{D}$ and the connectivity of the network simultaneously is at least ω, where $0 < \omega < 1$. For example, suppose that the CIS scheduling scheme is employed, then the network's ω-lifetime is $T_\omega = \mathrm{E}\left[\sum_{i=1}^{M} T_i\right]$, where T_i is the duration of the i-th round, and M is the maximum number of rounds during which the network can function properly. In other words, for any round i ($i \leqslant M$), the probability of guaranteeing both connectivity and k-coverage simultaneously, defined as $P_{\mathrm{c\&c}}$, is at least ω, but for round $(M+1)$, $P_{\mathrm{c\&c}}$ is smaller than ω.

B.2.2 Problem Statement

The problems we study in this appendix are the following:

1. What relation among n, p, r_0, and σ_s^2 would be the sufficient and necessary condition to guarantee that the probability of the entire field $\mathcal{D}$ being k-covered approaches 1 as n goes to infinity? This problem is referred to as the critical condition for asymptotic k-coverage. Although the answer to this problem can not be directly-applied to practical wireless sensor networks, such condition may give us insights on designing large-scale wireless sensor networks.

2. For a finite-size wireless sensor network, how to find the optimal parameters for the CIS scheme to maximize the ω-lifetime of the network? Compared with the first problem,

this problem is more realistic and the result may serve as a good guideline in deploying finite-size wireless sensor networks.

B.3 Critical Condition for Asymptotic k-coverage

In this section, we derive the sufficient and necessary condition for asymptotic k-coverage, i.e., the entire sensing field $\mathcal{D}$ is k-covered with probability one as the total number of deployed sensors n goes to infinity.

Lemma 5 *Let n points distributed independently and uniformly in a square field $\mathcal{D}$ of unit area within $\mathbb{R}^2$, then for sufficiently large n, these points form a stationary Poisson point process with density n.*

Lemma 5 is a well-known result and its proof is given by Hall in [41]. Let $\mathcal{P} \equiv \{\xi_i, i \geqslant 1\}$ denote the set of active sensors. It is shown in Lemma 6 that $\mathcal{P}$ is also a stationary Poisson point process with density np for sufficiently large n.

Lemma 6 *Let n points distributed independently and uniformly in a square field $\mathcal{D}$ of unit area within $\mathbb{R}^2$. Each point is marked independently as an active point with probability p, where $0 < p \leqslant 1$. Then the set of active points, $\mathcal{P} = \{\xi_i, i \geqslant 1\}$, is a stationary Poisson point process with density np for sufficiently large n.*

Let S_i denote a random disc with radius $r_{s,i}$ centered at the origin of $\mathbb{R}^2$, which is defined as $S_i \equiv \{x \in \mathbb{R}^2 : |x| \leqslant r_{s,i}\}$, where $r_{s,i}$ is the sensing radius of the i-th active sensor ξ_i. Here, we assume that all sensing radii are i.i.d random variables following an *unknown* distribution $F(r)$, with *known* mean r_0 and variance $r_0^2\sigma_s^2$, i.e., all S_i's are distributed as S:

$$S \equiv \{x \in \mathbb{R}^2 : |x| \leqslant r,\ r \sim F(r)\}. \tag{B.1}$$

Then, the sensing disc (abbreviated as disc) centered at active sensor ξ_i can be defined as $D_i \equiv \xi_i + S_i = \{\xi_i + y : y \in S_i\}$. The set of $\{D_i, i \geqslant 1\}$ forms a stationary coverage process. For such a coverage process, Lemma 7 gives the distribution of the number of discs with certain properties.

Lemma 7 *Let $\mathcal{Q} = \{\xi_i + S_i, i \geqslant 1\}$ denote a stationary coverage process, where $\{\xi_i\}$ is a stationary Poisson point process with density λ within $\mathcal{D}$, and S_i's are distributed as S defined in* (B.1). *For a given deterministic condition C, let Y denote the number of discs in $\mathcal{Q}$ that satisfy the condition C. Then, Y is Poisson-distributed with mean*

$$\mu = \lambda \cdot \mathrm{E}\Big[\|\{x : I_C(x+S) = 1\}\|\Big],$$

where $I_C(\cdot)$ is the indicator function of whether a disc satisfies the condition C or not, and $\|\cdot\|$ denotes the area.

The proofs of Lemma 6 and Lemma 7 are omitted due to space limitation. Interested readers can refer to the full version of this appendix [67].

Let $Y(x)$ denote the number of active sensors that cover a point x, and $I_k(x)$ denote the indicator function of whether the point x is covered by at most $(k-1)$ active sensors, i.e.,

$$I_k(x) = \begin{cases} 1, & \text{if } Y(x) < k, \\ 0, & \text{otherwise.} \end{cases}$$

Then, the expectation of Bernoulli random variable $I_k(x)$ is

$$\mathrm{E}[I_k(x)] = P(x \text{ is at most } (k-1)\text{-covered}) = P(Y(x) < k).$$

By Lemma 7, we know that $Y(x)$ is Poisson-distributed with mean

$$\mu = np \cdot \mathrm{E}\big[\|\{x : (x+S) \cap \{x\} \neq \emptyset\}\|\big] = np \cdot \mathrm{E}\big[\|x - S\|\big] = npa_s,$$

where $a_s \equiv \mathrm{E}\big[\|S\|\big] = \pi r_0^2(1+\sigma_s^2)$. Therefore,

$$\mathrm{E}[I_k(x)] = e^{-npa_s} \sum_{j=0}^{k-1} \frac{(npa_s)^j}{j!}. \tag{B.2}$$

Let the k-vacancy V_k denote the area within $\mathcal{D}$ that is covered by at most $(k-1)$ active sensors, then the random variable V_k can be expressed as $V_k = \int_{\mathcal{D}} I_k(x)\mathrm{d}x$. Using Fubini's theorem [10] and exchanging the order of integral and expectation, we obtain the expected value of the k-vacancy as:

$$\mathrm{E}[V_k] = \int_{\mathcal{D}} \mathrm{E}[I_k(x)]\mathrm{d}x = e^{-npa_s} \sum_{j=0}^{k-1} \frac{(npa_s)^j}{j!}. \tag{B.3}$$

K-coverage of the sensing field $\mathcal{D}$ means that each point in $\mathcal{D}$ should be covered by at least k active sensors, which implies $V_k = 0$. Because sensors are deployed independently and uniformly within $\mathcal{D}$, it cannot guarantee $P(V_k = 0) = 1$ with finite n for $a_s < 1$ regardless of the value of n. However, if $np \to \infty$ as $n \to \infty$, it is possible that $P(V_k = 0) \to 1$ as $n \to \infty$. Before studying the asymptotic behavior of $P(V_k = 0)$, we first give an upper bound and a lower bound on $P(V_k = 0)$ for finite n. Similar bounds have been proved in [121] for the case of deterministic sensing radius model and non-sleeping sensor networks. Theorem 8 is a generalization of the results in [121].

Theorem 8 *For $n > 1$, $0 < p \leqslant 1$, and $a_s < 1$*

$$P_l < P(V_k = 0) < P_u, \tag{B.4}$$

in which

$$P_u = \frac{4(k+1)!(1+\sigma_s^2)(np)^{-1}(npa_s)^{-k} \cdot e^{npa_s}}{1 + 4(k+1)!(1+\sigma_s^2)(np)^{-1}(npa_s)^{-k} \cdot e^{npa_s}}, \tag{B.5}$$

and

$$P_l = 1 - 2e^{-npa_s}\left(1 + (n^2p^2a_s' + 2npr_0)\sum_{i=0}^{k-1}\frac{(npa_s)^i}{i!}\right) \tag{B.6}$$

where $a_s' \equiv \pi r_0^2(1 + \sigma_s^2/2)$.

Proof: (i) Upper bound.

By the Cauchy-Schwartz inequality [41],

$$\mathrm{E}[V_k] = \mathrm{E}[V_k \cdot I(V_k > 0)] \leqslant \{\mathrm{E}[V_k^2]P(V_k > 0)\}^{1/2},$$

where $I(\cdot)$ denotes the indicator function, thus

$$P(V_k > 0) \geqslant \frac{(\mathrm{E}[V_k])^2}{\mathrm{E}[V_k^2]}, \tag{B.7}$$

where

$$\mathrm{E}[V_k^2] = \mathrm{E}\Big[\int\int_{\mathcal{D}^2} I_k(x_1)I_k(x_2)dx_1dx_2\Big] = \int\int_{\mathcal{D}^2} \mathrm{E}[I_k(x_1)I_k(x_2)]dx_1dx_2.$$

Let Y_1 denote the number of active sensors that cover x_1, Y_2 the number of active sensors that cover x_2, and Y_3 the number of active sensors that cover x_2, but not cover x_1, then

$$\mathrm{E}[I_k(x_1)I_k(x_2)] = P(Y_1 < k, Y_2 < k) \leqslant P(Y_1 < k, Y_3 < k). \tag{B.8}$$

Lemma 8 *For the random variables Y_1 and Y_3 defined above, we have the following results:*

- *Y_1 is Poisson-distributed with mean npa_s,*
- *Y_3 is Poisson-distributed with mean npb_s,*
- *Y_1 and Y_3 are independent,*

where

$$b_s \equiv \mathrm{E}\Big[\big\|\{x : (x+S)\cap\{x_1\} = \emptyset, (x+S)\cap\{x_2\} \neq \emptyset\}\big\|\Big].$$

The proof of Lemma 8 is omitted here due to space limitation. Interested users can refer to [67]. Using Lemma 8 and (B.8), we have

$$\begin{aligned}\mathrm{E}[I_k(x_1)I_k(x_2)] &\leqslant P(Y_1 < k)\cdot P(Y_3 < k) = \mathrm{E}[I_k(x_1)]\cdot P(Y_3 < k)\\ &= \mathrm{E}[I_k(x_1)]\cdot\Big(e^{-npb_s}\sum_{j=0}^{k-1}\frac{(npb_s)^j}{j!}\Big).\end{aligned} \tag{B.9}$$

Let $z = x_1 - x_2$, then

$$\begin{aligned}b_s &= \mathrm{E}\Big[\big\|\{x : (x+S)\cap\{x_1\} = \emptyset, (x+S)\cap\{x_2\} \neq \emptyset\}\big\|\Big]\\ &= \mathrm{E}\Big[\big\|\{x : (x+S)\cap\{z\} = \emptyset, (x+S)\cap\{0\} \neq \emptyset\}\big\|\Big]\\ &= a_s - \rho(z),\end{aligned}$$

where

$$\rho(z) = \mathrm{E}\Big[\big\|\{x : (x+S)\cap\{z\} \neq \emptyset, (x+S)\cap\{0\} \neq \emptyset\}\big\|\Big] = \int_0^\infty r^2 B(|z|/2r)dF(r),$$

and

$$B(x) = \begin{cases} 4\int_x^1 \sqrt{(1-y^2)}dy & \text{if } 0 \leqslant x \leqslant 1\\ 0 & \text{otherwise}\end{cases}$$

is the area of the lens of intersection of two unit discs centered $2x$ apart, and $F(r)$ is the distribution of sensing radius r_s.

It is shown in [67] that $B(x) \leqslant \pi(1-x)$ for $0 \leqslant x \leqslant 1$, then using the fact that $\rho(z) \geqslant 0$ and after some algebraic manipulation, we can bound $\rho(z)$ as

$$\begin{cases} \rho(z) \leqslant a_s - \pi r_s |z|/2 & \text{if } |z| < 2r_s(1+\sigma_s^2), \\ \rho(z) = 0 & \text{if } |z| \geqslant 2r_s(1+\sigma_s^2). \end{cases}$$

If $|z| \geqslant 2r_s(1+\sigma_s^2)$, then $b_s = a_s$. Using (B.9), we have

$$\mathrm{E}[I_k(x_1)I_k(x_2)] \leqslant \mathrm{E}[I_k(x_1)] \cdot \mathrm{E}[I_k(x_2)].$$

Therefore,

$$\begin{aligned} I_1 &\equiv \int\int_{\mathcal{D}^2 \cap \{|x_1-x_2| \geqslant 2r_s(1+\sigma_s^2)\}} \mathrm{E}[I_k(x_1)I_k(x_2)]dx_1dx_2 \\ &\leqslant \int\int_{\mathcal{D}^2} \mathrm{E}[I_k(x_1)] \cdot \mathrm{E}[I(x_2)]dx_1dx_2 = (\mathrm{E}[V_k])^2. \end{aligned} \tag{B.10}$$

Similarly, if $|z| < 2r_s(1+\sigma_s^2)$, then $b_s \geqslant \pi r_s|z|/2$. Using (B.9), we have

$$\mathrm{E}[I_k(x_1)I_k(x_2)] \leqslant \mathrm{E}[I_k(x_1)] \cdot \Big(e^{-np\frac{\pi r_s}{2}|z|} \sum_{j=0}^{k-1} \frac{(np\pi r_s|z|)^j}{2^j \cdot j!}\Big).$$

Therefore,

$$\begin{aligned} I_2 \equiv& \int\int_{\mathcal{D}^2 \cap \{|x_1-x_2| < 2r_s(1+\sigma_s^2)\}} \mathrm{E}[I_k(x_1)I_k(x_2)]dx_1dx_2 \\ \leqslant& \int_{\mathcal{D}} \mathrm{E}[I_k(x_1)]dx_1 \int_0^{2r_s(1+\sigma_s^2)} e^{-np\pi r_s z/2} \sum_{i=0}^{k-1} \frac{(np\pi r_s z)^i}{2^i \cdot i!} 2\pi z dz \\ =& \mathrm{E}[V_k] \cdot \Big(\int_0^1 e^{-\lambda u} \sum_{i=0}^{k-1} \frac{(\lambda u)^i}{i!} 8\pi r_s^2(1+\sigma_s^2)^2 u du \Big), \\ <& 4a_s(1+\sigma_s^2)k(k+1)\lambda^{-2}. \end{aligned}$$

where $\lambda = npa_s$. The proof of the last inequality above can be found in [67]. Hence, we have

$$I_2 < 4a_s(1+\sigma_s^2)k(k+1)(npa_s)^{-2} \cdot \Big(e^{-npa_s} \sum_{i=0}^{k-1} \frac{(npa_s)^i}{i!}\Big). \tag{B.11}$$

Since $\mathrm{E}[V_k^2] = I_1 + I_2$, combining (B.7), (B.3), (B.10), and (B.11), we can upper-bound $P(V_k = 0)$ as follows:

$$P(V_k = 0) = 1 - P(V_k > 0) \leqslant 1 - \frac{(\mathrm{E}[V_k])^2}{\mathrm{E}[V_k^2]} < \frac{\beta}{1+\beta},$$

where

$$\beta = \frac{4(1+\sigma_s^2)a_s k(k+1)(npa_s)^{-2}}{e^{-npa_s}\sum_{i=0}^{k-1}(npa_s)^i/i!} \leqslant 4(1+\sigma_s^2)(k+1)!(np)^{-1}(npa_s)^{-k}\cdot e^{npa_s}.$$

Therefore, we obtain the upper bound on $P(V_k = 0)$ as

$$P(V_k = 0) < \frac{4(k+1)!(1+\sigma_s^2)(np)^{-1}(npa_s)^{-k}\cdot e^{npa_s}}{1+4(k+1)!(1+\sigma_s^2)(np)^{-1}(npa_s)^{-k}\cdot e^{npa_s}}.$$

(ii) Lower bound.

Observe that

$$p(V_k = 0) = 1 - p_1 - p_2 - p_3,$$

where $p_1 = P(\text{no active sensors centered within } \mathcal{D}) = e^{-np} < e^{-npa_s}$. Here, we assume $a_s < 1$, meaning that, even for the random sensing radius model, the expected sensing area of one sensor will not cover the entire field $\mathcal{D}$.

$p_2 = P(\text{at least one disc centered within } \mathcal{D}, \text{ but none of the discs intersects}$
$\text{with any other disc, and none of the discs intersect the boundary of } \mathcal{D})$
$\leqslant P(\text{at least one disc centered within } \mathcal{D}) \times P(\text{a given disc intersects with no other discs})$
$= (1-e^{-np})\cdot e^{-np\pi \mathrm{E}[\pi(r_{s,1}+r_{s,2})^2]} = (1-e^{-np})\cdot e^{-2np\pi r_0^2(2+\sigma_s^2)} < e^{-npa_s},$

where $r_{s,1}$ and $r_{s,2}$ are sensing radii of two active sensors, which are i.i.d with mean r_0 and variance $r_0^2\cdot\sigma_s^2$, and the second equality is due to Lemma 7.

$p_3 = P(\mathcal{D} \text{ is not } k\text{-covered, at least one disc centered within } \mathcal{D}, \text{ and at least}$
$\text{one disc intersects with another disc or the boundary of } \mathcal{D}).$

Therefore

$$p(V_k = 0) > 1 - 2e^{-npa_s} - p_3. \tag{B.12}$$

Our next task is to derive an upper bound on p_3.

Define a *crossing* to be either an intersection point of the boundaries of two discs or an intersection point of the boundary of an disc and the boundary of the field $\mathcal{D}$. A crossing is said to be k-covered if it is within at least k discs. It is proved in [112] that, field $\mathcal{D}$ is k-covered if there exist crossings and every crossing is k-covered. Therefore, if $\mathcal{D}$ is not k-covered, if one

or more discs are centered within $\mathcal{D}$, and if there exist crossings in $\mathcal{D}$, then at least one of the discs has two or more crossings that are not k-covered. Thus

$$p_3 \leqslant P(M_k \geqslant 2) \leqslant \mathrm{E}[M_k]/2, \tag{B.13}$$

where M_k denotes the number of crossings that are not k-covered.

Define L_1 and L_2 as the number of crossings created by two discs intersecting with each other, and the ones created by a disc intersecting the boundary of field $\mathcal{D}$. We first study the expected value of L_1. The expected number of crossings created by a given active sensor ξ_1 with other active sensors is

$$\mathrm{E}[2np \cdot \pi(r_{s,1} + r_{s,2})^2] = 8npa'_s$$

where $a'_s \equiv \pi r_0^2(1+\sigma_s^2/2)$, and the expected number of discs centered within $\mathcal{D}$ is np. Therefore

$$\mathrm{E}[L_1] = np \cdot 8npa'_s/2 = 4n^2p^2a'_s.$$

If a disc intersects the edge of field $\mathcal{D}$, at most two crossings will be created; if a disc intersects the corner of field $\mathcal{D}$, at most four crossings will be created (due to the toroidal model assumption). Thus the expected value of L_2 is bounded by

$$\mathrm{E}[L_2] \leqslant 8npr_0.$$

The probability that a given crossing is not k-covered is given by (B.2). Therefore,

$$\mathrm{E}[M_k] = (\mathrm{E}[L_1] + \mathrm{E}[L_2])e^{-npa_s}\sum_{j=0}^{k-1}\frac{(npa_s)^j}{j!} \leqslant 4(n^2p^2a'_s + 2npr_0)e^{-npa_s}\sum_{j=0}^{k-1}\frac{(npa_s)^j}{j!}. \tag{B.14}$$

By (B.12), (B.13), and (B.14), we have

$$P(V_k = 0) > 1 - 2e^{-npa_s}\Big(1 + (n^2p^2a'_s + 2npr_0)\sum_{i=0}^{k-1}\frac{(npa_s)^i}{i!}\Big).$$

This completes the proof.

□

In what follows, we establish the sufficient and necessary condition for asymptotic k-coverage.

Theorem 9 *Assume $np \to \infty$ as $n \to \infty$, and let*

$$\pi r_0^2(1+\sigma_s^2) = \frac{\ln(np) + k\ln\ln(np) + c_1(np)}{np}, \tag{B.15}$$

then the entire unit square field $\mathcal{D}$ is k-covered with probability one as $n \to \infty$, if and only if $c_1(np) \to \infty$ as $n \to \infty$.

Proof: The entire unit square field $\mathcal{D}$ is k-covered with probability one means that $P(V_k = 0) \to 1$ as $n \to \infty$. First, we prove if $c_1(np) \to \infty$ as $n \to \infty$, $P(V_k = 0) \to 1$.

By (B.4) and (B.6) in Theorem 8, we have

$$P(V_k = 0) > 1 - 2e^{-npa_s} - (b_1 + b_2) \cdot (np)(npa_s)^k e^{-npa_s},$$

where $b_1 \equiv 2k\frac{1+\sigma_s^2/2}{1+\sigma_s^2} > 0$ is independent of n, and $b_2 \equiv \frac{4k}{\pi r_0(1+\sigma_s^2)np}$. Let $npa_s = \ln(np) + k\ln(\ln(np)) + c_1(np)$, then $npa_s \to \infty$, $e^{-npa_s} \to 0$, and $b_2 \to 0$, as $n \to \infty$. Therefore, when $c_1(np) \to \infty$,

$$\begin{aligned}
&\ln\Big((b_1 + b_2) \cdot (np)(npa_s)^k e^{-npa_s}\Big) \\
=&\ln(b_1 + b_2) + k \cdot \ln\Big(\ln(np) + k\ln(\ln(np)) + c_1(np)\Big) - k\ln(\ln(np)) - c_1(np) \\
\to&-\infty,
\end{aligned}$$

and consequently, $P(V_k = 0) \to 1$. The first part is proved.

If $c_1(np) \leqslant C_1$ for some finite $C_1 > 0$ as $n \to \infty$, then for sufficiently large n

$$4(k+1)!(1+\sigma_s^2)(np)^{-1}(npa_s)^{-k}e^{npa_s} = 4(k+1)!(1+\sigma_s^2)e^{c_1(np)} \leqslant 4e^{C_1}(k+1)!(1+\sigma_s^2),$$

Therefore, by (B.4) and (B.5) we have

$$P(V_k = 0) < \frac{4e^{C_1}(k+1)!(1+\sigma_s^2)}{1 + 4e^{C_1}(k+1)!(1+\sigma_s^2)} < 1.$$

It means that $P(V_k = 0) \to 1$ only if $c_1(np) \to \infty$ as $n \to \infty$. This completes the proof.

□

Remark: The bounds obtained in Theorem 8 is valid for finite n. Therefore, they can be used as performance criteria for designing finite-size sensor networks.

B.4 ω-lifetime of Finite-Size Wireless Sensor Networks

The second problem addressed in this appendix is how to find optimal parameters for the CIS scheme to maximize the ω-lifetime of a finite-size wireless sensor network.

Let A denote the event of the sensing field $\mathcal{D}$ being k-covered, and B denote the event of the sensor network being connected. The probability of guaranteeing simultaneously k-coverage of field $\mathcal{D}$ and connectivity of the network is $P_{\text{c\&c}} \equiv P(A \cap B)$.

Definition: The *ω-lifetime*, namely T_ω, of a sensor network is defined as the expectation of the time interval during which the probability of guaranteeing simultaneously k-coverage of field $\mathcal{D}$ and the connectivity of the network is no less than ω, i.e., $P_{\text{c\&c}} \geqslant \omega$, where $0 < \omega < 1$.

In order to study the ω-lifetime, we first introduce the energy consumption model of each wireless sensor. We assume that inactive sensors do not consume energy and the communication traffic is evenly distributed across the network. The energy consumption of an active sensor consists of two parts: *communication* and *sensing*. Thus, the power consumption P_0 of each active sensor can be modeled as

$$P_0 = Q \cdot \frac{1}{r_c} \cdot r_c^\beta + \Delta, \tag{B.16}$$

where

- r_c^β is proportional to the communication energy consumption per bit, and the typical values of β range from 3 to 4 for different propagation models [86];
- $1/r_c$ is proportional to the average traffic rate of active sensors (we assume that all active sensors have the same traffic rate, following the assumption of evenly distributed traffic.);
- Δ is the power consumption for continuous sensing;
- $Q > 0$ is a constant.

As the communication radius r_c decreases, the average number of hops required for packets transmitted from one point to another increases inversely. For this reason, we incorporate the factor of $1/r_c$ into the average traffic rate expression. We further assume that all active sensors

have the same communication radius r_c, which results in the same individual lifetime:

$$T_0(r_c) = \frac{E_0'}{P_0} = \frac{E_0}{r_c^{\beta-1} + \eta}, \tag{B.17}$$

where E_0' is the initial energy of each active sensor, $E_0 = \frac{E_0'}{Q}$, and $\eta = \frac{\Delta}{Q}$, respectively. This assumption is typical when analyzing the network's lifetime, e.g., in [121] and [11].

Next, we formally define the CIS scheme which can extend the ω-lifetime of a wireless sensor network. Suppose that time is divided into rounds. At the beginning of round i, there are $n^{(i)}$ alive sensors, and each alive sensor decides independently whether to remain sleeping (with probability $1 - p^{(i)}$), or become active (with probability $p^{(i)}$). All active sensors choose the same communication radius of $r_c^{(i)}$. Both $p^{(i)}$ and $r_c^{(i)}$ are chosen such that $P_{\text{c\&c}} \geqslant \omega$. Next, all active sensors will operate continuously until batteries die out. Since we assume that all active sensors have the same individual lifetime, they will die out at the same time instant, which is defined as the end of this round. The same procedure is repeated for the next rounds until there are not enough alive sensors to satisfy the "$P_{\text{c\&c}} \geqslant \omega$" requirement, regardless of the choices of p and r_c.

We call this scheduling scheme *Coordinated Independent Sleeping* since we assume that sensors are coordinated so that they may be able to choose $p^{(i)}$ and $r_c^{(i)}$ properly at the beginning of each round. The major differences between CIS and RIS in [59] are as follows. In CIS, p and r_c are chosen for each round to satisfy both connectivity and k-coverage requirements, and they may vary from round to round. Within each round, all active sensors operate continuously until batteries die out. In contrast, the values of p and r_c in RIS are fixed throughout the network operation, where p is chosen to satisfy the k-coverage requirement but with no optimization on r_c. Note that, with RIS, each individual sensor's lifetime is approximately the same as the network's lifetime when a sufficiently-small round duration is selected.

In the rest of this section, we study the ω-lifetime with the proposed CIS scheme and try to find the optimal parameters to maximize the ω-lifetime of the network.

B.4.1 ω-Lifetime Study

Suppose that n sensors are deployed independently and uniformly within a unit-area square field $\mathcal{D}$, and the network can operate M rounds following the CIS scheduling scheme. Then, the ω-lifetime of the wireless sensor network is

$$T_\omega = \mathrm{E}\left[\sum_{i=1}^{M} T_0(r_c^{(i)})\right] = \mathrm{E}\left[\sum_{i=1}^{M} \frac{E_0}{\left(r_c^{(i)}\right)^{\beta-1} + \eta}\right], \tag{B.18}$$

subject to both connectivity and k-coverage requirements, and the expectation is with respect to M. Define $n_{\text{eff}}^{(i)} = n^{(i)}p^{(i)}$, which is the expected number of active sensors in round i. It is easy to verify that the probability mass function (pmf) of M is

$$P(M=m) = \sum_{\substack{n=n^{(1)}\geqslant n^{(2)}\geqslant\cdots\geqslant n^{(m)}n^{(i)}\geqslant n_{\text{eff}}^{(i)} \\ i=1,\ldots,m}} \cdots \sum \sum_{n^{(m+1)}=0}^{n_{\text{eff}}^{(m+1)}-1} \prod_{i=1}^{m} \binom{n^{(i)}}{n^{(i+1)}} \left(1-p^{(i)}\right)^{n^{(i+1)}} \left(p^{(i)}\right)^{n^{(i)}-n^{(i+1)}},$$

Thus, the problem of maximizing the ω-lifetime of the network can be expressed as

$$T_\omega^{\max} = \max_{r_c^{(i)}, n_{\text{eff}}^{(i)}} T_\omega = \max_{r_c^{(i)}, n_{\text{eff}}^{(i)}} \mathrm{E}\left[\sum_{i=1}^{M} \frac{E_0}{\left(r_c^{(i)}\right)^{\beta-1} + \eta}\right], \tag{B.19}$$

$$\text{subject to} \qquad P_{\text{c\&c}} = P(A \cap B) \geqslant \omega \quad \text{for each round.} \tag{B.20}$$

Using the union bound, we have

$$\min\{P(A), P(B)\} \geqslant P_{\text{c\&c}} \geqslant P(A) + P(B) - 1. \tag{B.21}$$

Since it is hard to analyze $P_{\text{c\&c}}$ directly, we next focus on finding a lower bound and an upper bound on the optimal ω-lifetime, $T_\omega^{\max}$.

B.4.1.1 Lower bound

Restricting the constraint in (B.20) by replacing it with the lower bound in (B.21), and assuming that all $n_{\text{eff}}^{(i)}$ and $r_c^{(i)}$'s are the same for each round, we can obtain a lower bound on $T_\omega^{\max}$ by solving the following optimization problem:

$$\max_{n_{\text{eff}}, r_c, \epsilon} \mathrm{E}[M] \cdot \frac{E_0}{r_c^{\beta-1} + \eta}, \tag{B.22}$$

$$\text{subject to} \quad P(A) \geqslant \omega + \epsilon, \quad P(B) \geqslant 1 - \epsilon, \quad 0 < \epsilon < 1 - \omega. \tag{B.23}$$

Using the result $P(A) > P_l$ in Theorem 8, and the following result in [40]:

$$P(B) \approx 1 - P(\exists \text{ isolated active sensors}) > 1 - n_{\text{eff}} e^{-n_{\text{eff}} \pi r_c^2},$$

where the edge effects are avoided by the toroidal model assumption, we can restrict the constraints in (B.23) as

$$P_l \geqslant \omega + \epsilon, \quad r_c \geqslant \sqrt{[\ln(n_{\text{eff}}/\epsilon)]/(\pi n_{\text{eff}})}, \quad 0 < \epsilon < 1 - \omega. \tag{B.24}$$

Notice that the value of ω is usually larger than 90% in practice, then the P_l defined in (B.6) can be approximated as

$$P_l \approx 1 - g(n_{\text{eff}}) \equiv 1 - 2n_{\text{eff}}^2 a_s' e^{-a_s n_{\text{eff}}} \sum_{i=0}^{k-1} \frac{(a_s n_{\text{eff}})^i}{i!}. \tag{B.25}$$

Let X_i denote the number of active sensors in round i, then $n^{(m)} = n - \sum_{i=1}^{m-1} X_i$, and conditional on $n^{(i)}$, X_i is Binomial-distributed as $\text{BIN}\big(n^{(i)}, p^{(i)}\big)$. Next, we use the expectation of $n^{(i)}$ to obtain an approximation of $p^{(i)}$ as

$$p^{(i)} = \frac{n_{\text{eff}}}{n^{(i)}} \approx \frac{n_{\text{eff}}}{n - (i-1)n_{\text{eff}}} = \frac{1}{M_0 + 1 - i}, \tag{B.26}$$

where $M_0 \equiv n/n_{\text{eff}}$. Using (B.26) and the central limit theorem, we can approximate $n^{(m)}$ as a Gaussian random variable with mean $n - (m-1)n_{\text{eff}}$ and variance $A(m)n_{\text{eff}}$, where $A(m) = \sum_{i=1}^{m-1}(1 - p^{(i)})$. Then, we have

$$P(M \leqslant m) = P(n^{(m+1)} < n_{\text{eff}}) = Q\Big(\frac{n - (m+1)n_{\text{eff}}}{\sqrt{A(m+1)n_{\text{eff}}}}\Big),$$
$$P(M \geqslant m) = P(n^{(m)} \geqslant n_{\text{eff}}) = Q\Big(\frac{mn_{\text{eff}} - n}{\sqrt{A(m)n_{\text{eff}}}}\Big),$$

where $Q(\cdot)$ is complementary cumulative distribution function (CCDF) of Gaussian distribution. Therefore,

$$P(M \leqslant \lfloor M_0 \rfloor - 2) = Q\Big(\frac{n - (\lfloor M_0 \rfloor - 1)n_{\text{eff}}}{\sqrt{A(\lfloor M_0 \rfloor - 1)n_{\text{eff}}}}\Big) \leqslant Q\Big(\sqrt{\frac{n_{\text{eff}}}{A(M_0 - 1)}}\Big),$$

and

$$P(M \geqslant \lfloor M_0 \rfloor + 2) = Q\Big(\frac{(\lfloor M_0 \rfloor + 2)n_{\text{eff}} - n}{\sqrt{A(\lfloor M_0 \rfloor + 2)n_{\text{eff}}}}\Big) \leqslant Q\Big(\sqrt{\frac{n_{\text{eff}}}{A(M_0+1)}}\Big),$$

where the floor function $\lfloor x \rfloor$ denotes the largest integer that is not greater than x. For $m < M_0 + 2$, $A(m)$ can be upper-bounded as

$$A(m) \leqslant (m-1) - \int_{M_0+2-m}^{M_0} \frac{1}{x}\mathrm{d}x = (m-1) - \ln \frac{M_0}{M_0+2-m}.$$

Then, for n and n_{eff} in the range of our interests, we have

$$P(M \geqslant \lfloor M_0 \rfloor + 2) \leqslant Q\Big(\sqrt{\frac{n_{\text{eff}}}{A(M_0+1)}}\Big) \leqslant Q\Big(\sqrt{\frac{n_{\text{eff}}}{M_0 - \ln M_0}}\Big) \approx 0.$$

Similarly, we have $P(M \leqslant \lfloor M_0 \rfloor - 2) \approx 0$. Thus, the pmf of M are mostly concentrated at 3 points: $\lfloor \frac{n}{n_{\text{eff}}} \rfloor - 1$, $\lfloor \frac{n}{n_{\text{eff}}} \rfloor$, and $\lfloor \frac{n}{n_{\text{eff}}} \rfloor + 1$. Monte Carlo simulation results also verify this conclusion. Therefore, we have the lower bound on $\mathrm{E}[M]$ as

$$\mathrm{E}[M] \geqslant \Big\lfloor \frac{n - n_{\text{eff}}}{n_{\text{eff}}} \Big\rfloor. \tag{B.27}$$

Since $E_0/(r_c^{\beta-1} + \eta)$ is a decreasing function in r_c, using (B.24), (B.25) and (B.27), we obtain a new lower bound on $T_\omega^{\max}$ as

$$T_\omega^L = \max_{n_{\text{eff}}} T_1(n_{\text{eff}}) \equiv \max_{n_{\text{eff}}} \Big\lfloor \frac{n - n_{\text{eff}}}{n_{\text{eff}}} \Big\rfloor \cdot \frac{E_0}{\big(\frac{1}{\pi n_{\text{eff}}} \ln \frac{n_{\text{eff}}}{1-\omega-g(n_{\text{eff}})}\big)^{(\beta-1)/2} + \eta},$$

$$\text{subject to} \qquad n_{\text{eff}} > g^{-1}(1-\omega),$$

where $g^{-1}(\cdot)$ is the inverse function of $g(n_{\text{eff}})$. By temporarily removing the floor function $\lfloor \cdot \rfloor$, we have the following convex optimization problem (given $\beta > 3$):

$$\begin{aligned} &\max_{n_{\text{eff}}} \frac{E_0(n - n_{\text{eff}})}{n_{\text{eff}}\big(\frac{1}{\pi n_{\text{eff}}} \ln \frac{n_{\text{eff}}}{1-\omega-g(n_{\text{eff}})}\big)^{(\beta-1)/2} + \eta \cdot n_{\text{eff}}}, \\ &\qquad \text{subject to} \qquad n_{\text{eff}} > g^{-1}(1-\omega). \end{aligned} \tag{B.28}$$

The verification of the concavity of the objective function is omitted due to space limitation.

The convex optimization problem defined in (B.28) can be solved easily by numerical methods. Suppose that the solution of such problem is $\bar{n}_{\text{eff}}$, then

$$T_\omega^L = \max\{T_1(n_{\text{eff}}^1), T_1(n_{\text{eff}}^2)\},$$

where $n_{\text{eff}}^1 = n/\left\lfloor \frac{n}{\bar{n}_{\text{eff}}} \right\rfloor$, $n_{\text{eff}}^2 = n/\left\lceil \frac{n}{\bar{n}_{\text{eff}}} \right\rceil$, and $\lceil x \rceil$ denotes the smallest integer that is equal to or greater than x. We can also obtain the corresponding n_{eff}^L and r_c^L as

$$\begin{aligned} n_{\text{eff}}^L &= \arg\max_{n_{\text{eff}}^1, n_{\text{eff}}^2} T_1(n_{\text{eff}}), \\ r_c^L &= \sqrt{[\ln(n_{\text{eff}}^L/(1-\omega-g(n_{\text{eff}}^L)))]/(\pi n_{\text{eff}}^L)}. \end{aligned} \tag{B.29}$$

B.4.1.2 Upper bound

Next, we present an approximate upper bound on $T_\omega^{\max}$. Relaxing the constraint in (B.20) with the upper bound in (B.21), we obtain the relaxed constraints as

$$P(A) \geqslant \omega, \quad P(B) \geqslant \omega. \tag{B.30}$$

Then, we use the lower bounds to approximate $P(A)$ and $P(B)$ as

$$P(A) \approx P_l \approx 1 - g(n_{\text{eff}}^{(i)}), \quad P(B) \approx 1 - n_{\text{eff}}^{(i)} e^{-n_{\text{eff}}^{(i)} \pi \left(r_c^{(i)}\right)^2}. \tag{B.31}$$

Next, we assume that the number of active sensors in round i is approximately equal to $n_{\text{eff}}^{(i)}$. Then the maximum number of rounds, M, is a deterministic quantity, and satisfies the constraint $\sum_{i=1}^{M} n_{\text{eff}}^{(i)} \leqslant n$. Using (B.30) and (B.31), we obtain an approximate upper bound on $T_\omega^{\max}$ by solving the following optimization problem:

$$\begin{aligned} &\max_{n_{\text{eff}}^{(i)}} \sum_{i=1}^{M} \frac{E_0}{\left(\frac{1}{\pi n_{\text{eff}}^{(i)}} \ln \frac{n_{\text{eff}}^{(i)}}{\omega}\right)^{(\beta-1)/2} + \eta}, \\ &\text{subject to} \qquad n_{\text{eff}}^{(i)} \geqslant g^{-1}(1-\omega), \quad \sum_{i=1}^{M} n_{\text{eff}}^{(i)} \leqslant n. \end{aligned} \tag{B.32}$$

It is easy to verify that, given M, (B.32) is a convex optimization problem. By Lagrange multiplier, we obtain a new upper bound on $T_\omega^{\max}$ as

$$\begin{aligned} T_\omega^U &= \max_{n_{\text{eff}}} T_2(n_{\text{eff}}) \equiv \max_{n_{\text{eff}}} \left\lfloor \frac{n}{n_{\text{eff}}} \right\rfloor \cdot \frac{E_0}{\left(\frac{1}{\pi n_{\text{eff}}} \ln \frac{n_{\text{eff}}}{1-\omega}\right)^{(\beta-1)/2} + \eta}, \\ &\text{subject to} \qquad n_{\text{eff}}^{(i)} \geqslant g^{-1}(1-\omega). \end{aligned} \tag{B.33}$$

Similarly, we temporarily remove the floor function $\lfloor \cdot \rfloor$. It is easy to verify that the resulting optimization problem is a convex problem. Suppose that the solution of such problem is $\tilde{n}_{\text{eff}}$,

then

$$T_\omega^U = \max\{T_2(n_{\text{eff}}^1), T_2(n_{\text{eff}}^2)\},$$
$$n_{\text{eff}}^U = \arg\max_{n_{\text{eff}}^1, n_{\text{eff}}^2} T_2(n_{\text{eff}}),$$
$$r_c^U = \sqrt{[\ln(n_{\text{eff}}^U/(1-\omega))]/(\pi n_{\text{eff}}^U)},$$

where $n_{\text{eff}}^1 = n/\left\lfloor \frac{n}{\tilde{n}_{\text{eff}}} \right\rfloor$ and $n_{\text{eff}}^2 = n/\left\lceil \frac{n}{\tilde{n}_{\text{eff}}} \right\rceil$.

As an example, we let $E_0 = 1$, $\beta = 3.5$, $\eta = 0.001$, $\omega = 0.92$, and $k = 1$. Numerical results show that the relative difference between the lower bound (T_ω^L) and the upper bound (T_ω^U) is at the level of 10% for n from 10000 to 40000, which suggests that the derived lower bound is a good approximation of the optimal ω-lifetime of the sensor network.

B.4.2 CIS Scheme Design

We propose to choose the operational parameters for CIS scheme according to the derived lower bound on the optimal ω-lifetime, i.e., choosing $p^{(i)}$ and $r_c^{(i)}$ for round i as

$$p^{(i)} = \min\{n_{\text{eff}}^L/n^{(i)},\ 1\}, \quad r_c^{(i)} = r_c^L, \tag{B.34}$$

where $n^{(i)}$ is the number of alive sensors at the beginning of round i ($i \geqslant 1$), and n_{eff}^L and r_c^L are given in (B.29). Obviously, (B.34) provides a centralized solution, since $n^{(i)}$ is a global information. At the beginning of each round, such information is required for each alive sensor to calculate $p^{(i)}$ online.

In resource-constrained wireless sensor networks, we always prefer distributed solutions. In our case, distributed solutions mean that the choices of $p^{(i)}$'s should be independent of $n^{(i)}$. As shown in Section B.4.1, the expected number of active sensors in each round, $n^{(i)}p^{(i)}$, is the key parameter to determine whether the network satisfies the "$P_{\text{c\&c}} \geqslant \omega$" requirement or not. According to the lower bound on the optimal ω-lifetime, we define *outage* of round i as the event that $n^{(i)}p^{(i)} < n_{\text{eff}}^L$, which means that the "$P_{\text{c\&c}} \geqslant \omega$" requirement can not be satisfied at round i. The probability that an outage occurs at round i is denoted by $P_{\text{out}}^{(i)}$. For the centralized solution in (B.34), $P_{\text{out}}^{(i)}$ is always 0 for the rounds that $n^{(i)} \geqslant n_{\text{eff}}^L$.

As an approximation to (B.34), we propose a distributed solution as follows: for $1 \leqslant i \leqslant M$,

$$p^{(i)} = \begin{cases} \frac{n_{\text{eff}}^L\left(1+\epsilon^{(i)}\right)}{n-n_{\text{eff}}^L\sum_{l=1}^{i-1}\left(1+\epsilon^{(l)}\right)} & 1 \leqslant i < M \\ 1 & i = M \end{cases}, \quad r_c^{(i)} = r_c^L, \tag{B.35}$$

where M is the maximum number of rounds, $\epsilon^{(1)} = 0$, and for $1 < i < M$, $\epsilon^{(i)}$'s are chosen such that

$$P_{\text{out}}^{(i)} = P(n^{(i)}p^{(i)} < n_{\text{eff}}^L) = \delta, \tag{B.36}$$

where $\delta > 0$ is a pre-defined small quantity.

With the choice of $p^{(i)}$ in (B.35), where $1 < i < M$, we can approximate $n^{(i)}$ as a Gaussian random variable by the central limit theorem:

$$n^{(i)} \sim \mathcal{N}\Big(n - n_{\text{eff}}^L\sum_{l=1}^{i-1}(1+\epsilon^{(l)}),\ n_{\text{eff}}^L\sum_{l=1}^{i-1}(1+\epsilon^{(l)})(1-p^{(l)})\Big).$$

Then, $\epsilon^{(i)}$'s in (B.35) can be calculated recursively according to

$$\epsilon^{(i)} = \begin{cases} 0 & i = 1 \\ \frac{Q^{-1}(\delta)}{a^{(i)}-Q^{-1}(\delta)} & 1 < i < M \end{cases}, \tag{B.37}$$

and

$$a^{(i)} = \frac{n - n_{\text{eff}}^L\sum_{l=1}^{i-1}(1+\epsilon^{(l)})}{\sqrt{n_{\text{eff}}^L\sum_{l=1}^{i-1}(1+\epsilon^{(l)})(1-p^{(l)})}}, \tag{B.38}$$

where $Q^{-1}(\cdot)$ is the inverse function of $Q(\cdot)$. The maximum number of rounds M is defined as

$$M = \arg\max_{i>1}\{a^{(i)} > 0\}.$$

The idea of this distributed solution is to use the expected number of alive sensors to replace $n^{(i)}$ in (B.34), and increase the expected number of active sensors a little bit (by $n_{\text{eff}}^L\epsilon^{(i)}$) such that the outage probability ($P_{\text{out}}^{(i)}$) can be controlled at a given level (δ). In fact, this algorithm sacrifices the total number of rounds, equivalently network's lifetime, to achieve the distributed property.

B.5 Simulation Results

In this section, we use simulation results to demonstrate the performance of the proposed CIS scheduling schemes. The performance criterion is the ω-lifetime of the network. As a comparison, we include the results of a CIS-like scheme that simply fixes the communication range to be twice the mean of the sensing radius: $r_c = 2r_0$, and selects $n_{\text{eff}} = n^A_{\text{eff}}$ according to (B.31). It is based on the strategy described in [121] and we call it Zhang's scheme.

We simulate a square sensing field $\mathcal{D}$ of unit area in which n sensors are deployed independently and uniformly. The sensing radius r_s is assumed to be a uniformly distributed random variable on $[0.0384, 0.1216]$, which corresponds to $r_0 = 0.08$ and $\sigma_s = 0.3$. Let $E_0 = 1$, $\beta = 3.5$, $\eta = 0.001$, $\omega = 0.92$, and $k = 1$, i.e, we considerer 1-coverage as an example. With this network setup, the centralized and distributed CIS schemes select $p^{(i)}$ and $r_c^{(i)}$ according to (B.34) and (B.35), respectively. For the distributed CIS scheme, the outage probability threshold (δ) is set to 10^{-2}. Zhang's scheme selects $p^{(i)}$ and $r_c^{(i)}$ according to (B.34) with n^L_{eff} replaced by n^A_{eff}.

First, we simulate the operation of a network with $n = 10000$ using different scheduling schemes. We divide the field $\mathcal{D}$ into a grid of size 62×62, and approximate that the field $\mathcal{D}$ is k-covered if all grid points are k-covered. For the connectivity, we approximate that the network is connected if there is no isolated active sensors. The torus convention is also employed for simulations to avoid edge effects. Then, $P_{\text{c\&c}}$ at each round of the network operation is estimated as follows: given a deployment, the network is operated according to the particular scheduling scheme ($p^{(i)}$ and r_c) until the batteries of all sensors die out. Repeat this experiment 2500 times with the same deployment. For round i of experiment j, define $\delta^i_j = 1$ if the field $\mathcal{D}$ is k-covered and active sensors are connected, 0 otherwise. Then, $P_{\text{c\&c}}$ of round i can be estimated as $P^i_{\text{c\&c}} = \frac{1}{2500}\sum_{j=1}^{2500} \delta^i_j$.

Three snapshots of the network operation are shown in Fig. B.1, using Zhang's scheme, centralized and distributed CIS scheduling schemes, respectively. It is seen that all scheduling schemes can guarantee that the network satisfies the connectivity and k-coverage requirements as long as the expected number of active sensors is no less than n^L_{eff}. Therefore, in the simulation of the network's ω-lifetime, we only need to simulate how many rounds a network can operate

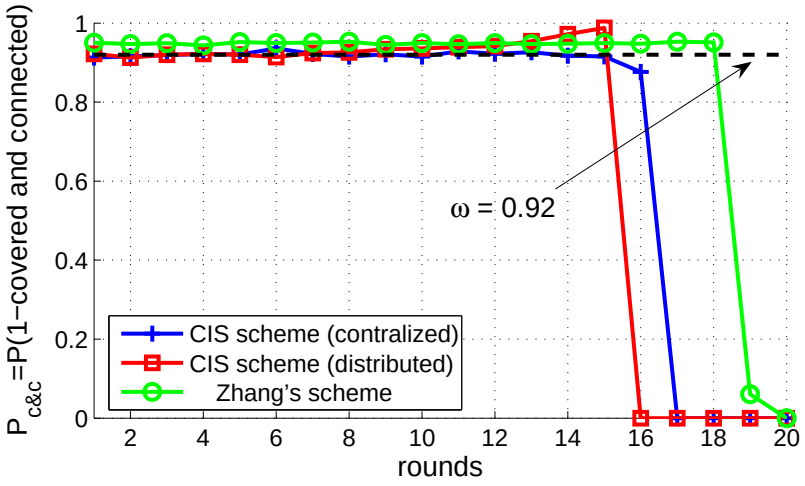

Figure B.1 Three snapshots of the network operation.

properly following a particular scheduling scheme. Notice that Zhang's scheme can operate more rounds than the CIS schemes. However, each round is shorter in Zhang's scheme, since r_c is not optimally selected. As seen in the next simulation, the CIS schemes have longer ω-lifetime than Zhang's scheme.

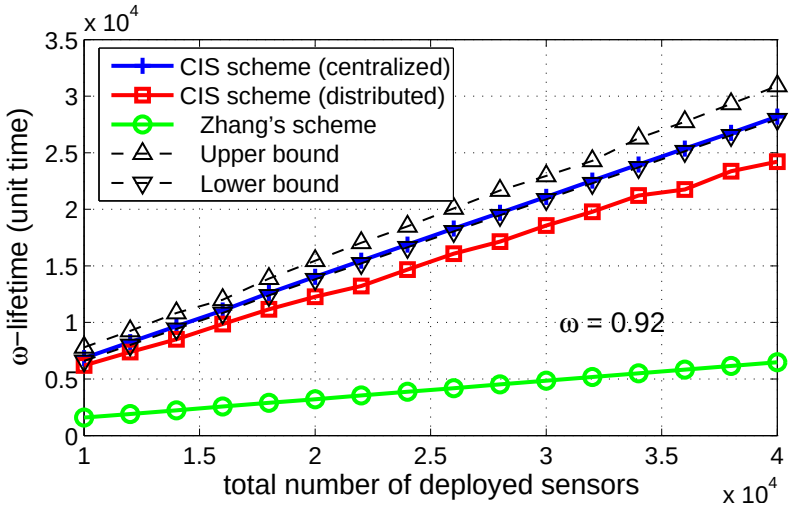

Figure B.2 ω-lifetime with different scheduling schemes.

Second, we compare the ω-lifetime of a network using different scheduling schemes with n from 10000 to 40000, and the results are plotted in Fig. B.2. The derived lower bound and upper bound for the CIS scheme are also shown in the figure. The estimate of the ω-lifetime

is calculated as:

$$\widehat{T}_{\text{net}} = \frac{1}{N}\sum_{i=1}^{N} M_i \cdot T_0(r_c), \tag{B.39}$$

where N is the number of Monte Carlo realizations, $T_0(r_c)$ is the duration of each round defined in (B.17), and

$$M_i = \arg\min_{i \geqslant 1} \left\{ n^{(i)} p^{(i)} < n_{\text{eff}}^L \right\}. \tag{B.40}$$

We observe that for the centralized CIS scheme, the simulation result is very close to the theoretical lower bound, T_ω^L, which was derived in Section B.4. By comparing the CIS schemes and Zhang's scheme, we clearly see that the ω-lifetime's of both centralized and distributed CIS schemes are much longer than that of Zhang's scheme, and the differences become larger with more deployed sensors. Such fact demonstrates the importance of joint optimization of lifetime, connectivity, and coverage. We also see that the ω-lifetime of the distributed CIS scheme is close to that of the centralized one, which suggests that the distributed CIS scheme is a good choice for real applications.

B.6 Summary

In this work, we investigate the fundamental limits of a wireless sensor network's lifetime under connectivity and k-coverage constraints. The contributions of our work are threefold. First, we derive the sufficient and necessary condition on the sensing radius for asymptotic k-coverage of the sensing field. Second, we study the lifetime of a wireless sensor network from a (new) probabilistic perspective and introduce a new concept, called network's ω-lifetime, which is defined as the expectation of the time interval during which the probability of guaranteeing connectivity and k-coverage simultaneously is at least ω. Third, we propose CIS (Coordinated Independent Sleeping) as a near-optimal scheduling scheme to maximize the ω-lifetime of a finite-size wireless sensor network, describe a possible distributed implementation of the CIS scheme, and demonstrate the CIS performance by simulation results.

Future work includes extending the analysis to more generic and realistic scenarios such as when only a portion of the sensing field needs to be k-covered, or when the sensing field is of irregular shape, or when the communication radius is also a random variable.

BIBLIOGRAPHY

[1] A. Abdi and M. Kaveh. A space-time correlation model for multielement antenna systems in and mobile fading channels. *IEEE J. Select. Areas Commun.*, 20(3):550–560, Mar. 2002.

[2] I. Akyildiz, W. Su, Y. Sankarasubramaniam, and E. Cayirci. A survey on sensor networks. *IEEE Commun. Mag.*, 40(8):102–114, Aug. 2002.

[3] S. M. Alamouti. A simple transmit diversity technique for wireless communications. *IEEE J. Select. Areas Commun.*, 16(8):1451–1458, Oct. 1998.

[4] C. Aldana and J. Cioffi. Channel tracking for multiple input, single output systems using em algorithm. In *Proc. Intl. Conf. on Com.*, pages 586–590, Helsinki, Finland, June 2001.

[5] K. Azarian, H. El Gamal, and P. Schniter. On the achievable diversity-multiplexing tradeoff in half-duplex cooperative channels. *IEEE Trans. Inform. Theory*, 51(12):4152–4172, Dec. 2005.

[6] K. Azarian, H. Gamal, and P. Schniter. On the achievable diversity-multiplexing tradeoff in half-duplex cooperative channels. *IEEE Trans. Inform. Theory*, 51(12):4152–4172, Dec. 2005.

[7] Z. Baranski, A. Haimovich, and J. Garcia-Frias. EM-based iterative receiver for space-time coded modulation with noise variance estimation. In *Proc. GLOBECOM*, volume 1, pages 355–359, Taipei, Taiwan, Nov. 2002.

[8] P. Bickel and K. Doksum. *Mathematical Statistics: Basic Ideas and Selected Topics*. Prentice Hall, Upper Saddle River, NJ, 2000.

[9] M. Biguesh and A. Gershman. MIMO channel estimation: optimal training and tradeoffs between estimation techniques. In *Communications, 2004 IEEE International Conference on*, volume 5, pages 2658–2662, 2004.

[10] P. Billingsley. *Probability and Measure*. New York: Wiley, 1979.

[11] D. Blough and P. Santi. Investigating upper bounds on network lifetime extension for cell-based energy conservation techniques in stationary ad hoc networks. In *MobiCom '02: Proceedings of the 8th annual international conference on Mobile computing and networking*, pages 183–192, New York, NY, USA, 2002. ACM Press.

[12] P. Bohlin and M. Lundberg. A blind and robust space-time receiver for a turbo coded system. In *Proceedings Asilomar Conference on Signals, Systems & Computers*, volume 1, pages 532–536, 2000.

[13] J. Boyer, D. Falconer, and H. Yanikomeroglu. Multihop diversity in wireless relaying channels. *IEEE Trans. Commun.*, 52(10):1820–1830, Oct. 2004.

[14] C. Budianu and L. Tong. Channel estimation for space-time orthogonal block codes. *IEEE Trans. Signal Processing*, 50(10):2515–2528, Oct. 2002.

[15] D. Chen and J. Laneman. The diversity-multiplexing tradeo for the multiaccess relay channel. In *Proceeding of Conference on Information Science and Systems*, Jan. 2006.

[16] J. Cheng, C. Tellambura, and N. Beaulieu. Performance of digital linear modulations on weibull slow-fading channels. *IEEE Trans. Commun.*, 52(8):1265–1268, Aug. 2004.

[17] W. Choi, K. Cheong, and J. Cioffi. Iterative soft interference cancellation for multiple antenna and systems. In *Proc. of Wireless Communications and Networking Conference*, volume 1, pages 304–309, 2000.

[18] C. Chuah, D. Tse, J. Kahn, and R. Valenzuela. Capacity scaling in MIMO wireless systems under correlated fading. *IEEE Trans. Inform. Theory*, 48(3):637–650, Mar. 2002.

[19] H. Cirpan and M. Tsatsanis. Stochastic maximum likelihood methods for semi-blind channel estimation. *IEEE Commun. Lett.*, 5:21–24, Jan. 1998.

[20] C. Cozzo and B. Hughes. Joint channel estimation and data detection in space-time communications. *IEEE Trans. Commun.*, 51(8):1266–1270, Aug. 2003.

[21] Y. de Jong and T. Willink. Iterative tree search detection for MIMO wireless systems. In *Proc. Vehicular Tech. Conf.*, volume 2, pages 1041–1045, 2002.

[22] A. Dempster, N. Laird, and D. Rubin. Maximum likelihood from incomplete data via the EM algorithm. *J. R. Stat. Soc.*, 39:1–38, July 1977.

[23] A. Dogandžić, W. Mo, and Z. Wang. Semi-blind SIMO flat-fading channel estimation in unknown spatially correlated noise using the EM algorithm. *IEEE Trans. Signal Processing*, 52(6):1791–1797, June 2004.

[24] A. Dogandžić and A. Nehorai. Finite-length mimo adaptive equalization using canonical correlation analysis. *IEEE Trans. Signal Processing*, 50:984–989, Apr. 2002.

[25] A. Dogandžić and A. Nehorai. Space-time fading channel estimation and symbol detection in and unknown spatially correlated noise. *IEEE Trans. Signal Processing*, 50(3):457–474, Mar. 2002.

[26] A. Dogandžić and A. Nehorai. Generalized multivariate analysis of variance- a unified framework for signal processing in correlated noise. *IEEE Signal Processing Mag.*, 20:39–54, Sept. 2003.

[27] A. Edelman. *Eigenvalues and Condition Numbers of Random Matrices*. PhD dissertation, Massachusetts Institute of Technology, 1989.

[28] D. Estrin, R. Govindan, J. Heidemann, and S. Kumar. Next century challenges: scalable coordination in sensor networks. In *MobiCom '99: Proceedings of the 5th annual ACM/IEEE international conference on Mobile computing and networking*, pages 263–270, New York, NY, USA, 1999. ACM Press.

[29] U. Fincke and M. Pohst. Improved methods for calculating vectors of short length in a lattice, including a complexity analysis. *Math. Comput.*, 44:463–471, Apr. 1985.

[30] G. Foschini, G. Golden, R. Valenzuela, and P. Wolniansky. Simplified processing for high spectral efficiency wireless communication employing multi-element arrays. *IEEE J. Select. Areas Commun.*, 17(11):1841–1852, Nov. 1999.

[31] G. J. Foschini and M. J. Gans. On limits of wireless communications in a fading environment when using multiple antennas. *Wireless Personal Communications*, 6(3):311–335, Mar. 1998.

[32] H. Gamal, G. Caire, and M. Damen. Lattice coding and decoding achieve the optimal diversity-multiplexing tradeoff of MIMO channels. *IEEE Trans. Inform. Theory*, 50(6):968–985, June 2004.

[33] G. Ganesan and P. Stoica. Space-time block codes: a maximum SNR approach. *IEEE Trans. Inform. Theory*, 47(4):1650–1656, Apr. 2001.

[34] C. Georghiades and D. Snyder. The expectation-maximization algorithm for symbol unsynchronized sequence detection. *IEEE Trans. Commun.*, 39:54–61, Jan. 1991.

[35] F. Gini, R. Reggiannini, and U. Mengali. The modified Cramer-Rao bound in vector parameter estimation. *IEEE Trans. Commun.*, 46(1):52–60, Jan. 1998.

[36] G. Golden, C. Foschini, R. Valenzuela, and P. Wolniansky. Detection algorithm and initial laboratory results using V-BLAST space-time communication architecture. *Electronics Letters*, 35(1):14–16, Jan. 1999.

[37] A. Goldsmith, S. Jafar, N. Jindal, and S. Vishwanath. Capacity limits of MIMO channels. *IEEE J. Select. Areas Commun.*, 21(5):684–702, May 2003.

[38] M. González-López, J. Míguez, and L. Castedo. Turbo aided maximum likelihood channel estimation for space-time coded systems. In *IEEE International Symposium on Personal, Indoor and Mobile Radio Communications*, volume 1, pages 364–368, 2002.

[39] D. Guo and X. Wang. Blind detection in MIMO systems via sequential Monte Carlo. *IEEE J. Select. Areas Commun.*, 21(3):464–473, Mar. 2003.

[40] P. Gupta and P. Kumar. Critical power for asymptotic connectivity. In *Decision and Control, 1998. Proceedings of the 37th IEEE Conference on*, volume 1, pages 1106–1110, 1998.

[41] P. Hall. *Introduction to the Theory of Coverage Process.* John Wiley and Sons, 1988.

[42] D. Harville. *Matrix Algebra From a Statistician's Perspective.* Springer-Verlag, New York, 1997.

[43] H. Hashemi. The m-distribution a general formula of intensity distribution of rapid fading. *Proc. IEEE*, 81:943–968, July 1993.

[44] M. Hasna and M.-S. Alouini. Application of the harmonic mean statistics to the end-to-end performance of transmission systems with relays. In *Proc. GLOBECOM*, volume 2, pages 1310–1314, 2002.

[45] M. Hasna and M.-S. Alouini. Performance analysis of two-hop relayed transmissions over Rayleigh fading channels. In *Proc. Vehicular Tech. Conf.*, volume 4, pages 1992–1996, 2002.

[46] M. Hasna and M.-S. Alouini. Outage probability of multihop transmission over Nakagami fading channels. *IEEE Commun. Lett.*, 7(5):216–218, May 2003.

[47] B. Hassibi. An efficient square-root algorithm for BLAST. In *Proc. Intl. Conf. on ASSP*, volume 2, pages II737–II740, 2000.

[48] B. Hassibi and B. Hochwald. High-rate codes that are linear in space and time. *IEEE Trans. Inform. Theory*, 48(7):1804–1824, July 2002.

[49] S. Haykin, M. Sellathurai, Y. de Jong, and T. Willink. Turbo-MIMO for wireless communications. *IEEE Commun. Mag.*, 42(10):48–53, Oct. 2004.

[50] O. Henkel. Sphere packing bounds in the grassmann and stiefel manifolds. *IEEE Trans. Inform. Theory*, 51(10):3445–3456, Oct. 2005.

[51] B. Hochwald and S. ten Brink. Achieving near-capacity on a multiple-antenna channel. *IEEE Trans. Commun.*, 51(3):389–399, Mar. 2003.

[52] T. Holliday and A. Goldsmith. Cross-layer design for mimo systems. In *Proceeding of Conference on Information Science and Systems*, Jan. 2006.

[53] B. Hughes. Differential space-time modulation. *IEEE Trans. Inform. Theory*, 46(7):2567–2578, July 2000.

[54] M. Ivrlac, W. Utschick, and J. Nossek. Fading correlations in wireless mimo communication systems. *IEEE J. Select. Areas Commun.*, 21(5):819–828, June 2003.

[55] G. Kaleh and R. Vallet. Joint parameter estimation and symbol detection for linear or nonlinear unknown channels. *IEEE Trans. Commun.*, 42:2406–2413, July 1994.

[56] S. Kay. *Fundamentals of Statistical Signal Processing: Estimation Theory*. Englewood Cliffs, NJ, Upper Saddle River, NJ, 1993.

[57] S. Kim. Log-likelihood ratio based detection ordering for the V-BLAST. In *Proc. GLOBECOM*, San Francisco, USA, Dec. 2003.

[58] M. Kopbayashi, J. Boutros, and G. Caire. Successive interference cancellation with SISO decoding and EM channel estimation. *IEEE J. Select. Areas Commun.*, 19(8):1450–1460, Aug. 2001.

[59] S. Kumar, T. Lai, and J. Balogh. On k-coverage in a mostly sleeping sensor network. In *MobiCom '04: Proceedings of the 10th annual international conference on Mobile computing and networking*, pages 144–158. ACM Press, 2004.

[60] J. Laneman, D. Tse, and G. Wornell. Cooperative diversity in wireless networks: Efficient protocols and outage behavior. *IEEE Trans. Inform. Theory*, 50(12):3062–3080, Dec. 2004.

[61] J. Laneman and G. Wornell. Energy-efficient antenna sharing and relaying for wireless networks. In *Proc. of Wireless Communications and Networking Conference*, volume 1, pages 7–12, 2000.

[62] J. Laneman and G. Wornell. Distributed space-time-coded protocols for exploiting cooperative diversity in wireless networks. *IEEE Trans. Inform. Theory*, 49(10):2415–2425, Oct. 2003.

[63] E. Larsson, P. Stoica, and J. Li. Orthogonal space-time block codes: maximum likelihood detection for unknown channels and unstructured interferences. *IEEE Trans. Signal Processing*, 51(2):362–372, Feb. 2003.

[64] T. Li and N. Sidiropoulos. Blind digital signal separation using successive interference cancellation iterative least squares. *IEEE Trans. Signal Processing*, 48(11):3146–3152, Nov. 2000.

[65] Y. Li, C. Georghiades, and G. Huang. Iterative maximum-likelihood sequence estimation for space-time coded systems. *IEEE Trans. Commun.*, 49(6):948–951, June 2001.

[66] G. McLachlan and T. Krishnan. *The EM Algorithm and Extensions*. Wiley, New York, 1997.

[67] W. Mo, D. Qiao, and Z. Wang. Mostly sleeping wireless sensor network: connectivity, k-coverage, and lifetime. Technical report, Electrical and Computer Engineering Department, Iowa State University, 2005.

[68] W. Mo, D. Qiao, and Z. Wang. Mostly-sleeping wireless sensor networks: Connectivity, k-coverage, and α-lifetime. In *Proc. of 43rd Allerton Conf.*, UIUC, Sept. 2005.

[69] W. Mo, D. Qiao, and Z. Wang. Lifetime maximization of sensor networks under connectivity and k-coverage constraints. In *Proc. of IEEE DCOSS'06*, San Francisco, CA, June 2006.

[70] W. Mo and Z. Wang. Average symbol error probability and outage probability analysis for general cooperative diversity system at high signal to noise ratio. In *Proc. 38th Conference on Information Sciences and Systems*, Mar. 2004.

[71] W. Mo and Z. Wang. Low-complexity nulling-canceling detection algorithm for coded MIMO systems with near-optimal performance. In *Signal Processing Advances in Wireless Communications, 2005 IEEE 6th Workshop on*, pages 570–574, 2005.

[72] W. Mo, Z. Wang, and A. Dogandžić. Em-based iterative receiver for coded mimo systems in unknown spatially correlated noise. *WILEY's Wireless Communications and Mobile Computing*, Mar. 2006. accepted for publication.

[73] T. Moon. The expectation-maximization algorithm. *IEEE Signal Processing Mag.*, 13:47–60, Nov. 1996.

[74] R. Muirhead. *Aspects of Multivariate Statistical Theory.* Wiley, New York, 1982.

[75] M. Nakagami. The m-distribution a general formula of intensity distribution of rapid fading. In *Statistical Methods in Radio Wave Propagation*, pages 3–36, W.G. Hoffman, Ed. Oxford: Pergamon Press, 1960.

[76] M. Nissila, S. Pasupathy, and A. Mammela. An em approach to carrier phase recovery in awgn channel. In *Proc. Intl. Conf. on Com.*, pages 2199–2203, Helsinki, Finland, June 2001.

[77] H. Niu, M. Shen, and J. Ritcey. Iterative channel estimation and LDPC decoding over flat-fading channels: A factor graph approach. In *Proc. of 37th Conf. on Info. Sciences and Systems*, Johns Hopkins University, March 12-14 2003.

[78] A. Nosratinia, T. Hunter, and A. Hedayat. Cooperative communication in wireless networks. *IEEE Commun. Mag.*, 42(10):74–80, Oct. 2004.

[79] A. Paulraj, D. Gore, R. Nabar, and H. Bolcskei. An Overview of MIMO Communications–A Key to Gigabit Wireless. *Proceedings of the IEEE*, 92(2):198–218, Feb. 2004.

[80] M. Pohst. On the computation of lattice vectors of minimal length, successive minima and reduced bases with applications. In *Proc. ACM SIGSAM*, pages 37–44, 1981.

[81] N. Prasad and M. Varanasi. Diversity and multiplexing tradeoff bounds for cooperative diversity protocols. In *Proc. IEEE Intl. Symp. on Info. Theory*, page 268, 27 June - 2 July, 2004.

[82] J. Proakis. *Digital communications*. New York: McGraw-Hill, 2000.

[83] J. Qin. Demodulation of binary psk signals without explicit carrier synchronization. In *Proc. Intl. Conf. on Com.*, pages 498–501, Geneva, Switzerland, May 1993.

[84] A. Ranheim. A decoupled approach to adaptive signal separation using an antenna array. *IEEE Trans. Veh. Technol.*, 48:676–682, May 1999.

[85] A. Ranheim, A. des Rosiers, and P. Siegel. An iterative receiver algorithm for space-time encoded signals. In *Proceedings Asilomar Conference on Signals, Systems & Computers*, volume 1, pages 516–520, 2000.

[86] T. Rappaport. *Wireless Communications: Principles and Practice*. Prentice Hall, 2001.

[87] A. Ribeiro, X. Cai, and G. Giannakis. Symbol error probabilities for general cooperative links. *IEEE Trans. Wireless Commun.*, 4(3):1264–1273, Mar. 2005.

[88] D. Samardzija and N. Mandayam. Pilot-assisted estimation of MIMO fading channel response and achievable data rates. *IEEE Trans. Signal Processing*, 51(11):2882–2890, Nov. 2003.

[89] M. Sandell, C. Luschi, P. Strauch, and R. Yan. Iterative channel estimation using soft decision feedback. In *Proc. GLOBECOM*, volume 6, pages 3728–3733, 1998.

[90] D. Schafhuber, G. Matz, and F. Hlawatsch. Kalman tracking of time-varying channels in wireless MIMO-OFDM systems. In *Signals, Systems & Computers, 2003 The Thrity-Seventh Asilomar Conference on*, volume 2, pages 1261–1265, 2003.

[91] A. Sendonaris, E. Erkip, and B. Aazhang. Increasing uplink capacity via user cooperation diversity. In *Proc. IEEE Intl. Symp. on Info. Theory*, page 156, 1998.

[92] A. Sendonaris, E. Erkip, and B. Aazhang. User cooperation diversity-part I: system description. *IEEE Trans. Commun.*, 51(11):1927–1938, Nov. 2003.

[93] N. Seshadri. Joint data and channel estimation using blind trellis search techniques. *IEEE Trans. Commun.*, 42:1000–1011, Apr. 1994.

[94] S. Sfar, L. Dai, and K. Letaief. Optimal diversity-multiplexing tradeoff with group detection for mimo systems. *IEEE Trans. Commun.*, 53(7):1178–1190, July 2005.

[95] S. Shakkottai, R. Srikant, and N. Shroff. Unreliable sensor grids: coverage, connectivity and diameter. In *IEEE INFOCOM*, volume 2, pages 1073–1083, 2003.

[96] N. Shepherd. Radio wave loss deviation and shadow loss at 900 mhz. *IEEE Trans. Veh. Technol.*, 26:309–313, Nov. 1977.

[97] M. Simon and M. Alouini. *Digital Communications over Fading Channels: A Unified Approach to Performance Analysis*. John Wiley & Sons, 2000.

[98] A. Stefanov and E. Erkip. Cooperative space-time coding for wireless networks. *IEEE Trans. Commun.*, 53(11):1804–1809, Nov. 2005.

[99] G. Stüber. *Principles of mobile communications*. Norwell, MA: Kluwer, 1996.

[100] S. Sun, T. Tjhung, and P. Fung. Soft decision-based iterative interference cancellation (IIC) in group-wise STBC (G-STBC) MIMO systems. In *Proc. Vehicular Tech. Conf.*, volume 2, pages 984–988, 2003.

[101] V. Tarokh, H. Jafarkhani, and A. R. Calderbank. Space-time block codes from orthogonal designs. *IEEE Trans. Inform. Theory*, 45(5):1456–1467, July 1999.

[102] I. E. Telatar. Capacity of multi-antenna Gaussian channels. *European Trans. on Telecomm.*, 10(6):585–596, Nov.–Dec. 1999.

[103] D. Tse, P. Viswanath, and L. Zheng. Diversity-multiplexing tradeoff in multiple-access channels. *IEEE Trans. Inform. Theory*, 50(9):1859–1874, Sept. 2004.

[104] M. Tuchler, R. Koetter, and A. Singer. Turbo equalization: principles and new results. *IEEE Trans. Commun.*, 50(5):754–767, May 2002.

[105] G. Tzeremes and C. Christodoulou. Use of weibull distribution for describing outdoor multipath fading. In *Proc. IEEE Antennas, Propagation Soc. Int. Symp.*, pages 232–235, San Antonio, TX, June 2002.

[106] P. Vaidyanathan. *Multirate Systems and Filter Banks*. Prentice-Hall, Englewood Cliffs, NJ, 1993.

[107] M. Valenti and B. Woerner. Iterative channel estimation and decoding of pilot symbol assisted turbo codes over flat-fading channels. *IEEE J. Select. Areas Commun.*, 19(9):1697–1705, Sept. 2001.

[108] S. Verdú. *Multiuser Detection*. Cambridge Press, 1998.

[109] M. Viberg, P. Stoica, and B. Ottersten. Maximum likelihood array processing in spatially correlated noise fields using parameterized signals. *IEEE Trans. Signal Processing*, 45(4):996–1004, Apr. 1997.

[110] E. Viterbo and J. Boutros. A universal lattice code decoder for fading channels. *IEEE Trans. Inform. Theory*, 45(5):1639–1642, May 1999.

[111] X. Wang and H. V. Poor. Iterative (Turbo) soft interference cancellation and decoding for coded CDMA. *IEEE Trans. Commun.*, 46(7):1046–1061, July 1999.

[112] X. Wang, G. Xing, Y. Zhang, C. Lu, R. Pless, and C. Gill. Integrated coverage and connectivity configuration in wireless sensor networks. In *SenSys '03: Proceedings of the 1st international conference on Embedded networked sensor systems*, pages 28–39. ACM Press, 2003.

[113] Z. Wang and G. Giannakis. Block spreading for multipath-resilient generalized multi-carrier CDMA. In *Signal Processing Advances in Wireless and Mobile Communications*, G.B. Giannakis, Y. Hua, P. Stoica, and L. Tong, Eds. vol. II, Chapter 6, Prentice-Hall, Inc, Oct. 2000.

[114] Z. Wang and G. Giannakis. A simple and general parameterization quantifying performance in fading channels. *IEEE Trans. Commun.*, 51(8):1389–1398, Aug. 2003.

[115] L. Weng, A. Anastasopoulos, and S. S. Pradhan. Diversity gain regions for mimo fading broadcast and multiple access channels. *IEEE Trans. Inform. Theory*, Apr. 2005 (submitted).

[116] P. Wolniansky, G. Foschini, G. Golden, and R. Valenzuela. V-blast: An architecture for realizing very high data rates over the rich-scattering wireless channel. In *ISSSE-98*, Sept. 1998.

[117] X. Xia. *Modulated Coding for Intersymbol Interference Channels*. Marcel Dekker, New York, 2000.

[118] F. Ye, G. Zhong, S. Lu, and L. Zhang. Energy efficient robust sensing coverage in large sensor networks. Technical report, UCLA, 2002.

[119] Y. Yuk, K. Ko, T. Kim, D. Hong, and C. Kang. An Iterative Decoded V-BLAST System using Maximum a Posteriori Criterion. In *Proc. GLOBECOM*, volume 2, pages 1099–1102, 2003.

[120] M. Yuksel and E. Erkip. Diversity-multiplexing tradeo in cooperative wireless sys- tems. In *Proceeding of Conference on Information Science and Systems*, Jan. 2006.

[121] H. Zhang and J. Hou. On deriving the upper bound of α-lifetime for large sensor networks. In *MobiHoc '04: Proceedings of the 5th ACM international symposium on Mobile ad hoc networking and computing*, pages 121–132. ACM Press, 2004.

[122] L. Zhang and D. Tse. The diversity-multiplexing tradeoff for non-coherent multiple antenna channels. In *Proceedings of the 40th Allerton Conference on Communication, Control, and Computing*, Oct. 2002.

[123] L. Zhao, W. Mo, Y. Ma, and Z. Wang. Diversity and multiplexing tradeoff in general fading channels. *IEEE Trans. Inform. Theory*, July 2006 (accepted).

[124] L. Zheng and D. Tse. Diversity and multiplexing: a fundamental tradeoff in multiple-antenna channels. *IEEE Trans. Inform. Theory*, 49(5):1073–1096, May 2003.